The Anti-Inflammatory Effects of INSL5 in a DSS-Induced Model of Ulcerative Colitis

By
Ian McNicol

A thesis submitted to the Faculty of Graduate Studies in partial fulfilment of the requirements for the Master of Science degree.

Department of Biology

Master of Bioscience, Technology and Public Policy
The University of Winnipeg
Winnipeg, Manitoba, Canada

Abstract

Insulin-like peptide 5 (INSL5) is a novel gastrointestinal (GI) hormone, primarily expressed in the distal colon and rectum. Its cognate receptor is the G-protein coupled receptor (GPCR) relaxin family peptide receptor 4 (RXFP4), which is expressed in a variety of tissues and cells, including the vagus nerve, colon, liver, heart, kidney, and gonads. Current research suggests that INSL5 is involved in satiety, glucose homeostasis, colonic propulsion, the male and female reproductive systems, and the progression of cancer. Our lab has recently found RXFP4 expression in all murine immune organs and some innate immune cells, implying that RXFP4 and therefore INSL5 may be involved in the immune system. Due to the high levels of INSL5 in the distal gut, it may play a homeostatic role in conditions of chronic inflammation, such as inflammatory bowel disease (IBD). The gut is intimately linked to the spleen via the spleen-gut axis and it is well documented that hyposplenism (splenic dysfunction) is correlated with GI disorders. The first objective of this study is to determine if DSS treatment induces inflammation in the spleen. The second objective is to determine if INSL5 influences immune cell responses in the murine spleen. I hypothesize that dextran sodium sulfate (DSS)-induced colitis will also induce hyposplenism. Additionally, I hypothesize that INSL5 exerts anti-inflammatory effects via RXFP4 expressed on splenic macrophages in a mouse model. To test these hypotheses, eight C57BL/6 strain male mice aged eight to twelve weeks were exposed to 2% DSS in their drinking water for seven days, while eight mice of the same strain and age were given regular drinking water as a control. Following euthanasia, blood samples were taken, the spleens were extracted, weighed, and some sections were kept for histological or molecular analysis while the rest were dissociated into RPMI cell culture media to generate primary culture of splenocytes. Histological preparations of whole spleen were stained with Prussian blue to test for thrombosis while blood smears were analysed for the presence of Howell-Jolly bodies and hypochromic erythrocytes, markers of hyposplenism. RNA was extracted from splenic macrophages of eight control and eight DSS-treated mice for qPCR analyses, and RNA from the spleens of four control and four DSS-treated mice was sent for RNA-sequencing. For the transcriptomic analysis, k-means clustering was performed to identify gene clusters associated with the largest standard deviation in gene expression across samples and the list of genes falling into each cluster were tested for enrichment using the GO Biological Process database. Subsequently, differentially expressed

genes (DEGs) were identified from the transcriptomic data using an FDR<0.1 and log fold change > 1.5; the list of DEG's was used for a gene enrichment analysis using the EnrichR database. Meanwhile, the aliquots of dissociated splenocytes were enriched for macrophages and then exposed to one of four treatments; control (no treatment), lipopolysaccharide (1.0 μg/ml LPS from *Escherichia coli* per well for 24 hours), co-treatment (100 nM INSL5 and 1.0 μg/ml LPS for 24 hours), and INSL5 pre-treatment (100 nM INSL5 hormone for 12 hours followed by 1.0 μg/ml LPS for 24 hours). Cytokine profiles and other macrophage markers were measured via qPCR and ELISA assay. Our histological, hematological, and qPCR results showed that DSS-induced colitis resulted in hyposplenism via the spleen-gut axis. According to the RNA seq data, DSS-treatment resulted in the upregulation of 146 genes and the downregulation of 21 genes, most of which were associated with the immune system or erythrocyte development. The results of the experiment on macrophage enriched splenocytes indicated that INSL5 played a minor role in alleviating inflammation by reducing the expression of some pro-inflammatory cytokines. However, the results of the cell culture experiment from the DSS-exposed murine spleens indicated that they experienced hyposplenism too extreme for LPS or INSL5 treatment to cause any significant change in immune gene expression. Unfortunately, the ELISA data did not show any significant effect of INSL5 in the spleen, however this may be a result of human error. Overall, our results indicate a strong relationship between the disorders of the gut and the spleen, however INSL5 appears to have a minimal role on immunological role of the spleen. Rather, the RNA-Seq data showed that DSS played a greater role in affecting its erythropoietic function. Further research is warranted, especially into the role of INSL5 in the gut, where it is most highly expressed, and where data mining indicate that its cognate receptor RXFP4 is found on diverse immune cell subsets. Research into the immunological role of INSL5 may be helpful for treating GI disorders such as ulcerative colitis.

Acknowledgments

I would like to thank my supervisor, Dr. Sara Good, for the opportunity to carry out this research in your lab. I have learned so much from you, both inside and outside of an academic context. Thank you so much for all of your support.

I would also like to thank my committee members Dr. Sanoji Wijenayake and Dr. Jean-Pierre Desforges for your guidance throughout my project. I would also like to thank Dr. Connie Willing for her support.

I would also like to thank my lab mates Drake Hechter and Cameron Rey-Dubois, as the three of us worked together on the mouse project, and without whom this research would not have been possible. I am also grateful for my other lab mates Ilya Kisselev, Avery Keen, Lara Peutz, Amy Pitzel, Patricia Montalvo-Rodriguez, and Hassan Nazari, as well as past lab members Tiana Tiede, Tamana Yasmin, and Coleen Soos. You've all given me tremendous support (and baking, thank you Amy) throughout my degree.

This project was funded by Dr. Good, as well as the Dr. Beni M. Sahai Fund for Cell and Molecular Biology for Advancement in Medical Research and NSERC Discovery Grant, and my CIHR Graduate Studies Research Award. Additionally, I thank the University of Winnipeg Research Office as they had awarded me a Graduate Student Research Travel Grant so I could present my findings at the 2023 Canadian Society of Zoologists conference.

Finally, I would like to thank my friends and family, who have given me so much support throughout my degree. Your support has helped me greatly, and without your encouragement, I would not be moving on to my PhD.

Table of Contents

Abstract……i
Acknowledgements……iii
Table of Contents……iv
List of Figures……vi
List of Tables……vii
Acronyms……viii
Introduction……1
1.1 The Insulin Gene Superfamily……1
1.1.1 Relaxin Family Peptide Receptors ……1
1.1.2 Insulin and Insulin-Like Growth Factors ……2
1.1.3 Insulin-Like and Relaxin Peptides……3
1.1.4 Insulin-Like Peptide 5……6
1.1.5 Stimulation of INSL5……7
1.2 Functions of INSL5……8
1.2.1 INSL5 as an Orexigenic Hormone ……8
1.2.2 INSL5 and Glucose Homeostasis ……9
1.2.3 INSL5 and Colonic Propulsion ……9
1.2.4 INSL5 and the Reproductive System ……10
1.2.5 INSL5 and Cancer ……11
1.2.6 INSL5 and the Immune System……12
1.3 Inflammatory Bowel Disease……13
1.3.1 Crohn's Disease……14
1.3.2 Ulcerative Colitis……15
1.3.3 Treatments for IBD……16
1.4 Pathways Associated with RXFP4……17
1.4.1 MAPK Pathways……17
1.4.2 JAK/STAT……18
1.4.3 SOCS3……18
1.5 The Immune System……19
1.5.1 Macrophages……21
1.5.2 Dendritic Cells……22
1.5.3 The Spleen……23
1.5.4 The Spleen-Gut Axis……25
1.5.5 Hyposplenism and GI Disorders……26
1.6 The Enteroendocrine System……28
Objectives and Hypotheses……30
Rationale……31
Methods……32
2.1 Animal Treatments……32
2.2 Disease Activity Index……32
2.3 Comparison of Spleens between Control and DSS-Treated Mice……32
2.3.1 Hematological Analysis of the Spleen……33
2.3.2 Histological Analysis of the Spleen ……34
2.4 RNA-Sequencing Analysis of Control and DSS-Treated Whole Spleen……34

2.5 Comparison of Macrophages Across Cell Treatments……35
2.5.1 Cell Culture Media……36
2.5.2 Analysis of Gene Transcript Abundance in Control vs DSS-Treated Mice……...36
2.5.3 Splenic Macrophage Treatments……38
2.5.4 Analysis of Gene Transcript Abundance Across Macrophage Treatments……..38
2.6 ELISA Assay……...39
2.7 Data Analyses……..40
Results……...42
3.1 Histological Analysis of the Spleen……42
3.2 Hematological Analysis of the Spleen……43
3.3 mRNA Transcript Abundance Analyses – Whole Spleen……..……44
3.3.1 RNA-SEQ Analysis……...45
3.3.2 Splenic Macrophages – Control Mice……48
3.3.3 Splenic Macrophages – DSS-Treated Mice……...50
3.3.4 The Effect of DSS on Splenic Macrophages……51
3.4 ELISA Assay……...52
Discussion……54
4.1 The Effects of DSS on the Murine Spleen……...54
4.1.1 Hyposplenism and DSS-Induced Colitis……..54
4.1.2 RXFP4 and the Spleen……..55
4.2 Control Mouse Transcript Data – *Il-6, Il-10,* and *Cd80*……..57
4.2.1 Remaining qPCR Data……..59
4.3 RNA-SEQ Data……60
4.4 Protein Evidence for INSL5 as an Immunological Hormone in the Spleen……61
4.5 Limitations……...62
4.6 Future Directions……63
Conclusion……65
References……..66
Appendices……80
Appendix A: Recipes for solutions used in Prussian blue experiment……..80
Appendix B: List of dissected mice with total weight from November–December 2022 Dissections……80
Appendix C: Howell-Jolly and Hypochromic Erythrocyte Counts……...81
Appendix D: K-Means Cluster Enrichment Data……..82
Appendix E: RNA Sequencing Significant Values (Control vs DSS)……100
Appendix F: Enrichment Pathways associated with the 158 differentially expressed genes identified using DESEQ2……103

List of Figures

Figure 1.1. The structure of an INS/INSL/RLN prepro-polypeptide, pro-polypeptide, and mature protein. INS/INSL/RLN prepro-polypeptides have an A-chain on the C-terminus, followed by a C-chain, a B-chain, and a signal peptide on the N-terminus. The signal peptide is cleaved out to form the pro-polypeptide, and then the C-chain is cleaved out to form mature peptide, leaving only the A and B-chains connected by two disulfide bridges, and one additional disulfide bridge on the A-chain. Generated with Microsoft Word……3
Figure 1.2. The structure of proteins in the human insulin gene superfamily. (**A)** Alignment of INSL/RLN proteins. (McNicol et al. in preparation) (**B)** Protein structure of INSL5 peptides A (orange) and B (green).Downloaded from RCSB Protein Data Bank, 2KBC..……...4
Figure 1.3. Phylogenetic tree of the RLN family peptides and the cognate receptors of RNL2, INSL3, RLN3, and INSL5. Generated with BioRender..……6
Figure 1.4. The sequential differences between human INSL5 and analog 13. Important residues are shown in green, while mutated residues are blue. Disulfide bonds are shown as black lines or arches. Generated with Microsoft PowerPoint……..11
Figure 1.5. The many potential roles of INSL5, including regulation of the immune system. Research suggests it may have many functions, including regulating energy homeostasis, colonic propulsion, glucose homeostasis, and inflammatory responses (Figure from Hechter et al. 2022) ……13
Figure 1.6. The distribution of inflammation in ulcerative colitis and Crohn's disease. UC affects the distal colon and rectum in a continuous fashion, while CD affects various parts of the gut in a patchy formation. Image source: http://sanmateorheumatology.com/condition/inflammatory-bowel-disease/……...16
Figure 1.7. Macrophages differentiate into M1 or M2 phenotype based on exposure to various stimulants. They can be distinguished based on cytokine profile……..22
Figure 1.8. Murine spleen weights of control vs DSS mice as recorded by Hechter et al., (in preparation) ……...28
Figure 2.1. The splenic macrophage treatments from both control and DSS-treated mice. Generated with Microsoft Powerpoint.……..38
Figure 3.1 A comparison of control and DSS-exposed murine livers stained using the Prussian blue staining technique. Blue pigmentation indicates the presence of ferric iron. Iron deposit images were made clearer in Photoscape X by isolating the colour blue and increasing the contrast, saturation, and vibrancy. **A)** Iron levels in the general area of the control spleen (top) and DSS-treated spleen (bottom). Magnified to 999 by 999 pixels. **B)** The blood vessel of the control spleen (top) and DSS-treated spleen (bottom). Magnified to 999 by 999 pixels. **C)** A full slide of a control spleen (top) and a DSS-treated spleen (bottom)……42
Figure 3.2 A) comparison of control (top) and DSS-treated (bottom) murine blood stains. **B)** A magnified to 250 by 250 pixels. image of control (top) and DSS-treated (bottom) murine blood stains. **C)** A comparison of Howell-Jolly bodies in control vs DSS-treated mice. N=16. **D)** A comparison of hypochromic erythrocytes in control vs DSS-treated mice. N=6 mice, three replicates per mouse for 18 total replicates. One asterisk on error bars: $p \leq 0.05$. Two asterisks: $p \leq 0.01$. Three asterisks: $p \leq 0.001$……..43-44
Figure 3.3 Gene transcript abundance differences between control and DSS-treated mouse spleens. dCt = delta Ct. Calculated by subtracting the Ct values of the housekeeping gene from the Ct values of the gene of interest..…….……45

Figure 3.4 A) boxplot and **B)** density of transformed transcript abundance values by treatment. **C)** Heatmap of k-mean unsupervised clustering of the top six clusters exhibiting the greatest cross-sample standard deviation in transcript abundance……..……...46
Figure 3.5 A) Tree visualization of significant GO: Biological Processes terms associated with cluster 3 and cluster 5 (shown in Figure 3.5 C)of the K-means unsupervised cluster analysis **B)** Normalized expression of log-transformed gene transcript abundance counts in control and DSS-treated expression.……..47
Figure 3.6 Transcript Abundance of *Rxfp4* between control and DSS-treated mouse across treatments. Higher *Rxfp4* levels imply more significant downstream effects triggered by binding *Insl5*.……...56
Figure 3.7 Transcript abundance of *Rxfp4* between control and DSS-treated mouse across cell treatments. Higher *Rxfp4* transcript abundance levels imply more significant downstream effects triggered by binding *Insl5*. dCt = delta Ct. Calculated by subtracting the Ct values of the housekeeping gene from the Ct values of the gene of interest.…….49
Figure 3.8 Gene transcript abundance differences across treatments in control mouse macrophages. dCt = delta Ct. Calculated by subtracting the Ct values of the housekeeping gene from the Ct values of the gene of interest……..50
Figure 3.9 Gene transcript abundance differences across treatments in DSS-treated mouse macrophages. dCt = delta Ct. Calculated by subtracting the Ct values of the housekeeping gene from the Ct values of the gene of interest……..51
Figure 3.10 Gene transcript abundance differences between mouse macrophages treated with and without DSS. dCt = delta Ct. Calculated by subtracting the Ct values of the housekeeping gene from the Ct values of the gene of interest…….52
Figure 3.11 Expression of IL-6, IL-13, and TNF-α across different treatments in control mouse macrophages as measured via ELISA assay. dCt = delta Ct. Calculated by subtracting the Ct values of the housekeeping gene from the Ct values of the gene of interest…….53
Figure 3.12 Expression of IL-1α, LIX, and TNF-α across different treatments in DSS-treated mouse macrophages as measured via ELISA assay. dCt = delta Ct. Calculated by subtracting the Ct values of the housekeeping gene from the Ct values of the gene of interest……53

List of Tables

Table 2.1. The scoring system of the disease activity index. **(A)** Weight loss scoring system. **(B)** Stool consistency scoring system. **(C)** Fecal occult blood test (Hemoccult II® SENSA® Fecal Occult Blood Test Systems, Beckman Coulter®, Medical Warehouse, Edmonton, AB, CA…...33
Table 2.2. The reaction volumes of each reagent according to the iScript protocol, and our altered volumes to account for low RNA yields.……...40
Table 2.3. The iScript reaction protocol in the MJ Research PTC-200 Thermal Cycler.……40
Table 2.4. qPCR protocol for optimization of primers and data collection……..41
Table 3.1 Genes exhibiting significantly different levels of transcript abundance between control and DSS-treated mice. For each gene, the gene symbol, ensemble ID, log2 fold change (log2FC) for control – DSS treated mice and the FDR adjusted p-value are given. Select genes associated with immune system functions **(A)** or erythrocyte traits **(B)** are given. The full list of 159 genes that exhibited differential transcript abundance between traits is given in Appendix D……...48

Acronyms

5-aminosalicylic acid	5-ASA
6-thioguanine	6-TG
α7nAChR	α7 subtype of nicotinic acetylcholine receptor
INSL5-A13	Analog 13
AMH	Anti-Müllerian hormone
CCL	CC-chemokine ligand
CD	Crohn's disease
CR	Caloric restriction
CRC	Colorectal cancer
CRP	C-reactive protein
CXCL	CXC-chemokine ligand
CXCR	CXC-chemokine receptor
DAI	Disease activity index
DPP IV	Dipeptidyl peptidase IV
DC	Dendritic cell
-FDC	Follicular dendritic cell
-mDC	Myeloid dendritic cell
-pDC	Plasmacytoid dendritic cell
-sDC	Splenic dendritic cell
DSS	Dextran sodium sulfate
EEC	Enteroendocrine cells
EC	Enterochromaffin cells
ELISA	Enzyme linked immunosorbent assay
FFAR	Free fatty acid receptor
FSHR	Follicle-stimulating hormone receptor
GF	Germ-free
GI	Gastrointestinal
GLP	Glucagon-like peptide
GPCR	G protein coupled receptor
HDAC	Histone deacetylase
HFD	High fat diet
HOV	Homogeneity of variance
HSC	Hematopoietic stem cells
IBD	Inflammatory bowel disease
IEC	Intestinal epithelial cell
IFN	Interferon
IkBα	Inhibitor of NF-kB
IKK	IkB kinase
IL	Interleukin
INS	Insulin
INSL or ILP	Insulin-like peptide
IP	Intervening peptide
JAK	Janus Kinase
KO or $^{-/-}$	Knockout

KW	Kruskal-Wallis
LPS	Lipopolysaccharide
M0	Naïve macrophage
M1	Type 1/classical macrophage
M2	Type 2/alternative macrophage
MAPK	Mitogen-activated protein kinase
MBC	Memory B-cell
MHC	Major histocompatibility complex
mTOR	Mammalian target of rapamycin
MZ	Marginal zone
NET	Neuroendocrine tumour
NF-kB	Nuclear factor kappa-light-chain-enhancer of activated-B-cells
NKT	Natural killer T-cells
NAFLD	Non-alcoholic fatty liver disease
NPC	Nasopharyngeal carcinoma
NPY	Neuropeptide Y
PAMP	Pathogen-associated molecular patterns
PBS	Phosphate buffer saline
PC	Prohormone convertase
PCOS	Polycystic ovary syndrome
PPAR-γ	Peroxisome proliferator-activated receptor gamma
PYY	Peptide tyrosine tyrosine
RLN	Relaxin
RPMI	Roswell Park Memorial Institute
RT-qPCR	Reverse transcription quantitative polymerase chain reaction
RXFP	Relaxin family peptide
S6RP	Ribosomal protein S6
SCFA	Short chain fatty acid
SIgA	Secretory immunoglobin A
SOCS	Suppressors of cytokine signaling
STAT	Signal transducer and activator of transcription
Th	T-helper
TLR	Toll-like receptor
TM	Transmembrane domain
TNF	Tumor necrosis factor
TYK	Tyrosine kinase
UC	Ulcerative colitis
WT	Wild type

Introduction

You're out for a walk one day, and you fall and scrape your knee. Soon after the initial injury, your knee starts to swell and turn red. It feels painful to the touch and you will most likely have difficulty moving it properly for the next couple of days. Numerous leukocytes (white blood cells) and other immune factors migrate to the area of the injury, protecting your body from infectious pathogens which would otherwise be stopped by your skin. You're experiencing inflammation. Inflammation is both a gift and a curse, it is often given as a prime example of having too much of a good thing. Inflammation is necessary to fight infections, keeping organisms safe and healthy, however it also causes us pain, allergic reactions, and in severe or chronic cases, is associated with cancer or other diseases. Fortunately, your body has ways of regulating inflammation. In this thesis, I aim to argue that via binding to the Relaxin family peptide receptor RXFP4, the insulin family peptide INSL5 is one of these regulators.

1.1 The Insulin Gene Superfamily

The insulin superfamily of peptides in humans includes insulin (INS), insulin-like peptides 3 to 6 (INSL3 to INSL6), insulin-like growth factors I and II (IGFI and IGFII), and Relaxin 1 to 3 (RLN1 to RLN3) (Belgi et al., 2013).

1.1.1 Relaxin Family Peptide Receptors

The receptors for the Relaxin family of peptides are known as the Relaxin Family Peptide Receptors (RXFP), however they belong to two distinct classes of highly conserved families of G-protein coupled receptors (GPCRs) (Bathgate et al., 2013). There have been four RXFP proteins discovered in mammals, known as RXFP1 to RXFP4, which are associated with the four Relaxin family peptides (Good et al., 2012). RXFP1 and RXFP2 belong to one class of GPCRs and are related to glycoprotein hormone receptors such as luteinizing hormone receptor (LHR) and follicle-stimulating receptor (FSHR) (Good et al., 2012). RXFP1 and RXFP2 are the cognate receptors for human RLN and INSL3, respectively, which primarily act as reproductive hormones (Good et al., 2012). RXFP1 and 2 are ~700 residues in length as they possess a long N-terminus, which contains a leucine-rich repeat that is involved in ligand binding, as do LHR and FSHR (Bathgate et al., 2013 and Hsu 2003).

RXFP3 and 4 belong to the other class of GPCRs and are related to the angiotensin receptor and somatostatin receptors (Good et al., 2012). RXFP3 and 4 are the cognate receptors for RLN3 and INSL5, respectively, which play a role in neuroendocrine signaling among other proposed functions in humans (Good et al., 2012). Formerly known as GPR100 and GPCR142, RXFP4 was discovered before INSL5, however it was considered an orphan GPCR (Bathgate et al., 2013, Ang et al., 2017a). RXFP4 shares about 40% amino acid similarity and 50% overall homology with RXFP3 (previously known as GPCR135) (Zhu et al., 2008). RLN3 binds to both receptors with high affinity, however INSL5 only weakly binds to RXFP3 (Hu et al., 2016). Both RXFP3 and RXFP4 are smaller peptides than RXFP1 and RXPF2, at ~400 residues in length with shorter N-terminal domains (Good et al., 2012, Bathgate et al., 2013). The negatively charged N-terminus and extracellular loop 2 residues (Glu100, Asp104, and Glu182) of RXFP4 bind to the positively charged B-chain residues (B13Arg and B23Arg) of INSL5 (Zhu et al., 2008, Li et al., 2020). The RXFP4 transmembrane domains TM2, TM3, and TM5 are necessary for receptor stimulation (Zhu et al., 2008).

1.1.2 Insulin and Insulin-Like Growth Factors

Insulin is an incredibly important hormone as it maintains glucose homeostasis, however both insulin and IGF proteins function in cell growth, carbohydrate metabolism, and fat metabolism (Good et al., 2012, Yang et al., 2022). Insulin is synthesized by pancreatic beta cells as preproinsulin (PPI), which contains an N-terminal signal peptide, a B-chain, a C-chain, and an A-chain on the C-terminal (Liu et al., 2018). The signal peptide guides the protein across the endoplasmic reticulum (ER) membrane and is then cleaved by signal peptidase, resulting in the formation of proinsulin (PI) (Yang et al., 2022). The PI then gains three disulfide bonds which are highly conserved in the vertebrate insulin superfamily (Liu et al., 2018). PI leaves the ER and enters the Golgi apparatus, where the C-chain is cleaved off by prohormone convertase 2 (PC2), PC1/3, and carboxypeptidase E (CPE), resulting in the formation of the mature insulin protein, 51 amino acids in length (Derewenda et al., 1989, Yang et al., 2022). The A and B-chains are connected by two disulfide bridges, and there is one intramolecular disulfide bond located within the A-chain (Haugaard-Jōnsson et al., 2009).

There are two IGF molecules in humans that play important roles in growth. IGF1 is 70 amino acids in length while IGF2 is 67 amino acids; both proteins have a longer C-terminus than

other insulin family peptides (Laron 2001, Rotwein and Baral 2019). Unlike insulin, mature IGF proteins include four domains, B, C, A, and D (Blyth et al., 2020). IGF pro-peptides include an E peptide, which is cleaved prior to the maturation of the peptide by alternative splicing (Brisson and Barton 2013). While mature IGF proteins include only domains A-D, the cleaved E-peptide isoforms still have a function, as they have been reported to increase the entry of mature IGF into cells (Pfeffer et al., 2009).

1.1.3 Insulin-Like and Relaxin Peptides

INSL and RLN preproproteins, proproteins, and mature peptides have nearly the same structure as INS and are cleaved by the same proteases (Figure 1.1) (Zhang et al., 2020). The RLN peptide family is part of the insulin superfamily, based on the similarity in the primary, secondary and tertiary structure of the hormones (Figure 1.2) (Hsu 2003).

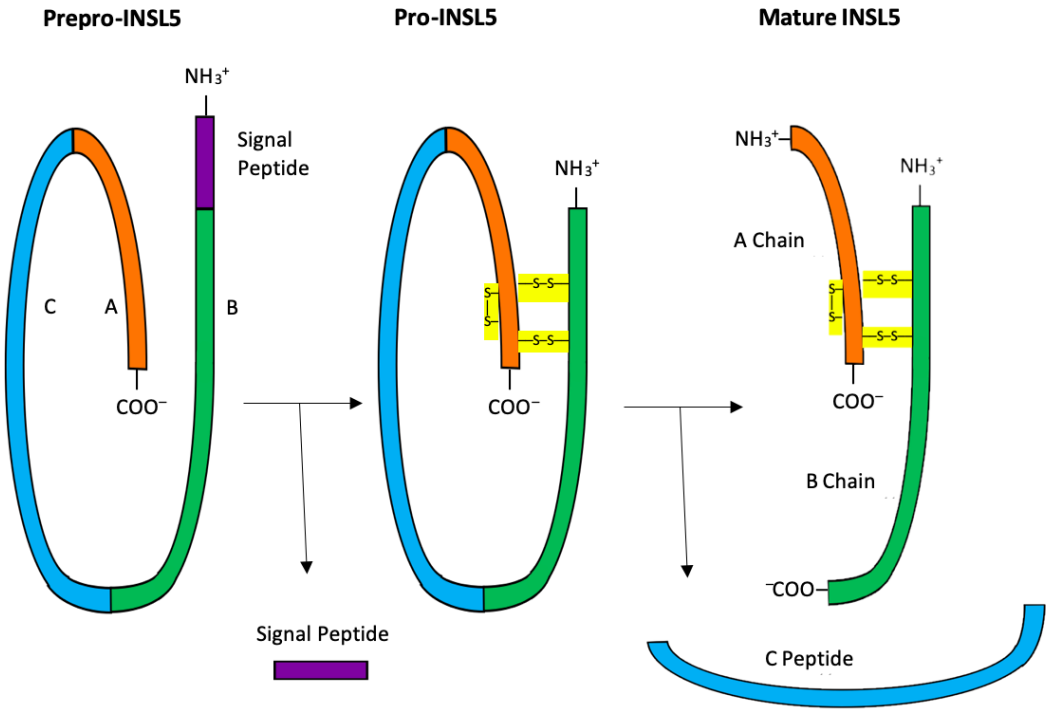

Figure 1.1. The structure of an INS/INSL/RLN prepro-polypeptide, pro-polypeptide, and mature protein. INS/INSL/RLN prepro-polypeptides have an A-chain on the C-terminus, followed by a C-chain, a B-chain, and a signal peptide on the N-terminus. The signal peptide is cleaved out to form the pro-polypeptide, and then the C-chain is cleaved out to form mature peptide, leaving only the A and B-chains connected by two disulfide bridges, and one additional disulfide bridge on the A-chain. Generated with Microsoft Word.

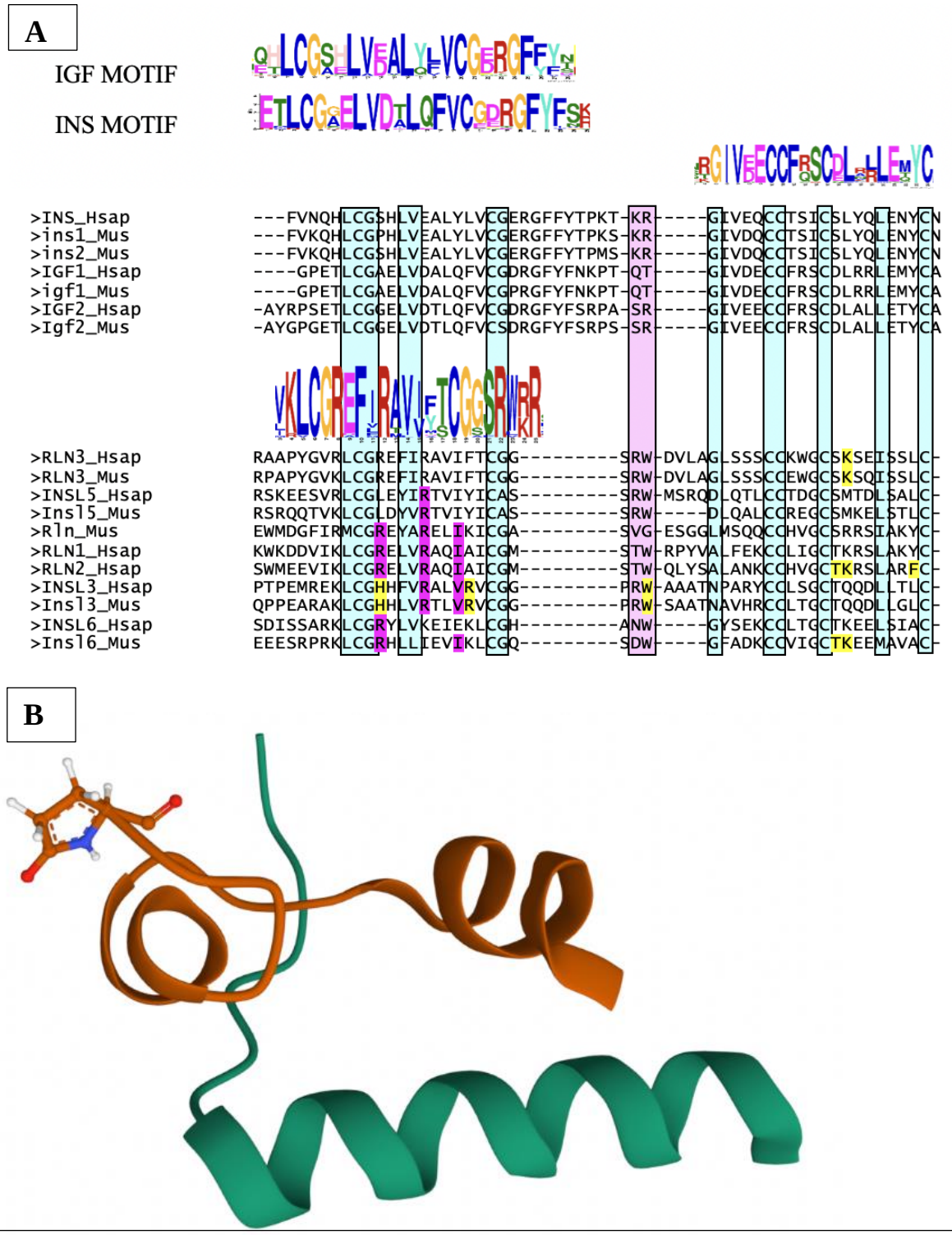

Figure 1.2. The structure of proteins in the human insulin gene superfamily. (**A)** Alignment of INSL/RLN proteins. (McNicol et al., in preparation) (**B)** Protein structure of INSL5 peptides A (orange) and B (green). Downloaded from RCSB Protein Data Bank, 2KBC.

The relaxin family peptides exert their function either primarily through the reproductive axis – these include the peptide hormones RLN (RLN1 and RLN2 in humans) and INSL3 (as well as mammalian specific hormones INSL4 and INSL6), or through the neuroendocrine axis primarily affecting stress and feeding behaviour, these include the peptide hormones RLN3 and INSL5. Relaxin plays a role in preparing the birth canal for parturition, tissue remodeling, wound healing, cardiovascular responses, and angiogenesis (Hsu 2003, Sherwood 2004). In humans there are two copies of the relaxin locus, RLN1 and RLN2, and both signal via RXFP1. RLN2 is primarily expressed by the corpus luteum and serves roles in reproduction, pregnancy, and maternity (Almeida-Pinto et al., 2023). INSL3 is primarily expressed in testicular Leydig cells where it regulates male reproductive health, and in ovarian theca cells where its function is less clear (Esteban-Lopez and Agoulnik 2020). INSL4 is primarily expressed in the placenta, where it plays an important role in the regulation of cell cycling, growth, and survival (Yang et al., 2019). INSL6 plays an important role in the development and motility of sperm (Burnicka-Turek et al., 2009). Both INSL4 and INSL6 are mammalian specific duplicates and signal via orphan receptors.

The relaxin family of peptides includes two peptide hormones, RLN3 and INSL5, which play neuroendocrine roles. The gene *RLN3* was discovered in 2001 by Bathgate et al. (2002) while searching for *RLN1* homologues. RLN3 has since been reported to play roles in learning, behaviours related to anxiety and motivation, memory, stress responses, and circadian rhythms (Ma et al., 2017). Finally, INSL5 is a novel gastrointestinal (GI) peptide hormone, and as such, there is much that we do not yet understand about it (Ang et al., 2018).

In the vertebrate ancestor, the primordial cluster A gene was subject to another duplication event, resulting in the evolution of vertebrate RLN3 and INSL5, as well as their cognate receptors RXFP3 and RXFP4 respectively (Good et al., 2012). Along with primate RLN1, the most recent members of the INSL/RLN family are INSL4 and INSL6, both of which are found only in mammals (Arroyo et al., 2012).

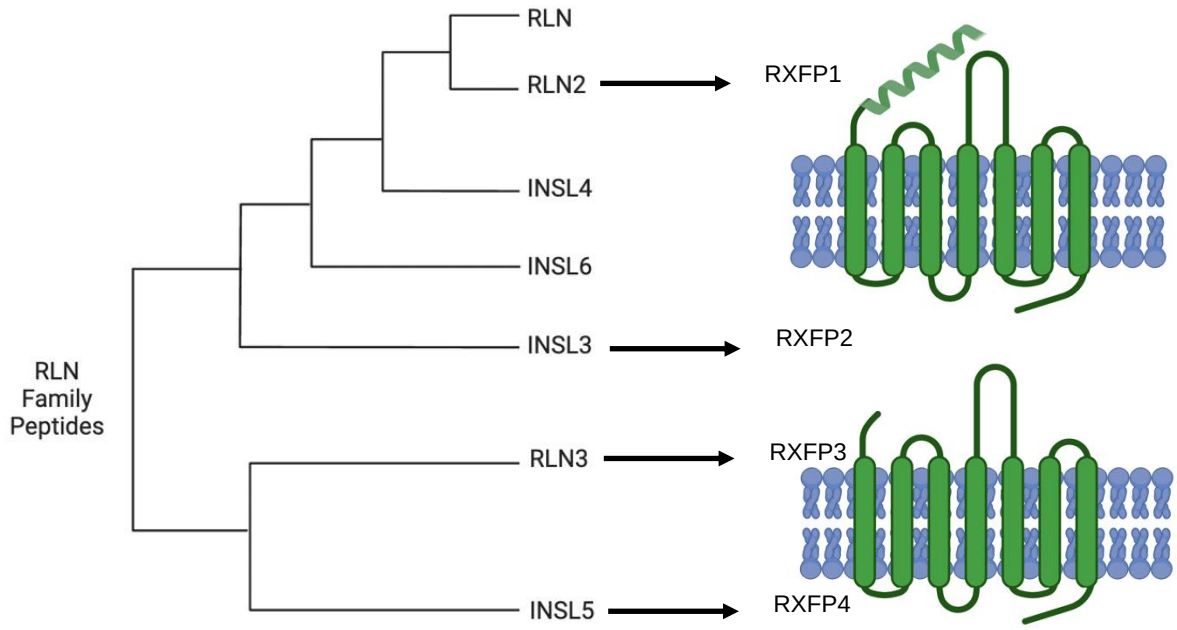

Figure 1.3. Phylogenetic tree of the RLN family peptides and the cognate receptors of RNL2, INSL3, RLN3, and INSL5.

1.1.4 Insulin-Like Peptide 5

INSL5 was first discovered in 1999 during an Expressed Sequence Tags (EST) database screening for the existence of the B-chain motif in the insulin superfamily (Conklin et al., 1999). Similar to the other INS/INSL/RLN proteins, the tertiary structure of the mature INSL5 peptide consists of a B-chain 25 residues in length and an A-chain 21 residues in length, with the chains connected via two interchain disulfide bonds, while the A-chain contains an additional intra-chain cysteine bond (Belgi et al., 2013). The primary binding residues of INSL5 are I^{B16}, W^{B24}, and R^{B23}, located on the B-chain (Praveen et al., 2019). Human and murine preproINSL5 both contain 135 amino acids while the mature peptide has 45, similar to other proteins in the insulin superfamily (Conklin et al., 1999, Zhang et al., 2020).

INSL5 was initially discovered in the uterus, colon, and rectum of humans (Conklin et al., 1999). Since then it has been found to be predominantly expressed by enteroendocrine L-cells in the rectum and distal colon, and is weakly expressed in other parts of the intestine (Grosse et al., 2014). It is also expressed elsewhere in the brain, thymus, kidneys, testes, prostate, ovary, thyroid, lung, placenta, and pituitary gland (Belgi et al., 2011). Liquid chromatography-mass spectrometry has shown that INSL5 is expressed along with glucagon-like peptide 1 (GLP-

1) and peptide tyrosine tyrosine (PYY) in colonic and rectal epithelial enteroendocrine L-cells (Ang et al., 2018, Gribble and Reimann 2019). INSL5 is co-secreted with GLP-1 and PYY *in vitro* when colorectal epithelial cells are exposed to physiological and pharmacological substances including bile acids and angiotensin II (Gribble and Reimann 2019). Curiously, PYY and GLP-1 are anorexigenic hormones, while INSL5 has orexigenic effects (Grosse et al., 2014). This suggests that INSL5 may be a homeostatic hormone.

RXFP4 is expressed in a wider group of organs of both humans and mice, including the vagus nerve, colon, liver, heart, kidney, and gonads of both sexes (Lewis et al., 2022). Research from our lab has found RXFP4 expression in all murine immune organs and some innate immune cells, suggesting that RXFP4 (and therefore INSL5) may have a role in the immune system (Vahkal et al., 2021).

1.1.5 Stimulation of INSL5

Various factors stimulate the expression of INSL5 in the gut, such as caloric restriction (CR) (Grosse et al., 2014). Grosse et al. (2014) proposed that INSL5 is an orexigenic hormone after finding that INSL5 is downregulated after eating and upregulated in CR mice. According to their results, CR is a major stimulant of INSL5 (Grosse et al., 2014), however other stimulants of INSL5 expression have been reported. Another stimulant of INSL5 is the absence of the gut microbiota, which are required to obtain nutrients from food, and therefore reducing gut microbiota yields similar effects to CR (Lee et al., 2016). A third stimulant of INSL5 includes short chain fatty acids (SCFAs), which are produced by the gut microbiota and are the primary energy source of colonocytes (Lee et al., 2016).

The intestinal microbiota evolved alongside the host, allowing the host to metabolize energy more efficiently (Wichmann et al., 2013). It has been found that in germ-free (GF) organisms, the lack of a gut microbiome decreases energy availability in the colon (Lee et al., 2016). Thus, the gut microbiome grants the host a metabolic advantage during conditions of CR, such as the scarcity of food (Wichmann et al., 2013). The colon and rectum have higher microbial densities than the small intestine, which further supports a possible role of INSL5 in energy metabolism in these regions (Arnoldini et al., 2018, Grosse et al., 2014; Hechter et al., 2022). Lee et al. (2016) found that GF mice and conventionally raised mice given anti-biotic

treatments show far higher expression of INSL5 than control mice, suggesting that the absence of an intestinal microbiome significantly increased the expression of INSL5.

It has been demonstrated that the composition of the intestinal microbiome is another major factor involved in INSL5 expression, as GLP-1 and INSL5 are upregulated in GF mice (Lee et al., 2016). The intestinal microbiome contains several enzymes which break down plant polysaccharides including resistant starch, pectin, and xylan (Gill et al., 2006). The gut microbiome converts these polysaccharides into a usable energy source for the host within the colon via the process of anaerobic fermentation, producing SCFAs (Wichmann et al., 2013, Silva et al, 2020).

1.2 Functions of INSL5

As it is a novel hormone, researchers are still looking for the functions of INSL5, and several hypotheses have been put forward (Hechter et al., 2022). Grosse et al. (2014) was one of the first papers to propose a function for INSL5, suggesting that it may function as an orexigenic hormone.

1.2.1 INSL5 as an Orexigenic Hormone

Grosse et al. (2014) reported that the levels of INSL5 in plasma were significantly higher in mice subjected to CR (60% of *ad libitum* food consumption) compared to *ad libitum* mice and high fat diet (HFD, 45% fat) fed mice. They found that INSL5 concentrations dropped after refeeding in the CR and the *ad libitum* fed mice, but not in the HFD fed mice (Grosse et al., 2014). They also reported that mice intraperitoneally injected with higher concentrations of INSL5 consumed more chow following periods of 20 and 60 minutes post-injection (Grosse et al., 2014). Additionally, they reported that INSL5 increased food consumption in wild type (WT) but not RXFP4 knockout (KO) mice (Grosse et al., 2014). They also found that RXFP4$^{-/-}$ mice had lower meal durations than WT mice following an overnight fast, and KO mice did not have the preference for HFD chow as seen in WT mice (Grosse et al., 2014).

Lewis et al. (2022) used a transgenic *Rxfp4*-Cre mouse model (murine strain engineered to express a reporter gene, in this case *Rxfp4*) to study the mechanisms by which INSL5 signaling on RXFP4 induces feeding behavior. They chemogenetically manipulated *Rxfp4*-expressing cells of the Cre-reporter mice and used designer drugs to activate the receptors (Lewis

et al., 2022). They reported expression of the Cre-reporter in the hypothalamus, indicating that murine hypothalamic neurons expressing RXFP4 regulate feeding behavior (Lewis et al., 2022). These results suggest that INSL5 plays a role in increasing food intake via RXFP4 during periods of CR, and that this function may predominantly be mediated via expression of RXFP4 in the hypothalamus. Since PYY and GLP-1 are anorexigenic, the putatively orexigenic properties of INSL5 raise questions about the co-release and co-expression of these three peptides from L-cells, as INSL5 expression in the colon may have the same orexigenic effect as INSL5 in the hypothalamus (Gribble and Reimann, 2016).

1.2.2 INSL5 and Glucose Homeostasis

Burnicka-Turek et al. (2012) reported that *Insl5*$^{-/-}$ mice suffered from reduced glucose homeostasis. They found that *Insl5*$^{-/-}$mice had significantly higher blood glucose levels following an overnight fast as measured by an oral glucose tolerance test compared to their WT counterparts, as well as an increase in hyperglycemia and glucose intolerance (Burnicka-Turek et al., 2012). They recorded a significant decrease in insulin levels in the bloodstream in *Insl5*$^{-/-}$ mice compared to WT mice, suggesting that this may be the cause of the hyperglycemia (Burnicka-Turek et al., 2012).

Lee et al. (2016) also demonstrated that *Insl5*$^{-/-}$mice suffer from reduced glucose homeostasis. They found that *Insl5*$^{-/-}$ mice experienced reduced glucose tolerance compared to WT mice, however they found no difference in systemic insulin levels between the two groups (Lee et al., 2016). They also reported that *Insl5*$^{-/-}$ mice had a higher insulin tolerance than WT mice, and theorized that *Insl5*$^{-/-}$ mice have an impaired ability to maintain glucose homeostasis following insulin injection (Lee et al., 2016). They tested pyruvate tolerance because pyruvate is an important substrate in hepatic gluconeogenesis, and found that glucose production was delayed and reduced in *Insl5*$^{-/-}$ mice (Lee et al., 2016). These results further suggest that INSL5 is involved in energy regulation, predominantly through hepatic glucose production (Lee et al., 2016).

1.2.3 INSL5 and Colonic Propulsion

RXFP4 is expressed on a subset of enteroendocrine cells (EECs) known as enterochromaffin cells (ECs), which secrete 5-hydroxy-tryptamine 5-HT, otherwise known as

serotonin (Fernando et al., 2023). Serotonin promotes colonic propulsion, and given its co-expression with RXFP4 on ECs, it has been shown that INSL5-RXFP4 signaling influences colonic propulsion (Fernando et al., 2023). Diwakarla et al. (2020) suggested that the simplified analog of INSL5, known as analog 13 (INSL5-A13), may accelerate colonic propulsion via binding to RXFP4 located on enteric neurons. They found that bead expulsion time decreased in mice treated with INSL5-A13, even with the addition of the constipation agent loperamide. They recorded an average bead expulsion time of 1018 seconds in mice given only loperamide, however for mice injected with 6 μg/kg, 20 μg/kg, and 60 μg /kg of INSL5-A13 dissolved in distilled water, average expulsion time was 424 seconds, 297 seconds, and 282 seconds respectively (Diwakarla et al., 2020). They also found that *Rxfp*$^{-/-}$ mice had an average bead expulsion time twice as long as their WT litter mates (Diwakarla et al., 2020). This lead Diwakarla et al. (2020) to propose that INSL5-A13 may be a potential treatment for constipation, since longer bead expulsion time indicates more solid stool. Thus, it has been suggested that a promising treatment for conditions including diabetes and inflammatory bowel disease (IBD) may be INSL5-A13, the structure of which is shown in Figure 1.4. (Zhang et al., 2020).

1.2.4 INSL5 and the Reproductive System

Burnicka-Turek et al. (2012) demonstrated that INSL5 plays a role in fertility in both sexes. They found that sperm counts in the epididymis of *Insl5*$^{-/-}$ mice were non-significantly lower than in WT males, as was the sperm count in the uterus of females inseminated by KO mice (Burnicka-Turek et al., 2012). Interestingly, they were not able to detect any sperm in the oviduct of females inseminated by male *Insl5*$^{-/-}$ mice, however they determined that this was because *Insl5*$^{-/-}$ mice had significantly reduced sperm motility and progressive motility, indicating that INSL5 affects sperm movement rather than (or significantly more than) sperm count (Burnicka-Turek et al., 2012). They also found that *Insl5*$^{-/-}$ females mated less regularly than WT females, and determined that this was the result of irregular estrous cycles in KO females, suggesting that INSL5 is involved in the timing of the estrous cycle (Burnicka-Turek et al., 2012). Yeganeh et al. (2017) reported results consistent with those of Burnicka-Turek et al. (2012), finding that INSL5 incubation increased human sperm motility.

Chen et al. (2022) reported that INSL5 is correlated with anti-Müllerian hormone (AMH) in humans. AMH is a polypeptide secreted by ovarian follicles which causes sexual

differentiation in males, inhibits primordial follicle recruitment, and is theorized to cause ovulation disorders via inhibiting follicle-stimulating hormone (Chen et al., 2022). AMH is an important biomarker of polycystic ovary syndrome (PCOS), which is a metabolic disorder in women that impairs fertility (Chen et al., 2022). The authors reported that women suffering from PCOS expressed significantly higher levels of both AMH and INSL5 than women without PCOS, however there was no significant relationship between AMH and INSL5 in the control cohort (Chen et al., 2022). These results suggest that INSL5 may be a potential marker of reproductive diseases such as PCOS (Chen et al., 2022).

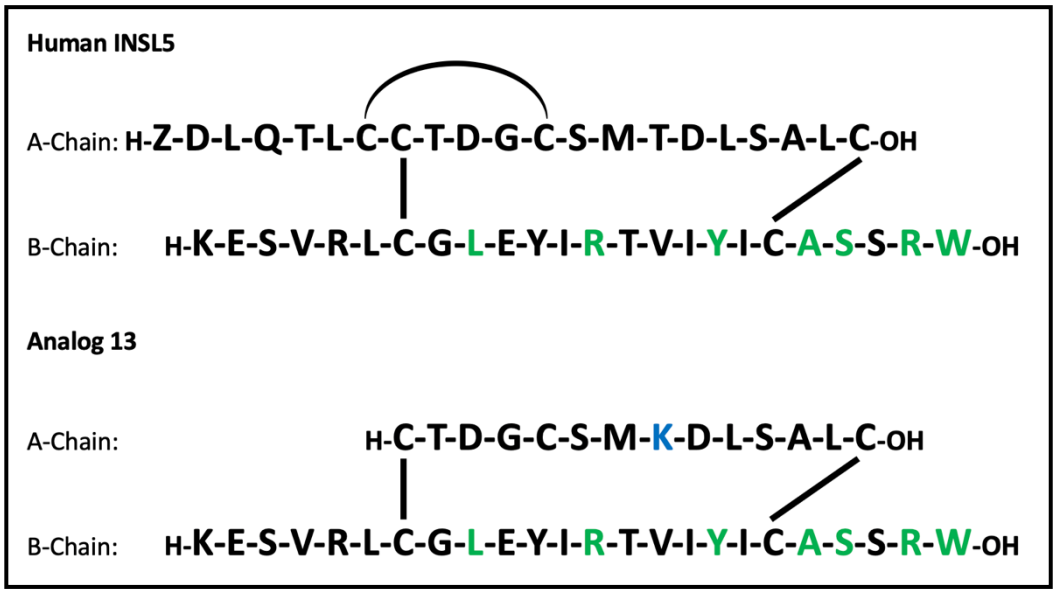

Figure 1.4. The sequential differences between human INSL5 and analog 13. Important residues are shown in green, while mutated residues are blue. Disulfide bonds are shown as black lines or arches. Generated with Microsoft PowerPoint.

1.2.5 INSL5 and Cancer

Like any cell, cancer cells need energy to grow, sustain themselves, and reproduce. To meet the demands of unrestricted growth found in cancer cells, they metabolize vast amounts of glucose and utilize most of their energy in the process of aerobic glycolysis (Li et al., 2020). The shift to aerobic glycolysis allows cancer cells to break down glucose into macromolecules required for unrestricted cell growth in a more efficient manner (Li et al., 2020). It has been long known that genes from the insulin superfamily are associated with tumors, promoting the survival, growth, migration, and invasion of cancer cells (Thanasupawat et al., 2013). Li et al. (2020) analyzed plasma and tissue samples from patients suffering from nasopharyngeal

carcinoma (NPC) to determine the metabolic role that INSL5 plays in NPC progression and proliferation. They reported that INSL5 was overexpressed in plasma and tissue samples from NPC patients, and that INSL5 enhances glycolysis in tumor cells, playing a significant role in cancer progression and proliferation (Li et al., 2020).

The first evidence of INSL5 and RXFP4 in human carcinoid neuroendocrine tumors (NETs, also known as carcinoid cells) in the intestine was reported by Mashima et al. (2013), who suggested that INSL5-RXFP4 autocrine/paracrine signaling may be involved in the growth of tumors. Thanasupawat et al. (2013). corroborated these findings, reporting that INSL5 and synaptophysin (a known entero-/neuroendocrine intestinal cancer marker) were co-expressed in NETs (Thanasupawat et al., 2013). They also found that INSL5 and RXFP4 are co-expressed in carcinoid cells, suggesting that there may be autocrine/paracrine INSL5-RXFP4 signaling within NETs (Thanasupawat et al., 2013). These results suggest that INSL5 is a marker of cancer in the human intestine.

1.2.6 INSL5 and the Immune System

Many hypothesized functions of INSL5 have been put forth, including its role as an orexigenic hormone (Grosse et al., 2014), a mediator of glucose homeostasis (Burnicka-Turek et al., 2012), in colonic propulsion, in male and female fertility (Diwakarla et al., 2020), and as a marker for cancer (Figure 1.5.) (Thanasupawat et al., 2013). Our lab is investigating the potential immune effects of INSL5. Vahkal et al. (2021) found that RXFP4 is expressed on all murine immune organs and some innate immune cells, particularly bone-marrow derived macrophages and most highly in splenic dendritic cells (sDCs). Murine *in vivo* i.p. injection of INSL5 altered levels of cytokines exerting homeostatic effects on macrophage proliferation (Vahkal et al., 2021). Mouse macrophage cell lines incubated with INSL5 exhibited impeded cell growth and reductions in pro-inflammatory cytokines (Vahkal et al., 2021). They showed changes to 27 cytokines following *in vivo* injection of INSL5 mice, and found significant differences in seven cytokines between 6 and 48 hours after injection (Vahkal et al., 2021). They also reported that pre-incubation of ANA-1 cells, a murine macrophage cell line, in INSL5 for 12, 24 or 36 hours prior to addition of lipopolysaccharide (LPS), lead to increasing downregulation of pro-inflammatory cytokines (Vahkal et al., 2021). These results suggest that INSL5-RXFP4 may play roles in gut immune homeostasis, particularly in a mouse model. In this thesis, I further

explore this hypothesis using primary cell lines cultured from healthy and inflamed murine spleens.

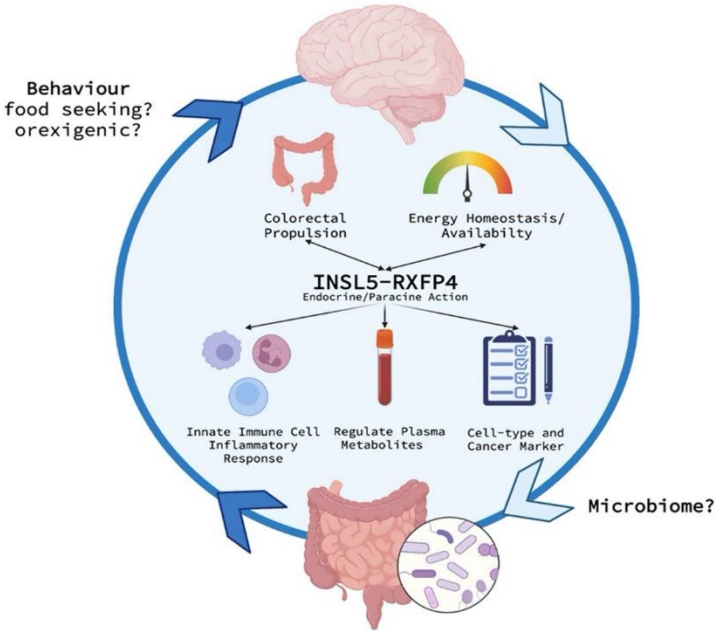

Figure 1.5. The many potential roles of INSL5, including regulation of the immune system. Research suggests it may have many functions, including regulating energy homeostasis, colonic propulsion, glucose homeostasis, and inflammatory responses (Figure from Hechter et al., 2022).

1.3 Inflammatory Bowel Disease

Immune regulation enables organisms to defend themselves against pathogens while preventing unnecessary immune responses against harmless antigens, thereby reducing harm to the organism (Li et al., 2012). An imbalance of the immune system can result in a reduced ability to fight infections, or may induce autoimmunity (Li et al., 2012). IBD is a type of chronic and recurrent autoimmune inflammatory disease which affects the GI tract (Sann et al., 2013). The prevalence of IBD worldwide is around 396/100,000 (Li et al., 2012). There are two main IBD phenotypes (Figure 1.6.), known as Crohn's disease (CD), which is more common in females, and Ulcerative colitis (UC), which occurs more frequently in males (Li et al., 2012).

The cause of IBD is still unknown, however the pathogenesis of IBD is associated with diverse genetic and environmental factors that result in an excessive immune response against the intestinal microbiota (McDaniel et al., 2016, Skok et al., 2021). IBD is characterized by a severe dysregulation of pro and anti-inflammatory cytokines and signalling pathways in the intestines (McDaniel et al., 2016). This diseased state disrupts the process of resolving inflammation in the gut and contributes to disorders and diseases in the GI system and possibly other organ systems (Skok et al., 2021). For example, chronic inflammation is linked to an

increased risk of cancer, and the chances of developing colorectal cancer (CRC) increases 0.5% to 1% with every passing year, for eight to ten years following diagnosis of IBD (Li et al., 2012). IBD is typically diagnosed by measuring levels of C-reactive protein (CRP), however low or normal CRP levels have been reported in a significant number of patients with IBD (Peyrin-Biroulet et al., 2016). Other biomarkers include fecal calprotectin and fecal neopterin, and for CD specifically, fecal lactoferrin (Peyrin-Biroulet et al., 2016). IBD contributes to only 1 to 2% of all CRC cases, however IBD-related CRC accounts for 15% of all deaths in people suffering from IBD (Li et al., 2012).

1.3.1 Crohn's Disease

Most CD patients present symptoms between 20 and 60 years of age, however symptoms can arise at any point in life (Jewell 2007). Globally, the incidence rate of CD ranges from 0.1 to 16/100,000 (Li et al., 2012). It is common in Europe and North America, with an approximate incidence rate of 6-10/100,000 per year, and a prevalence of 80-100/100,000 (Jewell 2007). It is not highly diagnosed in the developing world and it is uncommon in Japan, however the incidence rate in both Japan and the West is gradually increasing (Jewell 2007). CD is also becoming more common in Latin America, with prevalence rates around 24/100,000 in Brazil and 15/100,000 in Argentina (Avellaneda et al., 2023). CD is characterized by a patchy, transmural distribution of inflammation (Jewell 2007). It can affect any part of the gastro-intestinal tract from the mouth to the anus, however it most commonly affects the terminal ileum in 35% of patients, the ileocecal region in 40% of patients, the colon in 20% of patients, and the rectum is not usually affected (Jewell 2007). CD frequently flares up in patients, often resulting in further diseased states such as fibrotic stenosis or fistulae (Avellaneda et al., 2023). Monozygotic twins have a pairwise concordance of around 33.3 to 50% and a proband concordance of around 58.3 to 62.5% while dizygotic twins have a pairwise concordance of around 0 to 9.9% and a proband concordance of around 0 to 3.8% (Halfvarson et al., 2003). These data show that CD is caused by a combination of both genetic and environmental factors (Halfvarson et al., 2003).

1.3.2 Ulcerative Colitis

The global incidence rate of UC is between 0.5 and 24.5/100,000 and is therefore more common than CD (Li et al., 2012). Much like CD, UC is common in Europe and North America, with an approximate incidence rate of 6-20/100,000 per year, and a prevalence of 20-250/100,000 (Loftus 2004). Also like CD, UC is less common in Asia, Africa, and Latin America, however the ethnic gaps are narrowing (Loftus 2004). UC affects the colon and rectum (Sands et al., 2008). It is characterized by the presence of continuous and evenly distributed inflammation in the lamina propria, also known as the basement membrane, of the epithelial cells lining the intestinal tract (Li et al., 2012), and by the disruption of epithelial crypts leading to the generation of crypt abscesses (Li et al., 2012). Other symptoms of UC include diarrhea and rectal bleeding (Sands et al., 2008). During active UC, macrophages and granulocytes migrate to the gastrointestinal mucosa where they release proteases and reactive oxygen species which damage mucosal tissue (Sands et al., 2018). Monozygotic twins have a pairwise concordance of around 6.3 to 18.8% and a proband concordance of around 6.3 to 18.8% while dizygotic twins have both a pairwise and proband concordance of around 0 to 4.5% (Halfvarson et al., 2003). These data show that UC is less heritable than CD, and is therefore more highly influenced by environmental factors (Halfvarson et al., 2003).

Skok et al. (2021) performed a study to analyze the expression of cytokines in both UC and CD in humans. They obtained UC and CD patient microarray data from the National Center of Biotechnology Information. They selected only active UC samples for their analysis, however no such criteria was made for CD samples (Skok et al., 2021). Combining a discovery *in silico* bioinformatic analyses of publicly available microarray data followed by endoscopic biopsies and RT-qPCR to compare expression of the candidate genes in UC and CD, Skok et al. (2021) identified INSL5 as a potential biomarker differentiating UC vs CD. Their discovery bioinformatics analysis showed that INSL5 was down-regulated in CD and up-regulated in UC compared to a normal condition (Skok et al., 2021). Their experimental results showed that *INSL5* RNA was downregulated compared to normal in both conditions, but to a greater extent in CD (Skok et al., 2021). Despite these contrasting results, they were consistent with previous literature showing that INSL5 is expressed significantly more in UC than in CD (Skok et al., 2021). The author suggested that INSL5 is a potential marker to distinguish between the two

diseases (Skok et al., 2021). If INSL5 reduces pro-inflammatory cytokine levels, it may also be a viable treatment for IBD.

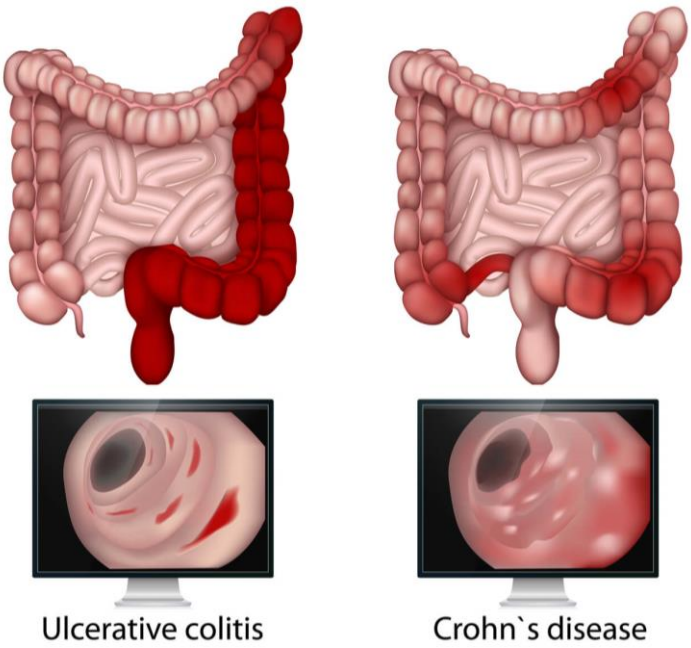

Figure 1.6. The distribution of inflammation in ulcerative colitis and Crohn's disease. UC affects the distal colon and rectum in a continuous fashion, while CD affects various parts of the gut in a patchy formation. Image source: http://sanmateorheumatology.com/condition/inflammatory-bowel-disease/

1.3.3 Treatments for IBD

Since intense inflammation is the primary symptom of IBD, the primary treatment for the disease includes anti-inflammatory and immunosuppressive pharmaceuticals (McDaniel et al., 2016). Much of the research into IBD over the last few decades has had the goal of identifying and characterizing immune signaling pathways which may be viable therapeutic targets (McDaniel et al., 2016). Sann et al. (2013) tested the efficiency of various drugs as treatments for dextran sodium sulfate (DSS) induced colitis in mice. They found that mesalazine was mostly inactive, budesonide worsened the disease, Cyclosporine A reduced DSS-induced weight loss but did not significantly reduce inflammation, 6-thioguanine reduced colitis symptoms, and olsalazine did not reduce most symptoms of colitis, other than myeloperoxidas activity and serum amyloid A levels (Sann et al., 2013).

It is clear that most treatments for IBD have proven inefficient. Our lab has studied the theorized functions of INSL5, with specific focus on its potential role in the immune system (Vahkal et al., 2021). We hypothesize that INSL5 exerts anti-inflammatory effects on immune cells, and therefore it may reduce the symptoms associated with UC, such as diarrhea, given the

involvement of INSL5 in colonic propulsion. If we are correct, then it is possible that future research may find that analogs such as INSL5-A13 are suitable as a treatment for IBD. Further research must also be done to determine which pathways RXFP4 acts on to carry out its proposed anti-inflammatory effects.

1.4 Pathways Associated with RXFP4

Several studies have examined the downstream effects of INSL5 stimulation of the RXFP4 receptor. The INSL5-RXFP4 axis activates extracellular signal-regulated protein kinases 1 and 2 (ERK1/2), p38 mitogen-activated protein kinases (p38MAPK), protein kinase B (PKB or Akt), and ribosomal protein S6 (S6RP) (Ang et al., 2017b). Mammalian target of rapamycin (mTOR) is a serine/threonine kinase in the P13k-related kinase family, and is primarily involved in cell growth, survival, and proliferation, as well as glucose metabolism (Xu et al., 2020). Ang et al. (2017a) found that the Akt-mTOR pathway activates S6RP (a component of the 40S ribosomal subunit) in RXFP4-expressing Chinese hamster ovary cells. They reported that stimulation of the RXFP4 receptors resulted in cellular growth and proliferation (Ang et al., 2017a). It is unknown exactly which downstream pathways RXFP4 may use to exert its anti-inflammatory effects.

1.4.1 MAPK Pathways

Among the most common transcription factors responsible for signal transduction are the MAPKs (Hecquet et al., 2002). MAPKs are required to carry out many cellular functions, such as development, proliferation, differentiation, apoptosis, and inflammatory responses (Zhang and Liu, 2002). The best characterized MAPKs are ERK1 and ERK2 (Hecquet et al., 2002). ERK1 and 2 are activated via stimulation of numerous GPCRs, receptor tyrosine kinases, and ion channels, and they play an important role in many cell functions including survival, proliferation, differentiation, and apoptosis (Wortzel and Seger, 2011). It is well documented that ERK1/2 is activated through GPCRs, however Belgi et al. (2013b) were the first to show that the ERK pathway is activated via RXFP4.

Another well studied MAPK transcription factor activated by RXFP4 in mammalian cells is p38MAPK (Zhang and Liu, 2002). The p38MAPK pathways are initiated by cellular stress factors including ultraviolet radiation, LPS, pro-inflammatory cytokines including IL-1 and

TNF-α, and protein synthesis inhibitors (Zhang and Liu, 2002). They play an important role in cellular proliferation, development, inflammation, apoptosis, and stress response (Zhang and Liu, 2002). The isoforms of p38, known as p38α, p38β, p38γ, and p38δ have been identified, and p38δ is required for interferon (IFN) signaling (Zhang and Liu, 2002). IFN stimulation of p38MAKP results in the phosphorylation of signal transducer and activator of transcription 1 (STAT1) (Zhang and Liu, 2002).

1.4.2 JAK/STAT

The STAT family consists of seven proteins (STAT1-4, STAT5A/B, and STAT6), and play significant roles in numerous important biological processes (Awasthi et al., 2021). Tyrosine phosphorylation occurs on STAT proteins via receptor activation, usually downstream of Janus Kinase (JAK) signalling (Awasthi et al., 2021). From 1989 to 1994, four JAK proteins were discovered, known as JAK1-3 and tyrosine kinase 2 (TYK2) (Hu et al., 2021). Velzquez et al. (1992) discovered the connection between JAK and STAT proteins after reporting that TYK2 is an important component of the IFN-α/β pathway. When cytokines bind to the JAK receptor, the JAK protein is activated (Li et al., 2012). The JAK protein now phosphorylates tyrosine residues on the JAK receptor, which binds STAT proteins (Li et al., 2012). JAK then phosphorylates to STATs, causing them to dimerize and migrate to the nucleus (Li et al., 2012). STAT-dimers bind DNA inside the nucleus and recruit cofactors to begin transcribing *STAT*-target genes (Li et al., 2012). The primary function of STAT3 in intestinal epithelial cells (IECs) during inflammation is to induce proliferation during healing, as IL-6 and IL-22 have both been found increase IEC reconstruction and proliferation via STAT3 signaling (Li et al., 2012). JAK/STAT signal transduction is inhibited by suppressors of cytokine signaling (SOCS) proteins (Li et al., 2012). Overexpression of SOCS3 has been reported to inhibit wound healing while increasing inflammation via inhibition of STAT3 (Li et al., 2012). Research from our lab has demonstrated that INSL5 and RXFP4 are regulated by STAT proteins, particularly STAT1, STAT4, and STAT5a/5b via the JAK/STAT pathway (Vahkal et al., 2021).

1.4.3 SOCS3

Another major regulatory factor involved in IBD immunogenesis is SOCS3 (Li et al., 2012). Unlike the above pathways, the downstream effects of RXFP4 on SOCS3 have not been

studied. There are eight proteins in the SOCS gene family, including cytokine-induced SH2 containing protein and SOCS1 to SOCS7 (Li et al., 2012). Every SOCS family member contains a central Scr Homology 2 (SH2) domain, which allows docking of phosphotyrosine residues on other peptides, such as STAT proteins (Li et al., 2012). The SOCS box is another region conserved in all SOCS proteins, which is a motif 40 amino-acids in length which mediates ubiquitination (Yoshimura et al., 2012). SOCS1 and 3 contain a kinase inhibitor region, which is necessary to inhibit cytokine signals, to inhibit JAK tyrosine kinases (Yoshimura et al., 2012). SOCS3 is upregulated following stimulation by pro and anti-inflammatory cytokines such as IL-6, IL-10, IL-12, TNF-α and IFN-γ, as well as by LPS (Miyanaka et al., 2007, Li et al., 2012). While SOCS3 inhibits STAT4, it primarily binds to STAT3 receptors (Yoshimura et al., 2012). STAT3 is associated with the survival and proliferation of CRC-tumor cells (Li et al., 2012). SOCS3 regulates STAT3 in an inflammatory environment, suggesting that SOCS3 has anti-tumor properties (Li et al., 2012). SOCS3 inhibits IL-6 but not IL-10, indicating that it restricts pro-inflammatory STAT3 activation but not anti-inflammatory STAT3 activation (Yoshimura et al., 2012). Egwuagu et al. (2002) reported high levels of SOCS3 mRNA and protein in $CD4^+$ T Th2 cells, and very little SOCS3 expression in naïve Th cells and Th1 cells. They suggest that SOCS3 may play a role in Th2 cell differentiation, and is therefore a Th lineage marker which can be used as a therapeutic target for immune modulation treatment (Egwuagu et al., 2002).

Suzuki et al. (2001) found that SOCS3 expression is increased in a DSS mouse model, where it was reported to reduce inflammation. They found that SOCS3 expression increased after DSS treatment, and remained highly expressed for two weeks (Suzuki et al., 2001). Miyanaka et al. (2007) analysed the *SOCS3* mRNA levels of eighteen UC patients in remission, over a twelve-month period. They found that patients with low *SOCS3* levels remained in remission for the entire twelve months, while patients with high *SOCS3* levels had lower remission lengths, suggesting that SOCS3 may be useful in determining the prognosis of UC remissions (Miyanaka et al., 2007). Interestingly, however, Li et al. (2012) recommended reducing SOCS3 as a treatment for IBD, given its correlation with cytokines secreted by M1 macrophages.

1.5 The Immune System

The innate immune system carries out immediate and general bodily defence, while the adaptive immune system is modified to attack specific antigens (Iwasaki and Medzhitov, 2015).

Leukocytes (or white blood cells) are the best known immune cell type in the body. They originate from hematopoietic stem cells (HSCs), which differentiate into various cell types (including leukocytes) in response to external stimuli (Geissmann et al., 2010). One group of leukocyte cell sub-types are the lymphocytes, which constitute the adaptive immune system. There are two types of lymphocytes, B-cells and T-cells. Naïve B-cells originate and develop in the bone marrow, and when they mature, they secrete immunoglobins (antibodies) to neutralize pathogens (Hoehn et al., 2022). T-cells are further divided into natural killer T-cells (NKT), $CD8^+$ T-cells (otherwise known as cytotoxic T-cells, or CTLs) and $CD4^+$ T-cells (otherwise known as Th cells, including Th1, Th2, and Th17) (Iwasaki and Medzhitov, 2015). All naïve T-cells originate in bone marrow and develop in the thymus (Iwasaki and Medzhitov, 2015). NKTs and CTLs function to directly kill pathogens and destroy cancerous or infected cells (Iwasaki and Medzhitov, 2015). Th cells upregulate the secretion of cytokines, which cause other immune cells to carry out a pro or anti-inflammatory response (Seong-Min et al., 2021). Th1 cells facilitate type 1 immune responses which attack intracellular microbes (Walker and McKenzie, 2018). Th2 cells facilitate type 2 immune responses which attack parasites and organize tissue repair, however they are also known to contribute to chronic inflammatory diseases (Walker and McKenzie, 2018). Th17 cells are characterized by the release of the pro-inflammatory cytokine IL-17, and facilitate immune responses against bacteria and fungi which Th1 and Th2 cells are not equipped to deal with (Tesmer et al., 2008).

Another group of leukocyte cell sub-types are the mononuclear phagocytes, innate immune cells which include monocytes, macrophages, and DCs (Geissmann et al., 2010). Monocytes are immune effector cells which fight infections by secreting inflammatory cytokines, releasing toxic molecules, and phagocytosing pathogens (Geissmann et al., 2010). Monocytes migrate to tissues and differentiate into various kinds of inflammatory macrophages and DCs during periods of inflammation (Geissmann et al., 2010). While macrophages and DCs often originate from the same progenitor cells and both serve sentinel roles, they are distinct varieties of immune cell (Weisheit et al., 2015). Macrophages function as resident effector cells of the innate immune system, while DCs migrate to activate the adaptive immune system, specifically T-lymphocytes (Weisheit et al., 2015).

1.5.1 Macrophages

Macrophages were discovered by Ilya Metchnikoff in the late 19th century (Epelman et al., 2014). Van Furth and Cohn (1968) suggested that circulating blood monocytes are the precursor cell type for all tissue macrophages, however evidence has been piling up over the decades that this is untrue (Sawyer et al., 1982). Several resident tissue macrophage types originate in embryonic development and are present in adulthood without being derived from blood monocytes (Epelman et al., 2014). The complexity of tissue macrophages is not fully captured in the dichotomy between monocyte-derived macrophages and embryonically derived macrophages, and macrophages of different origins have been found to co-exist and work together to perform specialized functions (Epelman et al., 2014). Macrophages are professional phagocytes which regulate tissue homeostasis by phagocytosing infected or damaged cells, releasing toxic metabolites, and upregulating proinflammatory cytokines to activate other immune cells (Weisheit et al., 2015).

Naïve macrophages (M0) can be polarized towards either the classical (Type 1, M1) or alternative (Type 2, M2) phenotype, depending on which stimulants they are exposed to (Chávez-Galán et al., 2015, Mohamed et al., 2021). The M1 phenotype is associated with a pro-inflammatory response which is necessary to fight infections, however in excess it can be harmful to the body (Bohlson et al., 2014). The M2 phenotype is associated with the resolving and healing response post-infection, and is therefore considered to be anti-inflammatory, however M2 macrophages are also known to combat fungal and parasitic infections (Atri et al., 2018). Major factors which stimulate M0 macrophages to the M1 phenotype include complement proteins C3a, C5a, and C5b-9, as well as pathogen-associated molecular patterns (PAMPS) (Bohlson et al., 2014). LPS is a major PAMP which is commonly used to induce inflammatory and stress responses (Bertani and Ruiz, 2018). Stimulants for an M2 phenotype include IL-4 and complement proteins C1q and C3b (Bohlson et al., 2014).

Recent research into macrophages has shed light into the complexities of macrophage characterization, as mixed M1/M2 phenotypes are expressed in various diseased states, and the lines between M1 and M2 macrophages are blurred and phenotypes have been known to overlap (Mohamed et al., 2021, Bhattacharya and Aggarwal 2019). M1 and M2 macrophages secrete various cytokines and other markers which are useful in distinguishing the two phenotypes, as seen in Figure 1.7. (Bohlson et al., 2014). Phenotypic characteristics associated with M1

macrophages include IL-1β, TNF-α, TLR2, TLR4, major histocompatibility complex class II (MHC-II), and surface molecules CD80 and CD86 (Mohamed et al., 2021). Phenotypic characteristics associated with M2 macrophages include surface proteins CD163, CD204, and CD206 (Mohamed et al., 2021). One reason why there are fewer reliable markers for M2 macrophages is because M2 macrophages can undergo further differentiation into M2a, M2b, M2c, and M2d macrophages (Bhattacharya and Aggarwal 2019).

1.5.2 Dendritic Cells

DCs were first described by Steinman and Cohn in 1973. They are the primary antigen presenting cell type of the immune system (Lewis et al., 2011), and are the bridge between innate and adaptive immunity (Iwasaki and Medzhitov, 2015). DCs are antigen presenting cells which phagocytose and then present antigenic peptides on MHC-II proteins to T-cells for T-cell activation (Seong-Min et al., 2021). Immature DCs use pattern recognition receptors including

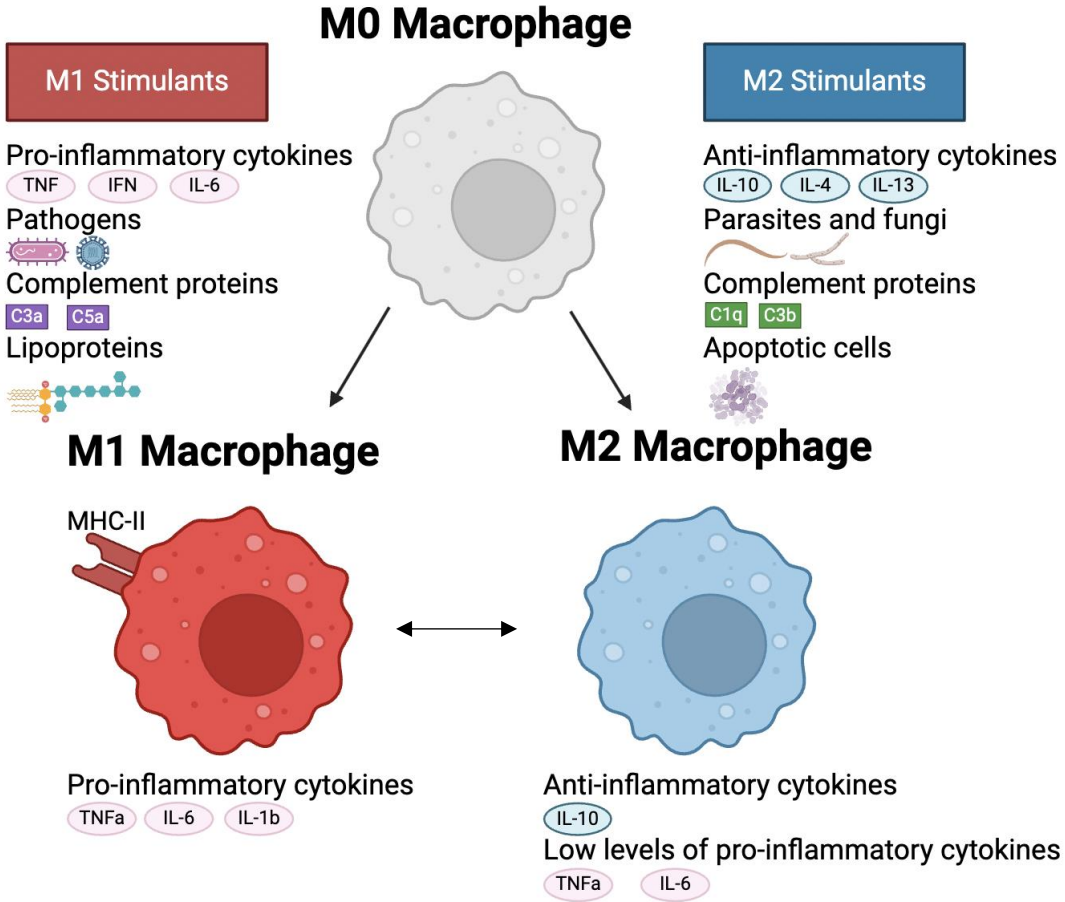

Figure 1.7. Macrophages differentiate into M1 or M2 phenotype based on exposure to various stimulants. They can be distinguished based on cytokine profile.

TLRs to recognize PAMPS and danger-associated molecular patterns (Wei et al., 2017, Weisheit et al., 2015). Following antigen phagocytosis, co-stimulatory molecules are upregulated, resulting in the increased expression of pro-inflammatory cytokines (Seong-Min et al., 2021). DCs travel to the lymph nodes to present antigens to specific T-cells, resulting in immunogenic T-cell activation (Weisheit et al., 2015). T-cell clones begin proliferating rapidly following stimulation by DCs, and then enter the circulation and migrate to the infected tissue to combat the infection (Weisheit et al., 2015). Other tissue-resident DCs secrete cytokines to regulate the activated T-cells migrating to the local tissues (Weisheit et al., 2015).

One of the main types of DCs is the myeloid dendritic cell (mDC, also known as conventional DC) (Seong-Min et al., 2021). There are two types of murine mDCs, the $CD8\alpha^+$ and $CD8\alpha^-$ variants (Seong-Min et al., 2021). In humans, BDCA3 is equivalent to $CD8\alpha^+$, while BDCA1 is equivalent to $CD8\alpha^-$ (Seong-Min et al., 2021). $CD8\alpha^+$ DCs phagocytose antigens and present them on MHC-I molecules to $CD8^+$ T-cells, causing them to differentiate into CTLs which target and kill infected or cancerous cells expressing cytosolic antigens (Seong-Min et al., 2021). $CD8\alpha^-$ cells phagocytose antigens and present them on MHC II molecules to $CD4^+$ T-cells, causing them to differentiate into Th cells, which upregulate the production of cytokines, activating other immune cells (Seong-Min et al., 2021).

Another important type of DCs are plasmacytoid dendritic cells (pDCs) (Ye et al., 2020). pDCs differentiate from myeloid and lymphoid precursor cells in the bone marrow before migrating to the bloodstream due to chemokine signaling (Ye et al., 2020). pDCs only make up 0.1 to 0.5% of human peripheral blood mononuclear cells, however upon activation, they account for most IFN-I released into the blood stream during viral infection in both humans and mice (Ye et al., 2020). Research has shown that pDCs are active in the intestinal mucosa of IBD patients, however their exact role in the disease is unclear (Ye et al., 2020).

1.5.3 The Spleen

Doctors in the 1960s discovered that splenectomy (removal of the spleen) increases the chances of developing sudden onset sepsis for two years post-operation (Muller and Toghill, 1995). It has since been found that patients are at risk of post-splenectomy sepsis for upwards of 30 years following splenectomy, and that as many as 2% of patients may be at risk (Muller and

Toghill, 1995). In contrast, only around 0.004% of individuals with an intact spleen share this risk (Muller and Toghill, 1995). In short, while the spleen is often overlooked, it is an important organ, and as such, asplenia often results in morbidity and mortality, as does dysfunction of the spleen resulting in reduced splenic function, known as hyposplenism (Lenti et al., 2022).

The spleen is an important source of macrophages and DCs (Mebius and Kraal, 2005). The spleen is an immune organ which functions to remove old erythrocytes from circulation, and removes cellular debris and blood-borne pathogens (Mebius and Kraal, 2005). It is one of the most ancient organs in the vertebrate immune system, first evolving in the infraphylum gnathostomata (Rosado et al., 2018). The spleen is important for immune homeostasis, as it is a secondary lymphoid organ involved in both innate and adaptive immune responses (Mebius and Kraal, 2005). Gualdrón-López et al. (2021) carried out multiparameter flow cytometry analysis on the human spleen, and found that it is comprised primarily of erythrocytes (70%), while neutrophils, $CD4^+$ T-cells, $CD8^+$ T-cells, and B-cells each comprised 1 to 5% of live cells, and monocytes, DCs, macrophages, NK cells, NKT cells, HSCs, and reticulocytes each comprised less than 1% of live splenocytes. The white pulp of the spleen is made up of lymphoid tissue surrounding the small arterial branches of the spleen, and is a site of activation for the adaptive immune system (Mebius and Kraal, 2005). The red pulp is made up of the large blood-filled sinuses which are found in the marginal zone (MZ), and is responsible for iron metabolism and erythrocyte phagocytosis (Mebius and Kraal, 2005, Andryukhova et al., 2022). The spleen also contains a marginal zone found between the white and red pulp which is responsible for both innate and adaptive immunity (Mebius and Kraal, 2005).

The spleen produces various sub-populations of macrophages in the red and white pulp (Fujiyama et al., 2018). The macrophages produced in the red pulp work to clear defective blood cells, recycle and metabolize iron, and clear bacteria from the bloodstream. (Fujiyama et al., 2018, Mebius and Kraal, 2005). The macrophages of the red pulp uptake erythrocytes, degrading the red blood cells and haemoglobin within (Mebius and Kraal, 2005). Bacterial pathogens compete with the host for iron in the serum and the tissue by secreting siderophores, which bind to iron and transport it into the bacteria (Mebius and Kraal, 2005). When bacteria encounter TLRs on macrophages, the macrophages secrete molecules including lipocalin-2, which binds siderophores, inhibiting bacterial growth (Mebius and Kraal, 2005). In addition to macrophages, the red pulp is also rich in B-cells (Mebius and Kraal, 2005). Plasmablasts (immature B-cells)

migrate to the red pulp following the upregulation of the chemokine receptor CXC-chemokine receptor 4 (CXCR4) which binds chemokine CXC-chemokine ligand 12 (CXCL12) in the red pulp (Mebius and Kraal, 2005). While this occurs, chemokine receptors in the red pulp which bind to homeostatic chemokines are downregulated (Mebius and Kraal, 2005). Plasmablasts in the red pulp require $CD11c^{hi}$ DCs to survive and become plasma cells (Mebius and Kraal, 2005).

The macrophages produced in the white pulp work to clear invasive antigens (Fujiyama et al., 2018). The white pulp resembles the structure of a lymph node, with T and B-cell compartments surrounding the arterial vessels (Mebius and Kraal, 2005). The T-cell zone is the area in which DCs and B-cells interact with T-cells, while the B-cell follicles are the areas in which activated B-cells clonally expand (Mebius and Kraal, 2005). CC-chemokine ligand 19 (CCL19) and CCL21 are responsible for the migration of DCs and T-cells to the T-cell zones, while CXCL13 signalling attracts B-cells to the B-cell follicles (Mebius and Kraal, 2005). These chemokines are upregulated by lymphotoxin-$\alpha_1\beta_2$ and TNF (Mebius and Kraal, 2005).

1.5.4 The Spleen-Gut Axis

While it may not be immediately obvious, the spleen and the gut are intimately linked. For example, the microbiota of the gut is essential for the development of secondary lymphoid structures of the spleen during the first two weeks of life (Rosado et al., 2018). At birth, the spleen is not fully developed, as it is missing the MZ and the follicular dendritic cell (FDC) network, and contains very few mature naïve lymphocytes (Rosado et al., 2018). However, the spleen at birth does contain B-cell precursors from the fetal liver, as well as innate lymphoid cells and immature DCs (Rosado et al., 2018). Three days after birth, bone marrow-derived B-cells migrate to the spleen and initiate the development of the FDC network (Rosado et al., 2018). Therefore, the spleen at birth is not able to supply the gut with precursor cells to produce secretory immunoglobin A (SIgA), as it does later in development (Rosado et al., 2018). Rosado et al. (2018) studied the impact of the gut microbiota on immunocompetent mice and found that SIgA in maternal milk increases the diversity of colonizing species in the neonatal gut microbiota. They reported that mice deprived of SIgA in milk did not develop a proper FDC network or primary splenic follicles, which led to an impaired T-cell response (Rosado et al., 2018).

The spleen-gut axis plays a vital role in regulating systemic inflammation, primarily through the vagus nerve (Zhang et al., 2021). The vagus nerve is the largest cranial nerve found in the body, and parasympathetically innervates the GI tract (Browning et al., 2017). In humans, it innervates 2/3 of the transverse colon, while the pelvic nerves innervate the remaining 1/3 of the transverse colon, the descending colon, and the rectum (Browning et al., 2017). The vagus nerve plays a role in gut physiology, as well as the immune system, the endocrine system, the respiratory system, and the cardiovascular system (Browning et al., 2017). It is widely recognized that the vagus nerve modulates appetite, obesity, and inflammation, and is activated by the gut microbiota under conditions of intestinal inflammation (Browning et al., 2017). Research has shown that stimulation of the vagus nerve by LPS-stimulated macrophages reduces the production of pro-inflammatory cytokines, such as IL-1β, IL-6, IL-18, and TNF, but not the anti-inflammatory cytokine IL-10 (Borovikova et al., 2000).

Berthoud et al. (1993) detected vagal nerves in the rat celiac ganglion while performing neuronal tracing studies, suggesting that the vagus nerve modulates splenic function. The primary vagal neurotransmitter is acetylcholine, which binds to the α7 subtype of nicotinic acetylcholine receptor (α7nAChR) on macrophages, primarily in the spleen (Berthoud et al., 1993, Browning et al., 2017). Interestingly, the activation of splenic nerves decreases splenic cytokine release independently of α7nAChR, suggesting that α7nAChR$^+$ macrophages migrate to the spleen from the gut during periods of inflammation (Browning et al., 2017). Splenic DCs then migrate to the gut to activate CD4$^+$ T-cells, eliciting an immune response (Lewis et al., 2011). It has been reported by McDermott et al. (2006) that CD4$^+$ T-cells regulate certain EEC types during intestinal inflammation, suppressing food intake via secretion of IL-4 and IL-13.

1.5.5 Hyposplenism and GI Disorders

As a result of the association between the spleen and the gut, hyposplenism can result in GI disorders, such as inflammation (Browning et al., 2017). In one such example, the spleen and gut are linked via the genes *RPSA*, which is linked to asplenia, and *NKX2-3*, which is important in the development of the murine spleen and gut vasculature (Kerkhofs et al., 2019). Kerkhofs et al. (2019) found that mutations on both genes results in idiopathic intestinal varices (dilated blood vessels) in the gut. Another example is anxiety. The drug reserpine (used to treat high blood pressure), associated with reduced acetylcholine levels in the gut, was reported by

Browning et al. (2017) to increases the severity of cases of DSS-induced colitis, however when given the antidepressant desipramine, the effects were reversed via the vagus nerve. Vagotomy (a procedure in which vagus nerve signalling is cut off) had no effect on T-cell transfer-induced colitis, nor did it affect colitis in macrophage-deficient mice, however an increase in the severity of colitis was seen in macrophage-deficient mice with macrophages transferred from vagotomised mice (Browning et al., 2017). Additionally, hyposplenism is involved with GI disorders including Ulcerative colitis, Crohn's disease, Coeliac disease, dermatitis herpetiformis, tropical sprue, Whipple's disease, idiopathic ulcerative enteritis, chronic ulcerative jejunitis, and intestinal lymphangiectasia (Foster and Losowsky 1987, Muller and Toghill, 1995).

There are numerous causes of hyposplenism, including GI diseases, liver diseases, oncohaematological diseases, immune-mediated diseases and immune deficiencies, infectious diseases, latrogenic causes, and splenic vascular alterations (Lenti et al., 2022). Due to the immunological communication between the digestive system via the hepatic portal system, GI diseases are commonly associated with hyposplenism as a result of the (Lenti et al., 2022). It is of note that most GI diseases (including IDB) can both be caused by hyposplenism or result in hyposplenism. Mice with DSS-induced colitis have been found to have hyperinflammed spleens. Hechter at al. (in preparation) found that mice given 2% DSS in their drinking water for seven days have significantly more massive spleens than control mice, as seen in Figure 1.8.

Many techniques have been developed to diagnose hyposplenism, such as taking a blood smear to observe the presence of Howell-Jolly bodies (basophilic nuclear debris) in erythrocytes, in addition to hypochromic erythrocytes (cells with low hemoglobin concentration) (Kirkineska et al., 2014). These conditions indicate the presence of splenic dysfunction as the spleen is not adequately filtering out anomalous erythrocytes. Some erythrocytes may be afflicted with one or both conditions. Additionally, IgM memory B-cell (MBC) counts can be used via flow cytometry, as has diagnostic imaging of the spleen to determine spleen size and structure, since larger spleens are a symptom of splenic dysfunction (Kirkineska et al., 2014). Another method commonly employed is measuring serum levels of the tetrapeptide tuftsin, as it's expression on neutrophils is reduced following splenectomy (Kirkineska et al., 2014).

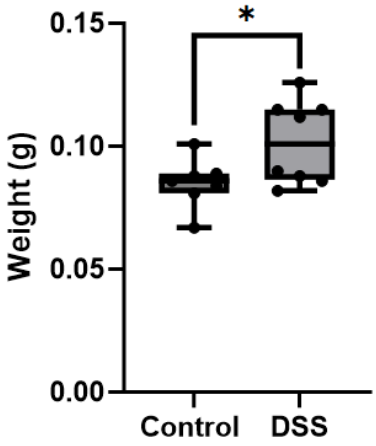

Figure 1.8. Murine spleen weights of control vs DSS mice as recorded by Hechter et al. (in preparation).

1.6 The Enteroendocrine System

The enteroendocrine system is responsible for sensing ingested food and releasing intestinal hormones which regulate glucose homeostasis, gastrointestinal secretion and motility, appetite, and other physiological responses (Psichas et al., 2015). The hormones of the enteroendocrine system have received much attention in recent years as their roles in appetite and glucose homeostasis make them prime targets for treatments for diabetes and obesity (Psichas et al., 2015). EECs are found in the epithelial lining of the stomach, large and small intestines, and the rectum of the GI tract (Gribble and Reimann, 2016). They make up one of the body's largest endocrine systems, and they play significant roles in nutrient absorption, energy homeostasis, gut motility, and intestinal transit (Thanasupawat et al., 2013). Despite the significant role of the intestine in the enteroendocrine system, EECs make up only 1% of all IECs (Psichas et al., 2015). There has been a renewed interest in EEC research in recent years as they play important roles in the brain-gut axis, the gut-pancreas axis, and the immune-endocrine axis (Thanasupawat et al., 2013). Nutrient ingestion stimulates EECs to release intestinal hormones which regulate the physiological roles of the enteroendocrine system (Gribble and Reimann, 2016). L-cells are expressed in the distal parts of the gut and produce PYY, GLP-1, GLP-2, and INSL5 (Gribble and Reimann, 2016, Bohórquez et al., 2011).

GLP-1 is a member of the glucagon family of peptides (Gupta, 2013). Like INSL5, GLP-1 is primarily expressed in enteroendocrine L-cells in the intestinal tract, however it has secondary sites of expression in organs such as the heart, lungs, kidneys, and hypothalamus, and cell types including neurons, microglia, and pancreatic β-cells (Lee and Jun, 2016). An important

and well-documented function of GLP-1 is the regulation of blood glucose levels by acting as an incretin to stimulate insulin release (Gribble and Reimann 2019). It further stabilises blood glucose levels by inhibiting glucagon secretion (which inhibits insulin release), delaying gastric emptying while increasing β-cell mass by stimulating the proliferation of β-cells and inhibiting their apoptosis (Lee and Jun, 2016). Research suggests GLP-1 exerts anti-inflammatory action on adipose and pancreatic tissue, reducing glucose levels in patients suffering from diabetes (Lee and Jun, 2016). The well-documented regulatory and anti-inflammatory effects of GLP-1 on blood glucose led to the development of GLP-1 analogs and other GLP-1 receptor (GLP-1R) agonists for the treatment of obesity and diabetes (Zhang et al., 2020). The anti-inflammatory properties of GLP-1 and its analogs suggest that it may be a useful target for treating other chronic inflammatory conditions, such as IBD (Villumsen et al., 2021). Villumsen et al. (2021) investigated the effect of GLP-1 based therapies on IBD compared to other antidiabetic treatments, by analysing IBD patient data between January 2007 and March 2019. They found that GLP-1 based therapies may improve the course of IBD, and had lower rates of negative clinical effects than other antidiabetic treatments (Villumsen et al., 2021).

PYY is a polypeptide hormone with 36 amino acid residues (Lafferty et al., 2018). It is released in response to proteins, lipids, and amino acids found in the gut lumen (Bohórquez et al., 2011). It is part of the neuropeptide Y (NPY) peptide family, which also includes NPY and pancreatic polypeptide (Albertsen et al., 2013). The cognate receptors for this peptide family are four GPCRs known as Y_1, Y_2, Y_4, and Y_5, collectively known as the NPY receptors (Albertsen et al., 2013). The NPY protein-receptor complexes are responsible for regulating appetite, gastrointestinal functions, blood pressure, and other physiological processes (Albertsen et al., 2013). Like GLP-1 and INSL5, PYY is mainly secreted postprandially from the endocrine L-cells in the GI tract (Albertsen et al., 2013). PYY functions as an anorexigenic hormone, reducing appetite and subsequently weight gain, however it also plays physiological roles such as delaying gastric emptying, regulating renal sodium excretion, and inhibiting motility in the colon and jejunum (Bohórquez et al., 2011). The similar functions of PYY to GLP-1 makes it a promising target for drug development in the treatment of obesity, diabetes, and inflammation (Lafferty et al., 2018). Further research into PYY's effects on pancreatic islet cells is required before we can develop and approve PYY analogs and other PYY receptor agonists (Lafferty et al., 2018).

Objectives and Hypotheses

The first objective of this study is to determine if DSS treatment induces inflammation in the spleen. It is known that DSS causes inflammation in the gut, however its role in splenic inflammation has yet to be confirmed. Inflammation will be induced in one cohort of mice at the start of the experiment, while the other cohort will be a control, and thus will be used to test the impact of INSL5 of splenic immune response starting from a native condition. Hematological and histological analysis in conjunction with RNA-sequencing and qPCR will be used to assess markers of inflammation in the spleen.

The second objective of this study is to determine if INSL5 influences immune cell responses in the murine spleen in either the native condition or in the context of DSS-induced UC. Splenocytes from both the control and DSS cohorts will be subjected to four different treatments; control (no treatment), LPS, INSL5-LPS co-treatment, and INSL5 pre-treatment followed by LPS treatment. Changes in the expression of pro- and anti-inflammatory cytokines will be measured by 1) analysing changes in secreted proteins using high sensitivity enzyme linked immunosorbent assay (ELISA) and 2) analysing changes in the expression of selected cytokines and chemokines using reverse transcription qPCR (RT-qPCR).

My first hypothesis is that the DSS-treated murine spleen will show signs of acute inflammation. I propose that the gut communicates with the spleen via the hepatic portal system, signalling to the spleen to polarize macrophages to the M1 phenotype.

My second hypothesis is that INSL5 polarizes splenic macrophages to the M2 phenotype, thereby reducing pro-inflammatory cytokine expression and/or increasing anti-inflammatory cytokine expression. Since M2 macrophages function to resolve inflammation, I hypothesize that polarizing macrophages to the M2 phenotype will increase the expression of anti-inflammatory cytokines and decrease the expression of pro-inflammatory cytokines.

My third hypothesis is that the SOCS3 pathway is activated downstream of RXFP4 stimulation. It is well documented that SOCS3 is more highly expressed in the inflamed colonic mucosa of UC patients than in inactive mucosa (Miyanaka et al 2007). While the downstream effects on RXFP4 on several other pathways have been studied, RXFP4 activity on SOCS3 has been largely ignored. Given the reported anti-inflammatory effects of SOCS3 (Suzuki et al., 2001) and the hypothesized role of RXFP4 in the reduction of inflammation (Vahkal et al., 2021), it stands to reason that SOCS3 may be upregulated following stimulation of RXFP4.

Rationale

The purpose of the LPS group was to simulate an *in vitro* a bacterial infection, thereby upregulating pro-inflammatory cytokines. LPS plays many roles in Gram-negative bacteria, most notably as an important part of the membrane structure (Bertani and Ruiz, 2018).

The purpose of the INSL5 pre-treatment group is to determine *in vitro* if higher rates of INSL5 prior to infection provides protection against inflammation. One of the major factors which contribute to INSL5 stimulation is the presence of SCFAs (Silva et al., 2020). Expression of pro-inflammatory cytokines is decreased in individuals with a high fiber diet, while inflammatory diseases are more common among people who consume low amounts of fiber (Li et al., 2018). SCFAs bind to enteroendocrine L-cells, stimulating the release of INSL5 (Silva et al., 2020). This suggests that INSL5 has protective effects against pro-inflammatory cytokines and inflammatory diseases. Therefore, we expect INSL5 pre-incubation to significantly inhibit the inflammatory effect of LPS relative to the LPS-alone treatment.

The purpose of the co-treatment group is to determine *in vitro* if INSL5 is effective as a treatment for inflammatory diseases. Prior research suggests that RXFP4 is a viable target for treatment of disorders such as obesity and diabetes, and if my hypotheses are correct, it may also be a viable treatment for IBD (Zhang et al., 2020). Vahkal et al. (2021) reported that pro-inflammatory cytokines are downregulated following INSL5 injection, suggesting that INSL5 not only has protective effects against inflammation, but can be used to hinder inflammation. We expect INSL5 to compete with LPS during co-treatment, thereby creating an environment with a lower level of pro-inflammatory cytokines than in the pre-treatment plates, but higher pro-inflammatory cytokine expression than in the LPS-alone treated plates.

Methods

2.1 Animal Treatments

Sixteen C57BL/6 strain male mice ages eight to twelve weeks were obtained from Jackson Laboratories. Over the course of four weeks (November 16 to December 11, 2022), four mice were the subject of experimentation each week. The mice were randomly divided into two cohorts, one cohort was the control group, and the other cohort was the colitis group. Colitis was induced by adding 2% DSS to their drinking water for seven days (day 1 to day 7), while the control mice were given regular drinking water. Following the 7-day period, there was a 3 day recovery period before the mice were sacrificed. The murine model of DSS-induced ulcerative colitis is generally considered useful for studying acute inflammation (Sann et al., 2013). It induces the main symptoms of UC including inflammation of the caecum and colon, diarrhea, ulceration, bloody stool, weight loss, and atrophy of the villi (Sann et al., 2013).

2.2 Disease Activity Index

The disease activity index (DAI) was measured during days 1 to 7 to determine the severity of colitis in the mice. The DAI scale ranges from 0 to 9 and is calculated from three different scores: weight loss, stool consistency, and intestinal bleeding (Table 2.1). The presence of blood in the stool was determined via a fecal occult blood test (Hemoccult II® SENSA® Fecal Occult Blood Test Systems, Beckman Coulter®, Medical Warehouse, Edmonton, AB, CA.) (Chassaing et al., 2014, Meers et al., 2018, Oldak et al., 2018).

2.3 Comparison of Spleens Between Control and DSS-Treated Mice

Whole spleens were collected following euthanasia (CO2 exposure). They were immediately placed in cold phosphate buffer saline (PBS) prior to being weighed and measured (Appendix B). Following this, some samples were used for a comparison of spleens between control and DSS-treated mice, while others were used in the cell experiment. Histological and hematological analyses were carried out to determine the presence of hyposplenism. Additionally, qPCR was carried out to test for transcript abundance differences of genes involved with inflammation, macrophage stimulation, and MBCs. Finally, an RNA sequencing analysis was carried out to test for transcript abundance differences of numerous genes.

Table 2.1. The scoring system of the disease activity index. **(A)** Weight loss scoring system. **(B)** Stool consistency scoring system. **(C)** Fecal occult blood test (Hemoccult II® SENSA® Fecal Occult Blood Test Systems, Beckman Coulter®, Medical Warehouse, Edmonton, AB, CA.

A		**B**		**C**	
Score	Range	Score	Description	Score	Description
0	0 ± 2%	0	Normal	0	Normal stool consistency and negative hemoccult
1	1 ± 5%	1	Soft	1	Soft stool and positive hemoccult
2	5 ± 10%	2	Diarrhea	2	Very soft stool, visible traces of blood, and positive hemoccult
3	10 ± 15%			3	Liquidly stool, visible rectal bleeding, and positive hemoccult
4	>15%				

2.3.1 Hematological Analysis of the Spleen

To determine if DSS-induced colitis resulted in hyposplenism, one hematological and one histological test were carried out. For the hematological analysis, blood smears from control and DSS mice (n=8, each group) were stained to identify abnormal erythrocytes. For the histological analysis, Prussian blue staining was carried out to identify differential levels of ferric iron in control and DSS spleens, as high iron levels correlate with splenic damage. As both procedures required Eosin, an Eosin Y stock solution was made with 1 gm of Eosin Y, 1 liter of 70% ethanol, and 5 ml glacial acetic acid. An Eosin working solution was made by diluting 1 volume of Eosin stock with 1 volume of 70% ethanol with two or three drops of glacial acetic acid.

To test for hyposplenism in DSS-treated mice, cardiac blood samples from six control and six DSS-treated mice were used in blood smears. Three slides were made from each control and DSS-treated mouse. The smears were stained in accordance with the Diff Quik® protocol. The slides were exposed to the fixative, Fast Green in methanol, in five one-second increments. The slides were then exposed to the Eosin solution in the same manner, rinsed with distilled water, and then exposed to the Methylene Blue stain in the same manner. The slides were rinsed with distilled water and left to dry, before cover slips were applied using permount. The slides were viewed using an Olympus CX41 microscope at 20x magnification. Images were randomly taken using the Infinity Analyze 5 application. One thousand erythrocytes per slide were counted

using ImageJ and Photoscape X. Abnormal erythrocytes, i.e. inclusion bodies and hyperchromic cells, were counted, and the mean number of abnormal erythrocytes was compared between treatments.

2.3.2 Histological Analysis of the Spleen

The Perl's Prussian blue staining technique was first used in 1867 by Dr. Max Perls (Ghio and Roggli, 2021). Hydrochloric acid (HCl) releases ferric ion (Fe^{3+}) from cells, which reacts with potassium ferrocyanide to form a blue pigment known as ferric ferrocyanide (Appendix A) (Ghio and Roggli, 2021). The protocol used in this thesis was based off of Lillie and Greer's (1965) method. A 0.5% HCl solution was made by mixing one volume of 6M HCl with 36.5 volumes of distilled water. A fresh staining solution was made by mixing 300 mg potassium ferrocyanide in 30 mL 0.5% HCl. The spleens of three control mice and three DSS-treated mice were utilized for this experiment. Two slides from each spleen were produced with multiple slices on each slide. The slides were washed with distilled water and then exposed to the staining solution for 30 minutes. The slides were washed with distilled water and then exposed to the Eosin counter stain solution for five minutes. The slides were once again washed with distilled water before dehydrating by exposing them to 50%, then 70%, then 80%, then 95%, then 100% ethanol for 5 minutes each. Finally, the slides were cleared using citrisolv clearing solution for five minutes. The slides were left to dry and then cover slips were added using permount. The slides were viewed using an Olympus CX41 microscope at 20x magnification. Image were taken using the Infinity Analyze 5 application.

2.4 RNA-Sequencing Analysis of Control and DSS-Treated Whole Spleens

RNA from four control and four DSS-treated mice was sent to Genome Quebec for RNA-sequencing on a NovaSeq 6000 sequencer together with 88 other samples. Poly A enriched stranded libraries were created and 100 bp forward and reverse reads generated, with an expected mean read depth of 25 million reads per sample. The RNA integrity number (RIN) of all samples was >8.0, except one control sample which did not generate suitable RNA-sequencing quality and was eliminated. The nf-core RNA sequencing pipeline was used to generate raw counts of the data (https://nf-co.re/rnaseq/3.14.0), using the GRCm39 mouse reference genome and annotation (GCF_000001635.27). Briefly, pre-processing of the reads was performed with

FastQC, reads with poor sequence quality were eliminated or trimmed using TrimGalore! The resulting high-quality reads were aligned to the mouse reference genome using the STAR aligner and the number of reads per gene were estimated using RSEM. This part of the pipeline was performed at Compute Canada. Subsequently, the raw count files were downloaded and used in differential gene transcript abundance analyses to compare up and down regulated genes and pathways between control and DSS-treated animals using DESEQ2 in R v 4.3.3.

The raw counts were first normalized using the normalization process in DESEQ2 plus a pseudocount c – 4 [in R: log2(counts(dds, normalized=TRUE) + 4)]. The normalized counts were then used to perform k-means clustering using an unsupervised method for clustering genes into groups based on their transcript abundance pattern across all samples. Genes are first ranked by standard deviation, and the genes with the 2000 highest standard deviation across all samples (and both treatments in this case) were used for clustering. To visualize the cluster's in a heat map, the data was scaled (for the purposes of graphing) to have the same sum across all genes per row. Using the genes identified in each of the six clusters, an enrichment analysis was conducted for the Gene Ontology Biological Processes, using the number of genes identified in each cluster pertaining to a given process relative to the total number of genes in the process. The fold enrichment and FDR adjusted p-value are reported for each Biological process found to be significantly enriched at FDR <0.05. Following this, the number of differentially expressed genes (DEGs) in the spleens of control vs DSS-treated mice was assessed using DESEQ2, and all genes with a fold change >|1.5| at an FDR <0.1 were retained. This list of DEGs was used to assess the enrichment of pathways according to the following databases: 1) GO Biological Processes 2023, 2) GWAS catalog 2023, 3) GTEx aging signatures (2021), 4) Clinvar (2019), 5) Mouse Genome Informatics Mammalian Phenotype, 6) Reactome 2022 and 7) Encode Histone Modifications reporting only pathways enriched at an FDR <0.01

2.5 Comparison of Macrophages Across Cell Treatments

Two 40 mL tubes of Spleen Dissociation Medium® (StemCell Technologies) were thawed at room temperature. The spleen samples from the two control mice were pooled and minced using scissors and forceps into <1 mm pieces in a 60 mm cell culture dish and the procedure repeated for the two DSS spleens. One tube of dissociation media was poured onto each culture dish and mixed. A 5 mL transfer pipette was used to return the suspension to the

media's original tube. The suspension was incubated at room temperature, and agitated every five minutes. Ethylenediaminetetraacetic acid was added to the dissociation solution to a concentration of 10 mM (80 μL of 0.5 M stock), and the spleen solution mixed and incubated at room temperature for five minutes. The fragments were then dissociated by passing the suspension through a 16-gauge blunt-end needle attached to a 3 cc syringe numerous times. A 70 μm nylon mesh filter was primed by passing 5 mL of Roswell Park Memorial Institute (RPMI) media through it. The cells were filtered through the nylon filter using the blunt end of the syringe into a 50 mL conical tube. The spleen dissociation media tube was rinsed with 5 mL RPMI and filtered into the 50 mL conical tube, twice. The cell suspension was centrifuged at 300 x g for 10 minutes. The supernatant was discarded and the pellet resuspended in 5 mL of RPMI. Following resuspension, the cells were diluted in 12 mL medium. An aliquot was counted using a hemocytometer.

2.5.1 Cell Culture Media

RPMI 1640 cell culture media with L-glutamine and Phenol Red was made from powder (Thermo Fisher, 31800105). The powder was mixed with 10 L ultrapure water and filtered into autoclaved glass bottles. 15% Fetal Bovine Serum was added to the RPMI medium to provide nutrients for the cells, with 25 μg/mL of gentamicin to protect against contamination. Gentamicin is a bactericidal aminoglycoside antibiotic, which is particularly useful against aerobic gram-negative bacteria (Phillips et al., 1977).

2.5.2 Analysis of Gene Transcript Abundance in Control vs DSS-Treated Mice

RNA was extracted from the whole spleens of both control and DSS-treated mice using the Qiagen RNeasy Mini Kit as per the manufacturer's instructions. To this end, we dissociated the spleen sections and added 600 μL of Buffer RLT®, and the lysate was homogenized with an 18 gauge needle. An equal volume of 70% ethanol (600 μL x 4 = 2400 μL per tube) was added to the lysate and mixed thoroughly by pipetting up and down numerous times, then we transferred 700 μL of the lysate to an RNeasy column inside of a collection tube and centrifuged for 15 seconds at 8000 x g in a Sigma 1-14 mini centrifuge. The flow-through was discarded and the columns were re-used until all of the lysate in the falcon tube had been flushed through. Subsequently, 700 μL of the Buffer RW1® was added to the RNeasy column and centrifuged for

15 seconds at 8000 x g. The flow-through was discarded and 500 µL of the Buffer RPE® was added to the column, the mixture was centrifuged for 15 seconds at 8000 x g and again the flow-through was discarded prior to repeating the process but with a longer spin of 2 minutes. The RNeasy column was placed into a new 2 mL collection tube, and 30 µL of nuclease-free water was added. The samples were centrifuged for 1 minute at 8000 x g and the process repeated resulting in a total of 60 µL RNA elution per sample. We stored the eluted RNA at -80ºC prior to complementary DNA (cDNA) synthesis.

We used the iScript cDNA Synthesis Kit protocol to perform two-step RT-qPCR. The reverse transcriptase used by the iScript kit is RNase H+, which supplies a higher level of sensitivity than RNase H– enzymes during qPCR. The enzyme iScript is a Moloney murine leukemia virus reverse transcriptase which has been modified for an optimal synthesis of cDNA from a wide variety of RNA. The iScript mix comes preblended with an RNase inhibitor and a selection of oligo(dT) and random hexamer primers, which are reliable in binding to several different targets.

Genes analysed included Lymphocyte antigen 75 *(Ly75),*Programmed death-ligand 1 *(Pd-l1),* Transforming growth factor beta 1 *(Tgfb1),* Macrophage colony stimulating factor *(Mcsf),* Interleukin-1beta *(Il-1β),* Monokine induced by gamma interferon *(Mig),* and Interferon gamma-induced protein 10 *(Ip-10),* the primers for which were purchased from Thermo Fisher. Ribosomal protein L13a *(Rpl13a)* (purchased from Millipore Sigma) and Ubiquitin-conjugating enzyme E2 *(Ubc-2)* (purchased from Invitrogen) were chosen as our reference genes, as they have been previously established to be reliable reference genes (Kuchipudi et al., 2012, Ho and Patrizi, 2021).

We used PowerTrack SYBR Green Master Mix from Applied Biosystems by Thermo Fisher Scientific to carry out qPCR. We optimized the primers by preparing the SYBR mix as per the PowerTrack protocol. We multiplied the volume of each solution needed per reaction by the number of reactions. qPCR was carried out in a QuantStudio™ 5 Real-Time PCR System for Human Identification according to the protocol shown in Table 2.5. Graphs representing qPCR results were generated using Prism Graphpad.

2.5.3 Splenic Macrophage Treatments

Splenocytes were counted using a hemocytometer prior to being cultured on 12-well plates at a density of ten million cells per well, and incubated at 37ºC with 5% CO_2. Sixteen hours following cell plating, the culture was enriched for macrophages by washing the cells with serum-free RPMI to remove non-adherent cells. Following enrichment for splenic macrophages by removing non-adherent cells, our cultures were subjected to one of four treatments: control (RPMI alone), LPS (1.0 μg/ml lipopolysaccharide from *E. coli* per well for 24 hours), co-treatment (100 nM INSL5 and 1.0 μg/ml LPS for 24 hours), and INSL5 pre-treatment (100 nM INSL5 hormone for 12 hours followed by 1.0 μg/ml LPS for 24 hours) (Figure 2.1.). INSL5 was diluted from a concentration of 1 M to 0.1 mM using dimethyl sulfoxide prior to being added to the appropriate wells (10 μL added to each well), in order to accurately pipette the required amount of peptide.

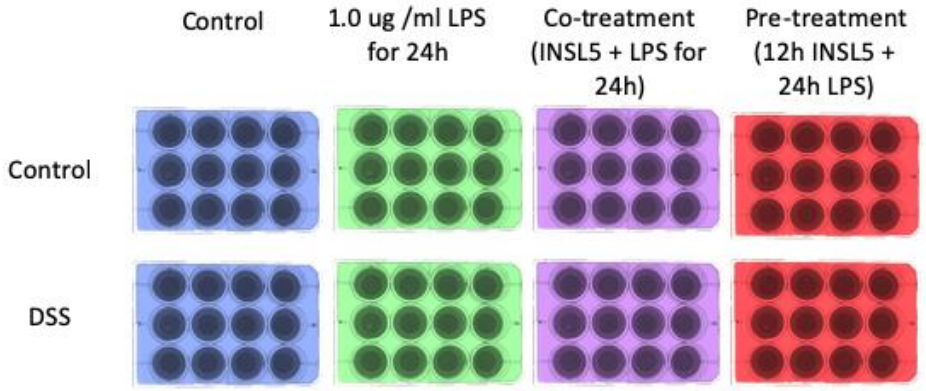

Figure 2.1. The splenic macrophage treatments from both control and DSS-treated mice. Generated with Microsoft Powerpoint.

2.5.4 Analysis of Transcript Abundance Across Macrophage Treatments

The Qiagen RNeasy Mini Kit was used to extract RNA from the cells following the manufacturer's instructions. First, we aspirated the RPMI media and washed the wells with PBS. Following this, we added 600 μL of Buffer RLT via pipette to each well. We disrupted the cell monolayer by scraping the pipette against the wells multiple times, as well as by pipetting the buffer up and down. The lysate from each row was combined into one 15 ml falcon tube (four wells per one tube) and homogenized with an 18 gauge needle. The remaining steps are the same as described in section 2.5 We used the iScript cDNA Synthesis Kit protocol to perform two-step RT-qPCR, as per section 2.5.

Unfortunately, most of our RNA samples resulted in a low yield. We altered the volume of each component of the cocktail to account for this. For many of our RNA samples, we were only able to obtain a maximum of 0.5 μg in an elution of 39.5 μL. Therefore we opted to synthesize 500 ng of cDNA rather than 1000 ng. Reaction mix volumes are shown in Table 2.3. Following this, we incubated the reaction mix in an MJ Research PTC-200 Thermal Cycler. The reaction protocol is shown in table 2.4. Once the reaction was finished and the thermal cycler cooled down to 4ºC, we transferred the cDNA to a –20ºC freezer prior to qPCR.

Primers purchased for the cell experiment included Interleukin-10 *(Il-10),* Interleukin-6 *(Il-6),* Tumor necrosis factor alpha *(Tnfα),* Suppressor of cytokine signaling 3 *(Socs3),* Cluster of differentiation 80 *(Cd80),* and *Rxfp4* from Millipore Sigma, and *Mcsf* from Thermo Fisher. *Rpl13a* and *Ubc-2* were chosen as our housekeeping genes, as they have been previously established to be reliable reference genes (Kuchipudi et al., 2012, Ho and Patrizi, 2021). *Il-10* was chosen as it is a classic anti-inflammatory hormone and marker of M2 macrophages, while *Il-6* and *Tnfα,* are classic pro-inflammatory hormones and markers of M1 macrophages (Chávez-Galán et al., 2015). *Cd80* was chosen as it is a surface marker of M1 macrophages (Chávez-Galán et al., 2015). *Socs3* was chosen for its role as a marker of inflammation in IBD (Miyanaka et al 2007). *Rxfp4* was chosen as we believe it has anti-inflammatory properties, and is therefore a M2 surface marker (Vahkal et al., 2021). Macrophage colony stimulating factor *(Mcsf)* was chosen as it upregulates the production of pro-inflammatory cytokines (Chávez-Galán et al., 2015). qPCR was carried out as described in section 2.5.

2.6 ELISA Assay

Prior to RNA extraction, the cell culture plates were spun down in an Eppendorf Centrifuge 5804R at 2000 x g for 2 minutes. Each week, over the course of four weeks, 700 μL RPMI media from four wells per treatment was collected, and pipetted into 2 mL centrifuge tubes in pooled groups of two (i.e. each week, we collected two tubes per treatment, each containing 1400 μL RPMI media). The samples were stored at -80ºC prior to being concentrated via centrifugation into filters, obtaining a total volume of 350 μL per sample. The filtered samples were then sent to EVE Technologies for a high sensitivity discovery ELISA to measure levels of pro-inflammatory cytokines and other immune proteins. Proteins measured included Granulocyte-macrophage colony-stimulating factor (GM-CSF), Interferon gamma (INFγ),

Interleukin-1 alpha (IL-1α) and beta (IL-1β), Interleukin 2 (IL-2), IL-4, IL-5, IL-6, IL-7, IL-10, IL-12p70, IL-13, IL-17A, Keratinocytes-derived chemokine (KC), Epithelial-derived neutrophil-activating peptide 78 (ENA-78 or LIX), monocyte chemoattractant protein-1 (MCP-1), Macrophage inflammatory protein-2 (MIP-2), and TNFα.

Table 2.2. The reaction volumes of each reagent according to the iScript protocol, and our altered volumes to account for low RNA yields.

Reagent	**iScript Protocol Volume (µL)**	**Low Yield Volume (µL)**
NF Water	Variable	Variable
5x iScript Select Reaction Mix	4	10
RNA template	Variable (1 µg)	Variable (0.5 µg)
iScript Reverse Transcriptase	1	0.5
Total Volume (Pre-cycle)	**20**	**50**
Total Volume (Post cycle)	**100** (80 µL NF-water added)	**50** (no NF-water added)

Table 2.3. The iScript reaction protocol in the MJ Research PTC-200 Thermal Cycler.

Step	**Temperature**	**Time**
Priming	25ºC	5 mins
Reverse Transcription	46ºC	20 mins
RT inactivation	95ºC	1 mins
Optional	4ºC	Hold

2.7 Data Analyses

For the cell culture analysis, the delta cycle threshold (ΔCt) method was used to analyse the qPCR data. This method is used on qPCR data to compare relative fold transcript abundance by calculating the difference between the difference in Ct value (ΔCt) between the gene of interest and housekeeping gene. This is done on both the experimental and control treatments to compare the expression of genes in both control and experimental treatments.

$$\Delta Ct = Ct\ (\text{gene of interest}) - Ct\ (\text{housekeeping gene})$$

For the whole spleen analysis, the delta delta cycle threshold (ΔΔCt) published by Livak and Schmitgen in 2001 was used. This method allows one to compare the relative difference in expression of experimental treatments relative to the control treatment. Thus, the ΔCt value of the control average is subtracted from the ΔCt of the experimental treatments.

ΔΔCt = ΔCt (mean experimental treatment) – ΔCt (mean control)

Table 2.4. qPCR protocol for optimization of primers and data collection.

Stage	Step	Ramp Rate (°C/sec)	Temperature (°C)	Time
Hold	1	4.14	95.0	2 min
PCR	1	4.14	95.0	5 sec
	2	3.17	58.0	30 sec
Melt	1	1.99	95.0	15 sec
	2	1.77	60.0	1 min
	3	0.1	95.0	15 sec

Finally, statistical analyses were carried out in IBM® SPSS. First, a Levene's test was carried out to determine homogeneity of variance (HOV) amongst treatments. The null hypothesis was that the variance of transcript abundance amongst treatments were equal, while the alternative hypothesis was that the variance of transcript abundance amongst treatments were not equal. If the null hypothesis was met, then an ANOVA test was carried out to determine significance levels of cytokine transcript abundance between treatments. The null hypothesis was that the transcript abundance between treatments was equal, while the alternative hypothesis was that the transcript abundance between treatments were not equal. If the null hypothesis was met, then a Tukey test was carried out post-hoc to compare multiple treatments. If the null hypothesis of the Levene's test was not met, then a Kruskal-Wallis (KW) test with post-hoc was carried out instead of an ANOVA.

Results

3.1 Histological Analysis of the Spleen

During the mouse experiment, we noted how some DSS-treated mice had been plagued by large blood clots in their spleens. It was thus reasoned that Prussian Blue Staining may be an appropriate histological test to determine the presence of hyposplenism. No difference in colouration was observed between the control and DSS-treated spleen slides as a whole. However, a major splenic blood vessel in a DSS-treated mouse was heavily stained, while control blood vessels were not. No other blood vessels were observed in the DSS-treated spleens. This same spleen had generally lower levels of iron compared to the other two DSS-treated spleens, however it was covered in black dots, possibly a further sign of hyposplenism, however this evidence is not statistically supported (Figure 3.1).

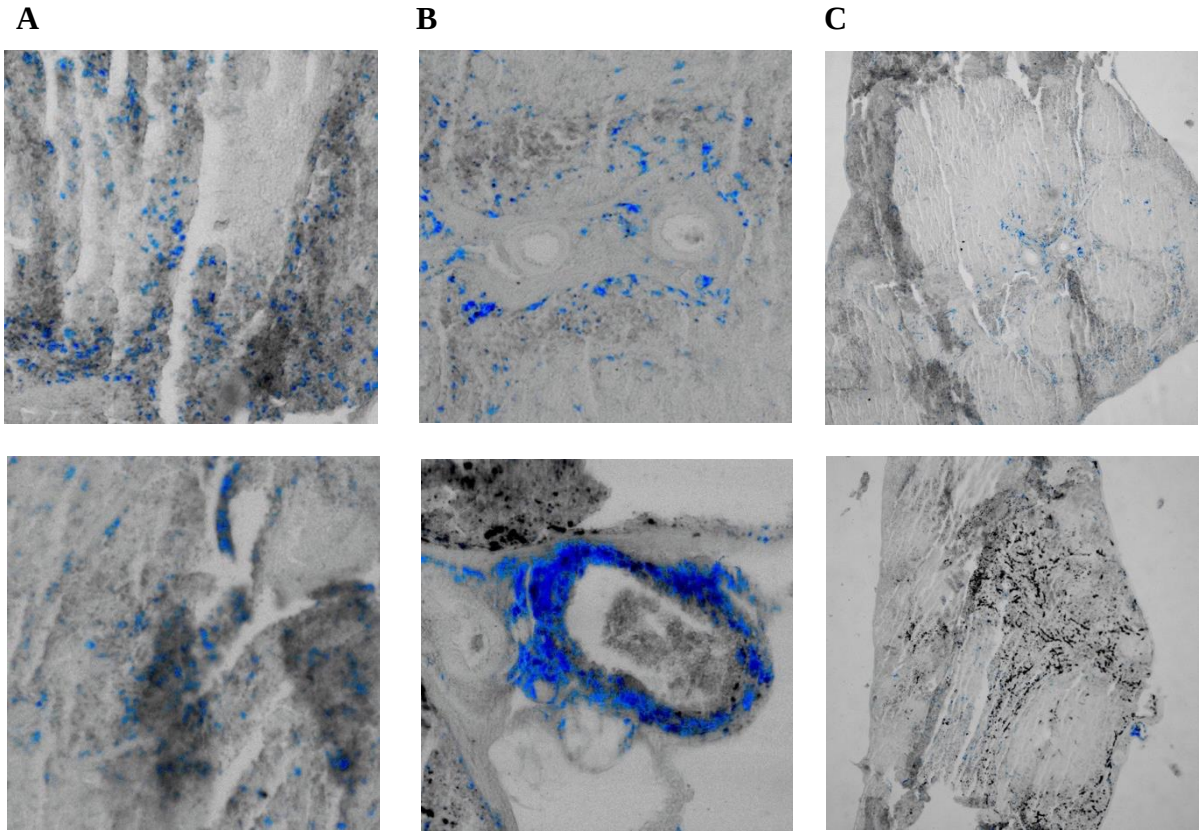

Figure 3.1 A comparison of control and DSS-exposed murine livers stained using the Prussian blue staining technique. Blue pigmentation indicates the presence of ferric iron. Iron deposit images were made clearer in Photoscape X by isolating the colour blue and increasing the contrast, saturation, and vibrancy. **A)** Iron levels in the general area of the control spleen (top)

and DSS-treated spleen (bottom). Magnified to 999 by 999 pixels. **B)** The blood vessel of the control spleen (top) and DSS-treated spleen (bottom). Magnified to 999 by 999 pixels. **C)** A full slide of a control spleen (top) and a DSS-treated spleen (bottom).

3.2 Hematological Analysis of the Spleen

In addition to the Prussian blue stain, blood smears were carried out to measure levels of Howell-Jolly bodies and hypochromic erythrocytes. Few Howell-Jolly bodies and hypochromic erythrocytes were counted in the control mice, with 2.3% containing Howell-Jolly bodies and 1.3% showing a hypochromic phenotype. Meanwhile, 5.7% of DSS-treated mice contained Howell-Jolly bodies (HOV: $p<0.001$***, KW: $p<0.001$***) and 42% showing a hypochromic phenotype (HOV: $p=0.011$*, KW: $p<0.001$***) (Figure 3.2 and Appendix C).

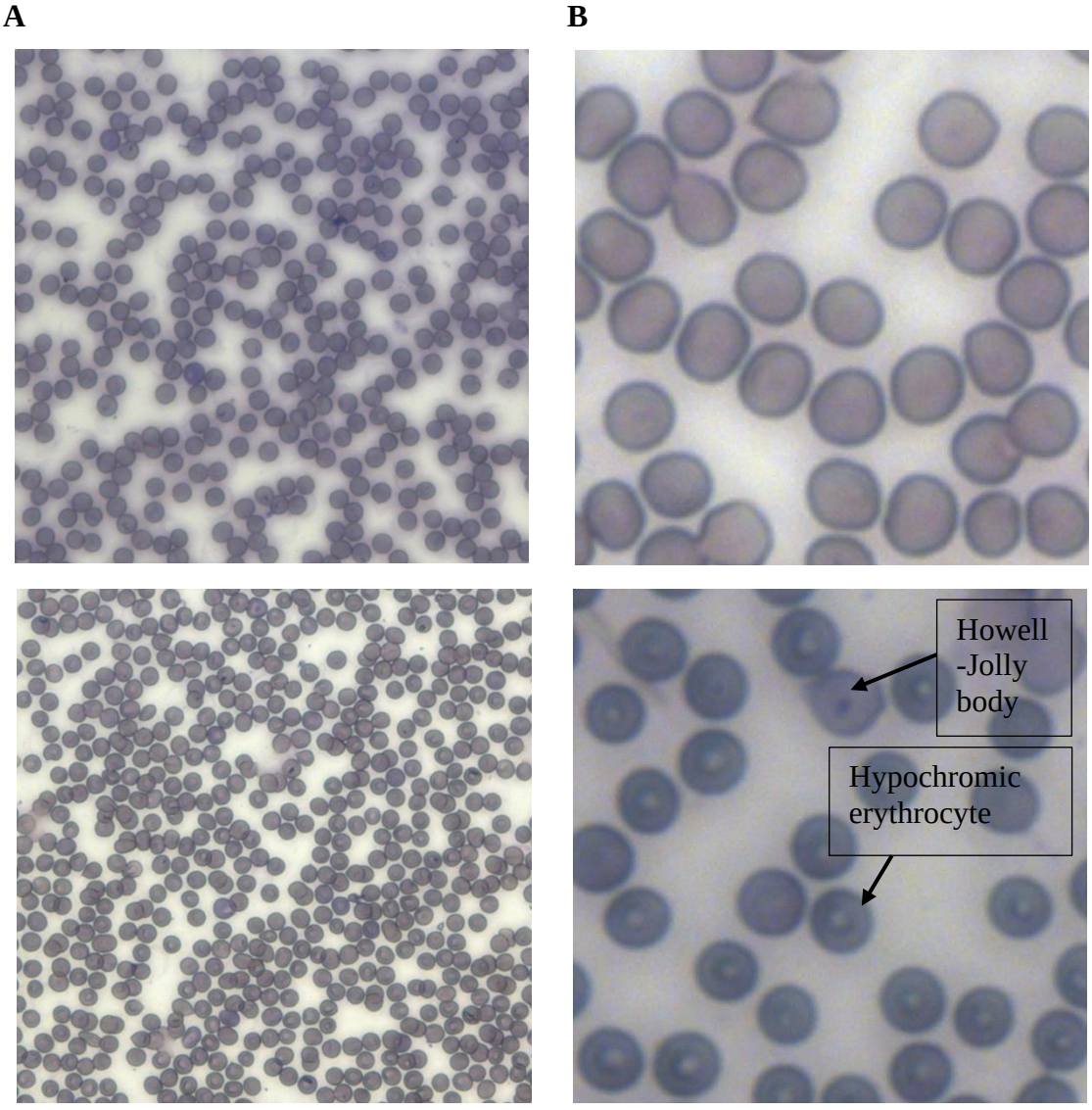

C **D**

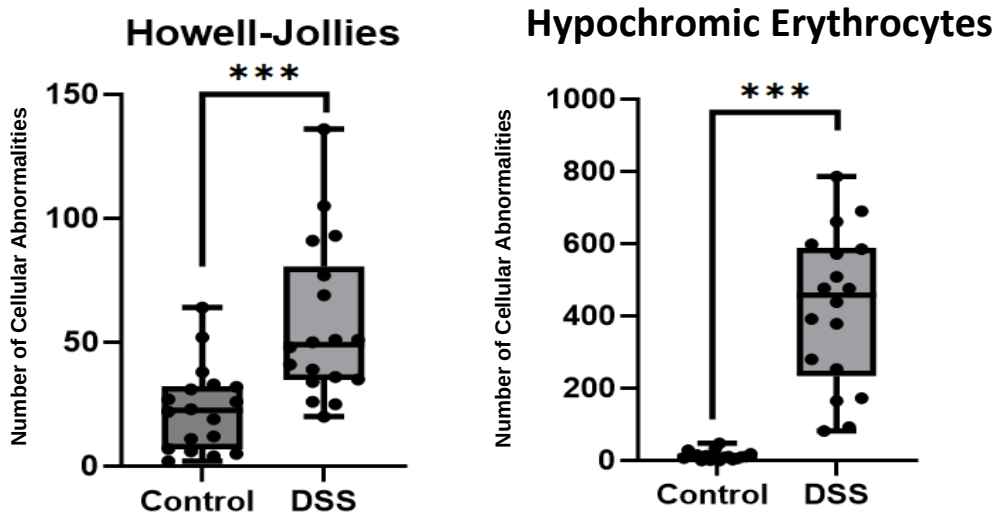

Figure 3.2 A) comparison of control (top) and DSS-treated (bottom) murine blood stains. **B)** A magnified to 250 by 250 pixels. image of control (top) and DSS-treated (bottom) murine blood stains. **C)** A comparison of Howell-Jolly bodies in control vs DSS-treated mice. N=16. **D)** A comparison of hypochromic erythrocytes in control vs DSS-treated mice. N=6 mice, three replicates per mouse for 18 total replicates. One asterisk on error bars: $p \leq 0.05$. Two asterisks: $p \leq 0.01$. Three asterisks: $p \leq 0.001$.

3.3 mRNA Transcript Abundance Analyses – Whole Spleen

mRNA transcript abundance analyses of the whole spleen were carried out via qPCR. The MBC marker *Cd274* was more highly expressed in control mouse spleens compared to the colitis mouse spleens, (HOV: p=0.008**, KW: p=0.046*), however *Ly75* was not. The *Il-6*-associated gene *Tgfb1* was not more significantly highly expressed in the control mouse spleens compared to the colitis mouse spleens, however it was more variably expressed in the DSS-treated mice than in the control mice (HOV: p=0.051) (Figure 3.3).

The pro-inflammatory cytokine *Mcsf* was significantly more variably expressed in DSS-treated mouse spleens than in control mouse spleens (HOV: p=0.035*). *Il-1β* was highly expressed in control mouse spleens compared to DSS-treated mouse spleens (ANOVA: p=0.037*) (Figure 3.3).

The pro-inflammatory chemokine *Mig* was significantly variably expressed in the DSS-treated mouse spleens compared to the control mouse spleens (HOV: p=0.004**), as was *Ip-10* (HOV: p=0.011*) (Figure 3.3).

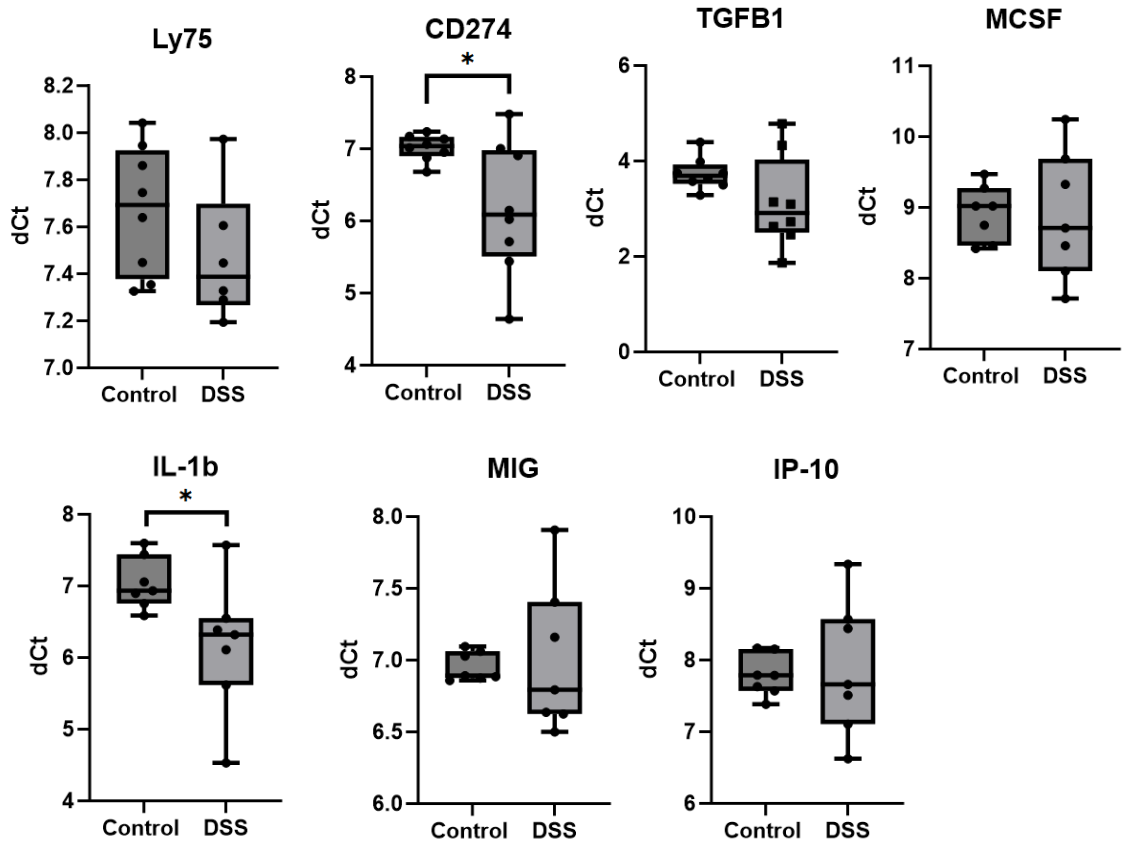

Figure 3.3 Gene transcript abundance differences between control and DSS-treated mouse spleens. dCt = delta Ct. Calculated by subtracting the Ct values of the housekeeping gene from the Ct values of the gene of interest.

3.3.1 RNA-SEQ Analysis

RNA-SEQ analysis was carried out to measure gene transcript abundance differences in the whole spleen between control and DSS-treated mice. The RNA sequencing of one control sample with an RNA-integrity (RIN) score =6.3 was unsuccessful, but the RIN score of all other samples was >8.1 and the raw number of reads per sample ranged from 10.1 million to 28 million. Following normalization and log transformation, both the distribution and density of log transformed transcript abundance values were highly similar across samples (Figure 3.5A and B). Using k-mean unsupervised clustering with k=6, identified two clusters, 3 and 5 that harboured genes that were consistently upregulated in the DSS-treated mice. Cluster 3 harboured genes the GO Biological Processes of Erythrocyte and myeloid cell differentiation, homeostasis

and development, as Immune system process and a few other pathways (Figure 3.6 A and Appendix D). Cluster 5 harboured genes involved predominantly in the cell cycle and mitosis (Figure 3.6 A and Appendix D).

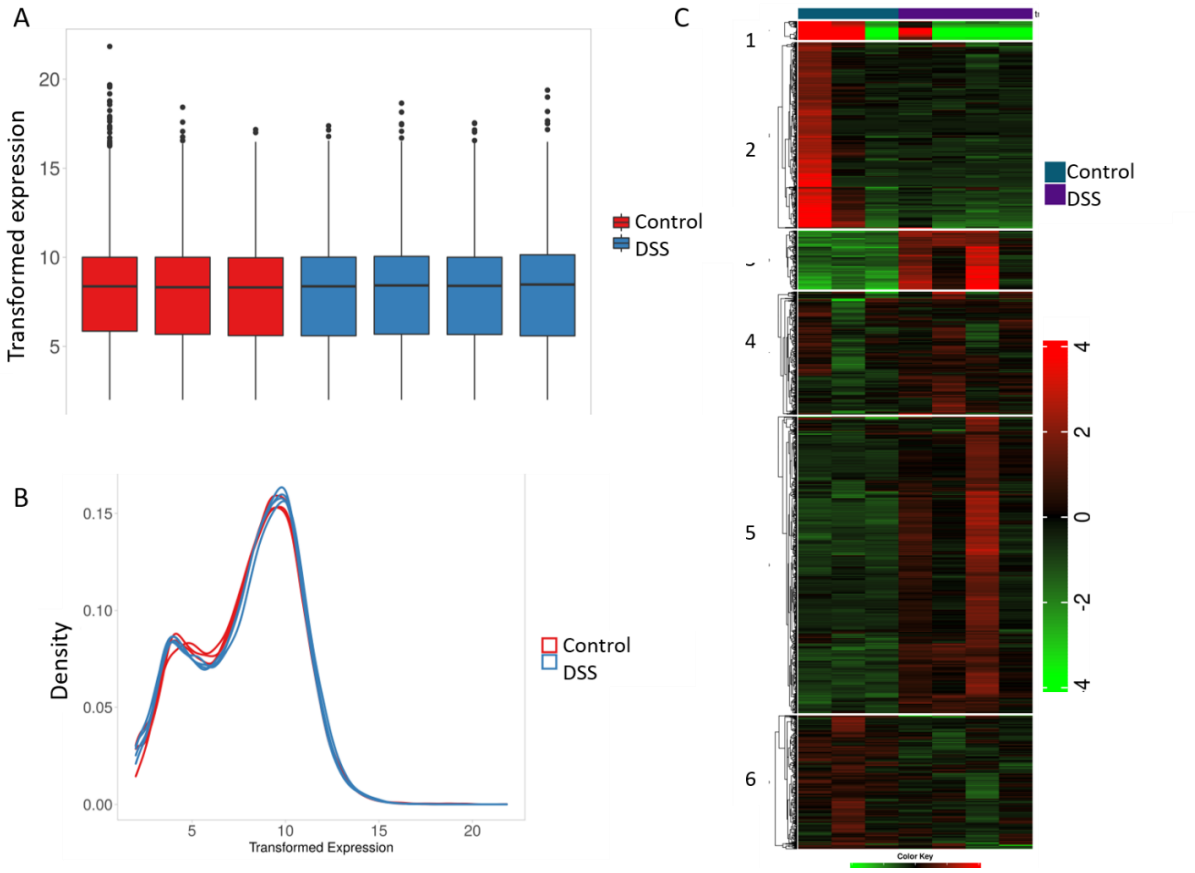

Figure 3.4 A) Boxplot and **B)** density of transformed transcript abundance values by treatment. **C)** Heatmap of k-mean unsupervised clustering of the top six clusters exhibiting the greatest cross-sample standard deviation in transcript abundance.

The differential transcript abundance analyses in DESEQ2 identified only 158 genes that were differentially up or down regulated between treatments: 140 of these genes were upregulated in the DSS treated mice and 18 upregulated in the control mice (Appendix E). Two of the genes upregulated in the control mice were *Fgf21* and *Foxa3* (Figure 3.6 B). On the other hand, genes upregulated in the DSS-treated mice included *Il1r2*, *Socs3*, and *Pklr* (Figure 3.6 B). Several other genes that were found to be differentially expressed between treatments have been previously shown to be associated with erythrocyte or immune related functions (Table 3.1).

Submitting the list of all 159 genes to the EnrichR database identified that 1) the top predicted GTEx tissue was spleen; 2) predicted relevant Clinvar disease was hereditary

spherocytosis; 3) GWAS catalogue associated traits included elevated mean spherical cell volume, mean corpuscular hemoglobin, reticulocyte count, immature fraction of reticulocytes and mean spherical corpuscular volume; 4) GO Biological Process enriched terms included erythrocyte differentiation and neutrophil migration, 5) MGI mammalian phenotype contained similar terms all related to increased spherocytosis as well as other traits related to red blood cells; 6) the Reactome database identified both neutrophil degranulation and Innate Immune System pathways, while finally 7) the encoded histone modification predicted changes in H3K4me1 bone marrow macrophages. (Appendix F).

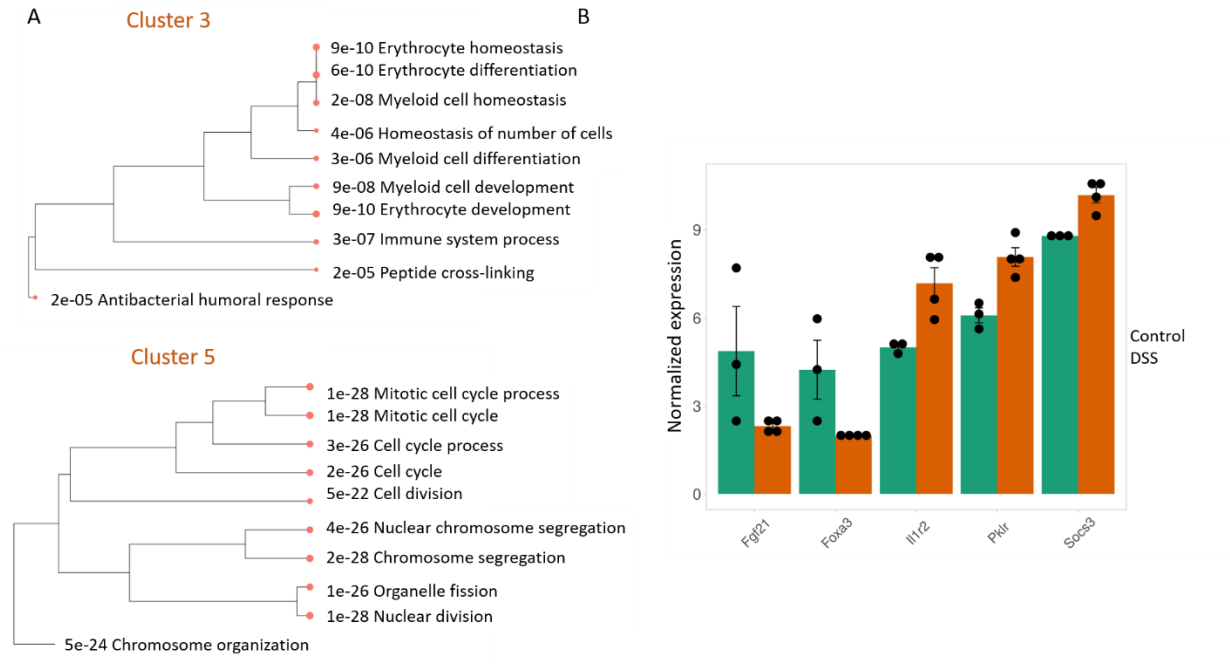

Figure 3.5 A) Tree visualization of significant GO: Biological Processes terms associated with cluster 3 and cluster 5 (shown in Figure 3.5 C) of the K-means unsupervised cluster analysis. **B)** Normalized expression of log-transformed transcript abundance counts in control and DSS-treated expression.

Table 3.1 Genes exhibiting significantly different levels of transcript abundance between control and DSS-treated mice. For each gene, the gene symbol, ensemble ID, log2 fold change (log2FC) for control – DSS treated mice and the FDR adjusted p-value are given. Select genes associated with immune system functions **(A)** or erythrocyte traits **(B)** are given. The full list of 158 genes that exhibited differential transcript abundance between traits is given in Appendix D.

A. Immune-Associated Genes

Symbol	Ensembl_ID	log2FC	Adjusted P-Value
S100a9	ENSMUSG00000056071	-3.709382736	9.93E-07
Il36g	ENSMUSG00000044103	-2.404618713	9.93E-07
S100a8	ENSMUSG00000056054	-3.834910306	1.73E-06
Ifitm1	ENSMUSG00000025491	-1.528914907	0.000972137
Fcgr4	ENSMUSG00000059089	-2.050240633	0.006189535
Foxa3	ENSMUSG00000040891	7.275093318	0.011039245
Cd177	ENSMUSG00000052212	-3.36980746	0.029199092
Fpr1	ENSMUSG00000045551	-1.462218832	0.032509638
Socs3	ENSMUSG00000053113	-1.466857772	0.049756628
Cxcr2	ENSMUSG00000026180	-1.227037613	0.05659309

B. Erythrocyte-Associated Genes

Symbol	Ensembl_ID	log2FC	Adjusted P-Vlue
Hp	ENSMUSG00000031722	-2.445868203	4.38E-07
Rhd	ENSMUSG00000028825	-5.370983911	0.006189535
Fgf21	ENSMUSG00000030827	6.146197809	0.007691583
Gypa	ENSMUSG00000051839	-4.889813148	0.009772425
Cldn13	ENSMUSG00000008843	-4.771040843	0.010026092
Hemgn	ENSMUSG00000028332	-4.882044463	0.024037867
Il1r2	ENSMUSG00000026073	-2.595719549	0.027439035
Ank1	ENSMUSG00000031543	-4.521696022	0.028332127
Trim10	ENSMUSG00000073400	-4.242687019	0.037977743
Tmcc2	ENSMUSG00000042066	-4.389581238	0.064943838
Tal1	ENSMUSG00000028717	-3.21087441	0.181431214
E2f2	ENSMUSG00000018983	-1.63954691	1

3.3.2 Splenic Macrophages – Control Mice

mRNA transcript abundance analyses of the splenic macrophages were carried out via qPCR. *Rxfp4* was significantly downregulated as a result of DSS treatment compared to control (HOV: p=0.047*, KW: p=0.034*), however the cells of DSS-treated mice exposed to LPS

expressed higher levels of *Rxfp4* than DSS-treated murine cells not exposed to LPS (ANOVA: p=0.052). *Rxfp4* was not differentially expressed between control and DSS-treated mice that were either co-treated or pre-treated with INSL5 (Figure 3.7).

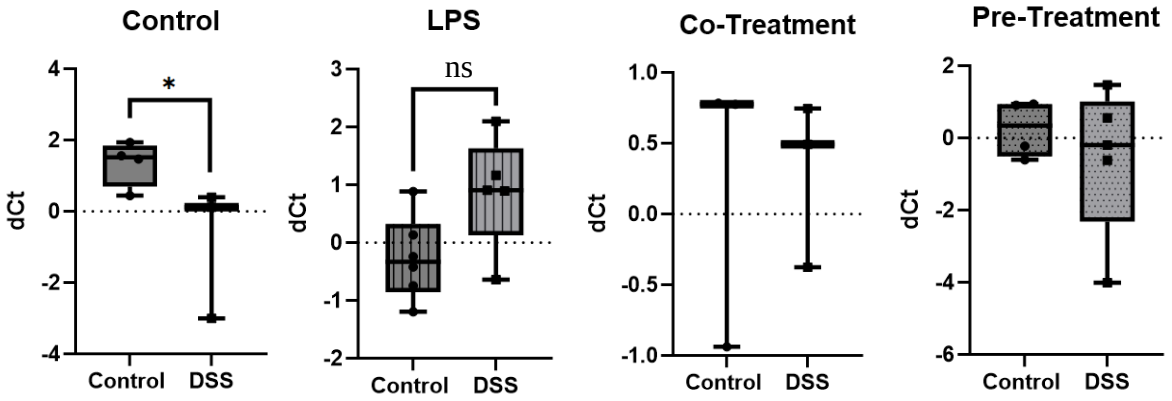

Figure 3.7 Transcript abundance of *Rxfp4* between control and DSS-treated mouse across cell treatments. Higher *Rxfp4* transcript abundance levels imply more significant downstream effects triggered by binding *Insl5*. dCt = delta Ct. Calculated by subtracting the Ct values of the housekeeping gene from the Ct values of the gene of interest.

The M1 Surface marker *Cd80* (HOV: p=0.039*) was significantly highly expressed in the LPS and pre-treatment samples compared to the control samples (KW: p=0.014*) and compared to the co-treatment samples (KW: p=0.012*). Transcript abundance of SOC3 remain unchanged with LPS and co-treatment. (Figure 3.8), though it was significantly upregulated in the DSS-treated spleens based on the RNA-sequence data analysis (Table 3.1).

The pro-inflammatory cytokine *Il-6* (HOV: p=0.011*) was statistically highly expressed in the pre-treatment samples compared to the control samples (KW: p=0.047*) and co-treatment samples (KW: p=0.012*). *Tnf-α* was statistically highly expressed in the co-treatment samples compared to the control samples (ANOVA: p=0.045*), and transcript abundance in the LPS and pre-treatment samples was similarly high (Figure 3.8).

The anti-inflammatory cytokine *Il-10* (HOV: p=0.017*) was significantly highly expressed in the LPS-treated samples compared to the control samples (KW: p=0.025*). *Rxfp4*

had a significant higher transcript abundance in the control samples compared to the LPS-treated samples (ANOVA: p=0.028*) (Figure 3.8).

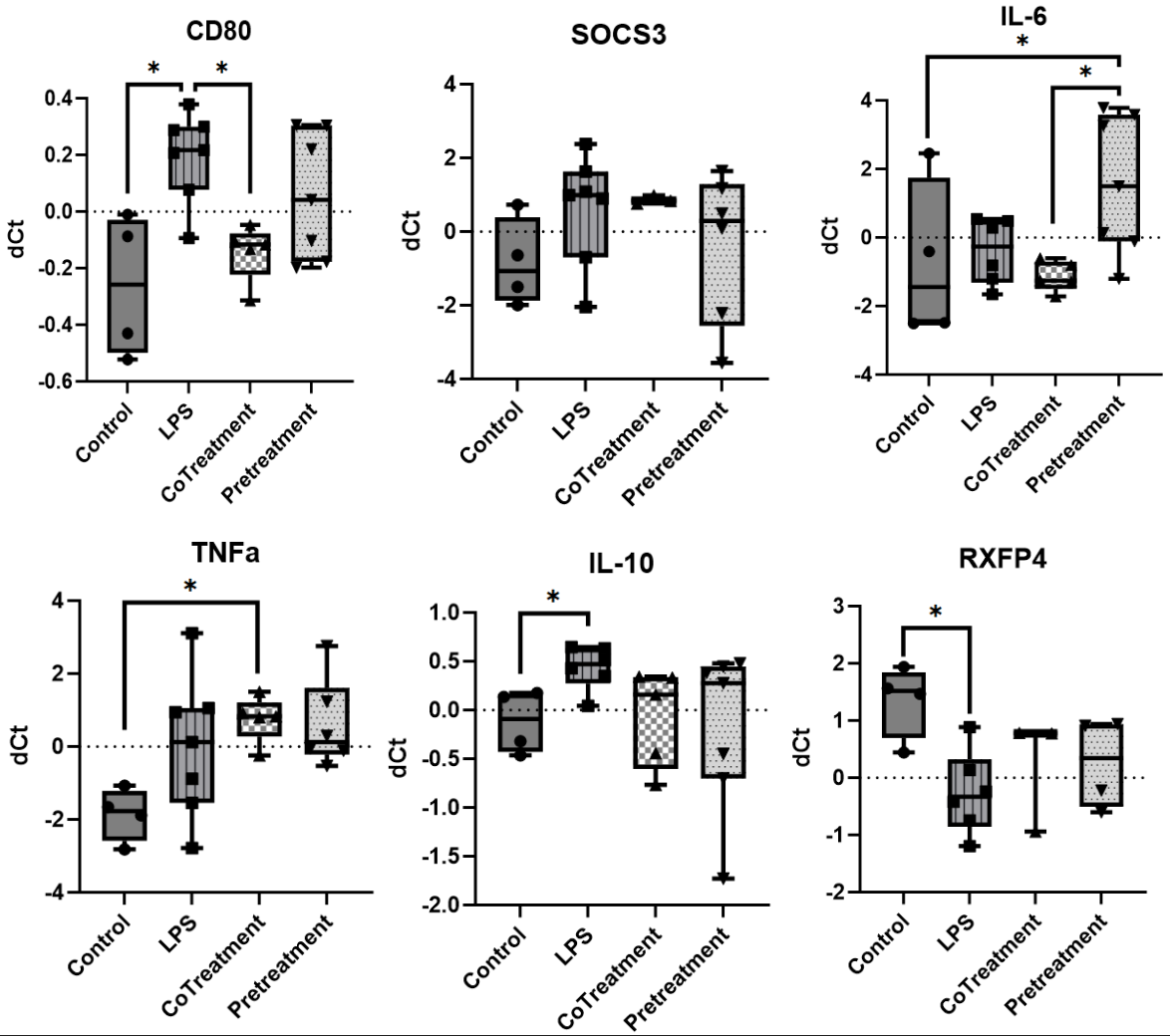

Figure 3.8 Gene transcript abundance differences across treatments in control mouse macrophages. dCt = delta Ct. Calculated by subtracting the Ct values of the housekeeping gene from the Ct values of the gene of interest.

3.3.3 Splenic Macrophages – DSS-Treated Mice

Overall, transcript abundance differences transcript abundance amongst the four treatments were less pronounced in the DSS-treated murine macrophages than in control mice macrophages. *Cd80*, *IL-10* and *Rxfp4* were not differentially expressed across treatments. *Socs3* (HOV: p=0.032*) was marginally higher expressed in the LPS-treated samples. *Il-6* was not differentially expressed across treatments. *Tnf-α* failed the HOV test (HOV: p=0.032*) and

exhibited somewhat higher transcript abundance in the LPS and pre-treated samples, relative to control and co-treatment (Figure 3.9).

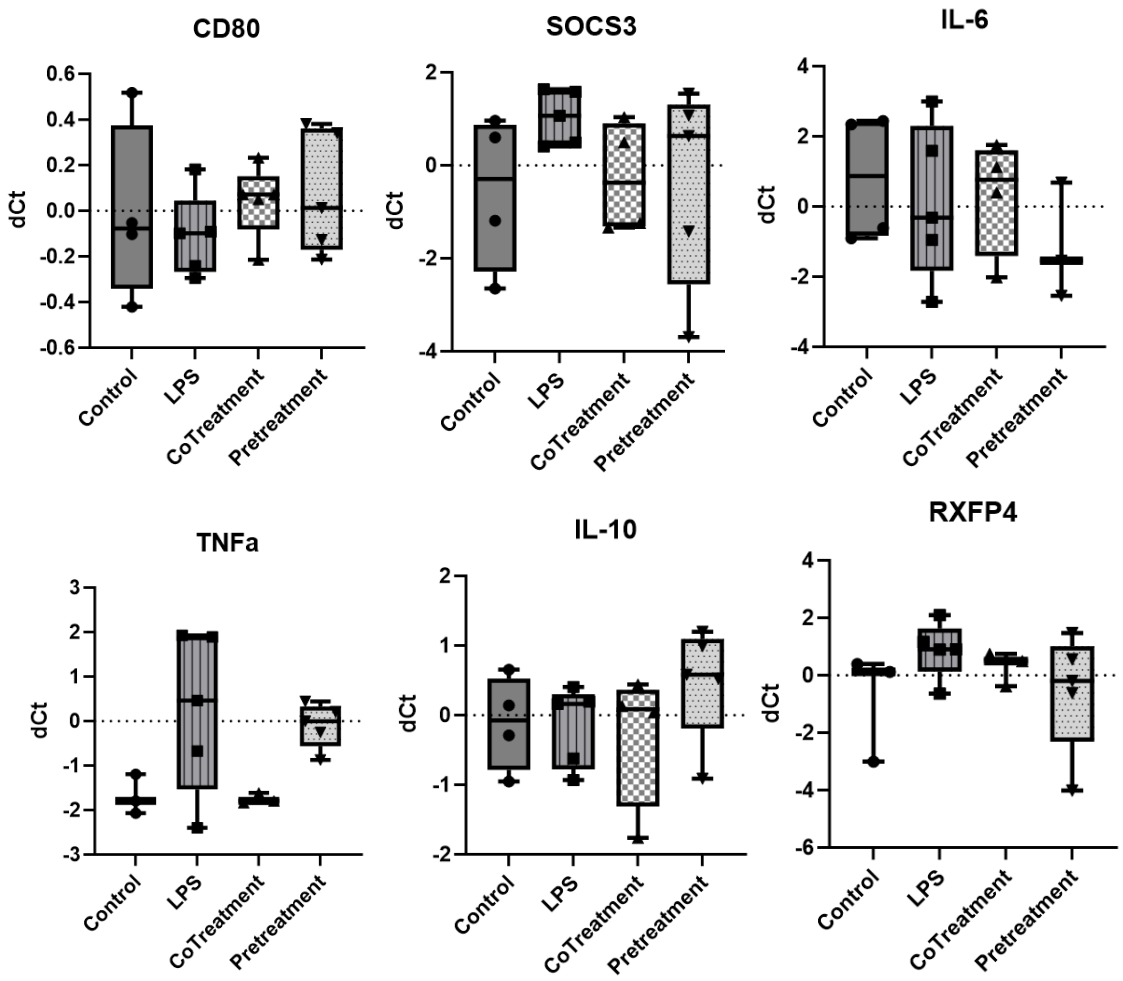

Figure 3.9 Gene transcript abundance differences across treatments in DSS-treated mouse macrophages. dCt = delta Ct. Calculated by subtracting the Ct values of the housekeeping gene from the Ct values of the gene of interest.

3.3.4 The Effect of DSS on Splenic Macrophages

Interestingly, there were no significant differences in gene transcript abundance in control macrophages between the control and DSS-treated mice (Figure 3.10), with the exception of RXFP4 as mentioned above in figure 3.7. While *Socs3, Cd80, Mcsf, and Il-6* were all marginally upregulated in the DSS-treated cells compared to the control cells, there was no average difference in *Il-10 or Tnfα* transcript abundance.

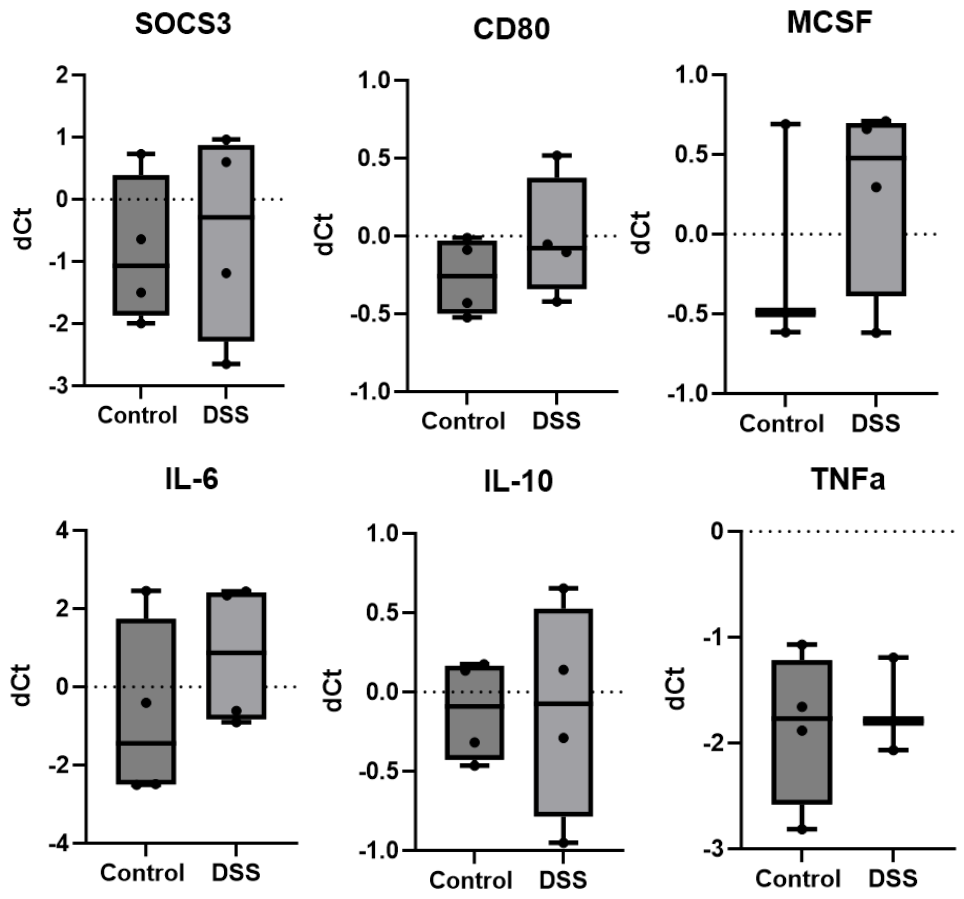

Figure 3.10 Gene transcript abundance differences between mouse macrophages treated with and without DSS. dCt = delta Ct. Calculated by subtracting the Ct values of the housekeeping gene from the Ct values of the gene of interest.

3.4 ELISA Assay

Unfortunately, the ELISA assay showed that most cytokines and chemokines had little to no differential expression across treatments in either the control or DSS-treated mice. The assay did not detect expression of GM-CSF, IFN-γ, or IL-17A. The cytokine IL-13 (HOV: p=0.033*) was significantly more highly expressed in the LPS and pre-treatment samples relative to the control (KW: p=0.036*), however no other protein was statistically differently expressed across any treatment. The anti-inflammatory cytokine IL-10 was not differentially expressed across the various treatments. IL-6 was somewhat more highly expressed in the LPS sample (Figure 3.11).

Similar to the control mouse samples, the ELISA assay showed that most cytokines and chemokines had little to no differential expression across treatments in DSS-treated murine macrophages. IL-10 protein levels were barely detectable. IL-1α (HOV: p=0.002**) was

significantly upregulated in the pre-treated samples compared to the control samples (KW: p=0.034*), while in the LPS-treated samples, expression was somewhere in between. LIX was significantly downregulated the LPS-treated samples compared to the control samples (KW: p=0.039*), while the pre-treated samples were similarly expressed to the LPS-treated samples. TNF-α was significantly upregulated in the co-treated samples (KW: p=0.017*), while it was visibly higher expressed in the LPS-treated samples (Figure 3.12).

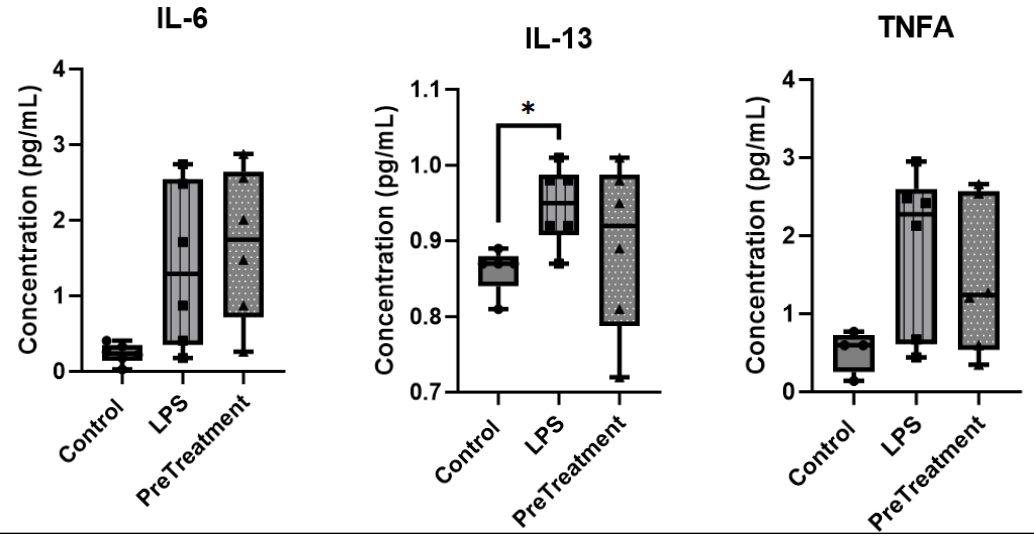

Figure 3.11 Expression of IL-6, IL-13, and TNF-α across different treatments in control mouse macrophages as measured via ELISA assay. dCt = delta Ct. Calculated by subtracting the Ct values of the housekeeping gene from the Ct values of the gene of interest.

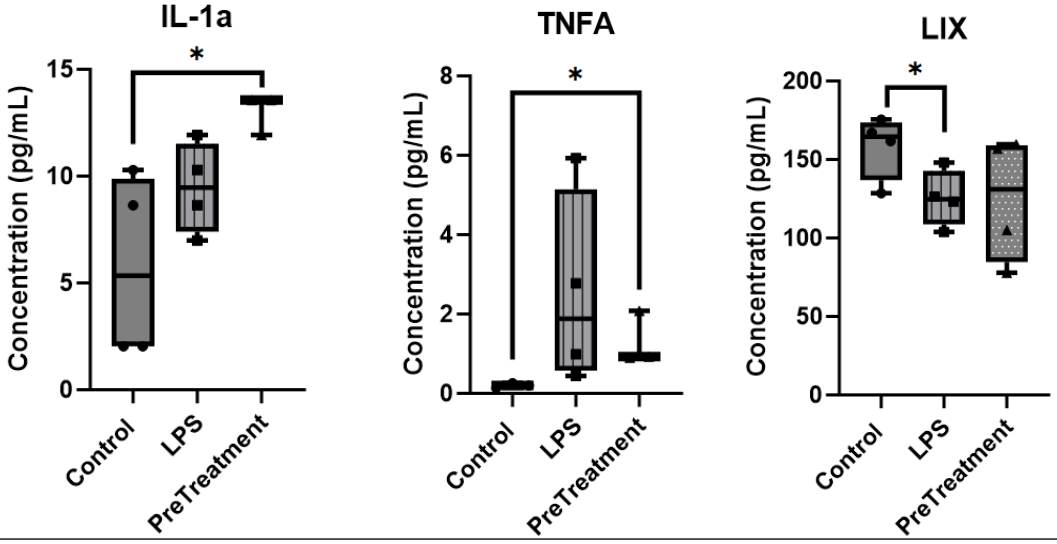

Figure 3.12 Expression of IL-1α, LIX, and TNF-α across different treatments in DSS-treated mouse macrophages as measured via ELISA assay. dCt = delta Ct. Calculated by subtracting the Ct values of the housekeeping gene from the Ct values of the gene of interest.

Discussion

4.1 The Effects of DSS on the Murine Spleen

While performing the mouse experiment, I noticed that around half of the DSS-treated mouse spleens were plagued with large black blood clots, while none of the control mice had this issue. The fact that these splenic blood clots were clearly visible to the naked eye was a sure sign that the DSS treated mice were not just suffering from colitis, but from hyposplenism as well. The Prussian blue analysis and the qPCR analysis provided weak evidence for hyposplenism, however stronger evidence was present in the hematological analysis and the RNA-seq analysis.

4.1.1 Hyposplenism and DSS-Induced Colitis

It is well documented that patients suffering from hyposplenism are at increased risk for arterial and venous thrombosis, blood clots which result in blood vessel blockages (Thomsen et al., 2010). Thrombosis and inflammation are highly correlated conditions, which often result in thrombo-inflammation (Kohli et al., 2022). Murotomi et al. (2016) found that high levels of splenic iron are associated with obesity and diabetes in mice, suggesting further evidence for a link between splenic iron levels and inflammation. Therefore, we decided that a Prussian blue stain would prove adequate as a determiner of hyposplenism, since blood clots indicate a significant increase in ferric ion, reacting with potassium ferrocyanide to form the characteristic blue pigment (Ghio and Roggli, 2021). We found no noticeable difference in the level of ferric iron between the control and DSS-treated spleens across the organ generally, as blood coagulation tends to be located separately from inflammation (Kohli et al., 2022). However, one DSS-treated splenic blood vessels was detected, which showed extreme levels of iron. Several blood vessels were detected in control spleens, none of which showed iron expression. This indicates the presence of thrombosis in the DSS-treated spleens, and therefore hyposplenism, as a direct result of acute exposure to DSS, at least in this one spleen. Additionally, the spleen containing evidence of thrombosis was covered in black dots, possibly the remnants of a blood clot, indicating further evidence of hyposplenism. This is a purely observational result and is not statistically supported.

In contrast to the Prussian blue stain, the hematological analysis provided far stronger evidence of hyposplenism as a result of DSS-induced colitis. Few Howell-Jolly bodies and hypochromic erythrocytes were found in the control mouse blood smears, however they were

common in the DSS-treated blood smears. Patients suffering from asplenia and hyposplenism are more prone to infections as they have a reduced number of circulating MBCs (Lenti et al., 2020), meaning that a reduced level of MBC markers may indicate the presence of hyposplenism. Additionally, *Il-1β* was significantly more highly expressed in the control mice than in the DSS-treated mice, which may be surprising given that *Il-1β* is traditionally classified as a pro-inflammatory cytokine. However, in 2022, Eislmayr et al. reported that IL-1β is crucial for splenic homeostasis, and that IL-1β deficiency was correlated with extreme inflammatory conditions in the colon. Additionally, IL-1α deficiency resulted in a weaker inflammatory state (Eislmayr et al., 2022). It therefore follows that the lack of *Il-1β* expressed in the DSS-treated murine spleens is indicative of splenic dysbiosis and hyposplenism.

Tgfb1 is a growth factor which is associated with balance of the immune response in the spleen via inducing Treg differentiation (Wang et al., 2022). It is therefore expected that *Tgfb1* transcript abundance was somewhat reduced in the DSS-treated mice than in the control mice, as DSS induces dysregulation. Additionally, it is of note that the homogeneity of variances test showed that the DSS-treated spleens expressed *Tgfb1* more variably than control spleens, just shy of statistical significance. While no significant difference in average transcript abundance was seen, higher variability of transcript abundance of *Mcsf*, *Mig*, and *Ip-10* were all observed in the DSS-treated spleens compared to the control spleens, albeit insignificantly in *Ip-10* but significantly for *Mcsf* and especially *Mig*. Much like the variable transcript abundance of *Tgfb1*, this is likely also a result of splenic dysfunction. Taken together with the histological and hematological results, our data indicates that DSS-induced colitis results in hyposplenism in a mouse model. This likely explains certain qPCR results, specifically the transcript abundance of M1 and M2 macrophage markers in the DSS-treated spleens as described below in Section 4.2.1.

4.1.2 RXFP4 and the Spleen

RXFP4 was significantly more highly expressed in the control macrophages of control mice than in the control macrophages of DSS-treated mice. This is consistent with Vahkal et al. (2021) who found that *Rxfp4* was downregulated in splenic macrophages of mice suffering from colitis. Additionally, we found that *Rxfp4* transcript abundance was more variable in the DSS-treated mice than in the control mice. Taken together, these results suggest that DSS significantly reduces the transcript abundance of *Rxfp4* to varying degrees in mice. These results indicate that

the anti-inflammatory properties of INSL5 may not be as effective in DSS treated mice since it decreased the transcript abundance of INSL5's cognate receptor. At first this seemed to explain the lack of variation amongst DSS-treated samples, however *Rxfp4* was significantly more highly expressed in the LPS-treated macrophages of DSS-treated mice than in LPS-treated macrophages of control mice. It is possible that RXFP4 is upregulated to combat inflammation. Additionally, *Rxfp4* was not significantly differentially expressed between the macrophages of control and DSS-treated mice in the co-treatment or pre-treatment groups. This suggests that INSL5 has homeostatic properties on RXFP4 expression, working to offset the damaging effects of DSS, however seemingly having no effect in counteracting the damaging effects of LPS. Or, perhaps INSL5 works in tandem with LPS to increase the expression of RXFP4. Regardless, it is evident that the lack of effect of INSL5 on the DSS-treated samples was not merely due to a downregulation of its receptor. Additionally, LPS had little to no effect on the DSS-treated samples. Taken together with the results of the histological, hematological, and qPCR data, it appears that DSS exposure primarily affects splenic filtering function rather than immune function, causing LPS and INSL5 treatments to have little to no effect.

Rather than directly causing intestinal inflammation, DSS damages the lining of the colonic epithelial monolayer, allowing pathogens from the lumen to enter the mucosa (Eichele and Kharbanda, 2017). The bacteria and antigens disseminate from the mucosa into the underlying tissue, eliciting an inflammatory response from the immune system (Eichele and Kharbanda, 2017). The mechanics by which LPS cause inflammation are entirely different. Lipid A, the most conserved structure of LPS, binds to TLR-4, which upregulates the expression of pro-inflammatory cytokines (Bertani and Ruiz, 2018). It is possible that *Rxfp4* may be downregulated by DSS and upregulated by LPS as a result of these different mechanisms, or it may be a difference in responses to acute vs chronic inflammation. It is also possible that these results are the result of an *in vivo* vs *in vitro* difference, as mice were exposed to DSS in their drinking water while splenic murine macrophages were directly exposed to LPS post-sacrifice. While these are possible explanations, the most likely reason for this difference is simply splenic dysfunction as a result of DSS-induced colitis.

4.2 Control Mouse Transcript Data – *Il-6, Il-10,* and *Cd80*

There were significant differences in mRNA transcript abundance of *Il-6, Tnf-α, Il-10,* and *Rxfp4* across treatments in the control cohort. *Il-6* had only a marginally higher average transcript abundance in the LPS-treated samples compared to the control and co-treated samples, however interestingly, it was significantly more highly expressed in the pre-treated samples than in the control or co-treatment samples. While INSL5 may have had some downregulatory effect on *Il-6* in the co-treated samples, it seems to have upregulated *Il-6* in the pre-treated samples. While *Il-6* is traditionally characterized as a pro-inflammatory marker, its role as a homeostatic cytokine has been established for decades, however its anti-inflammatory effects are not well understood (Andres-Hernando et al., 2017, Xing et al., 1998). *Il-6* elicits pro or anti-inflammatory immune responses depending on the cells, organs, and diseases studied (Andres-Hernando et al., 2017). Xing et al. (1998) reported that *Il-6* regulates the transcript abundance of pro-inflammatory cytokines, but not anti-inflammatory cytokines. However, in 2017, Andres-Hernando et al. reported the first evidence that *Il-6* does regulate the transcript abundance of the most potent anti-inflammatory cytokine, *Il-10*. They also reported that the organ in which *Il-6* upregulation of *Il-10* mainly occurs is the spleen (Andres-Hernando et al., 2017). They found that *Il-10* was not upregulated in *Il-6*$^{-/-}$ mice, indicating that *Il-6* upregulates *Il-10* in some splenocytes in order to limit *Il-6*-mediated inflammation (Andres-Hernando et al., 2017). This may explain the heightened transcript abundance of *Il-6* in the pre-treated samples, however this does not explain the slightly reduced transcript abundance of *Il-6* in the co-treated samples compared to the LPS-treated samples. Perhaps INSL5 reduces *Il-6* transcript abundance contemporaneous with inflammatory conditions like colitis, however following pre-treatment, *Il-6* seems to have both pro and anti-inflammatory effects based on *Il-10* transcript abundance.

Il-10 was significantly more highly expressed in the LPS-treated samples compared to the control samples, despite being an anti-inflammatory hormone. The average levels of *Il-10* mRNA in the co-treated and pre-treated samples were between that of the control and LPS-treated samples. Given the high level of *Il-6* transcript abundance in the pre-treated samples, a low level of *Il-10* would indicate that *Il-6* was secreted as a pro-inflammatory hormone, while a high level of *Il-10* would indicate that *Il-6* was secreted as an anti-inflammatory hormone. The fact that *Il-10* is expressed at similar levels in the co and pre-treated samples while *Il-6* is not suggests that the high transcript abundance of *Il-6* takes on both pro and anti-inflammatory properties. In terms of the slightly elevated *Il-10* transcript abundance in the LPS-treated

samples, Andres-Hernando et al. (2017) reported increased *Il-10* transcript abundance in the murine spleen following acute kidney injury. The fact that *Il-10* was upregulated in the LPS treatment suggests that it downregulated pro-inflammatory cytokines to a greater degree in the LPS treatment than in the other treatments. This may explain the apparent lack of effect in many co-treated and pre-treated samples, as they lacked the aid off *Il-10.* Additionally, the pre-treatment may have been especially offset by the increased *Il-6* transcript abundance in the pre-treated samples. It is likely that without the heightened transcript abundance of *Il-6* in the pre-treated mice, the transcript abundance levels of the other cytokines may have been more similar to their transcript abundance levels in the co-treatment samples. An examination of the surface marker *Cd80* may provide some insight into the nature of *Il-6* and *Il-10* transcript abundance in the pre-treated samples.

The gene most significantly differentially expressed across treatments in the control cohort was *Cd80,* which significantly more highly expressed in the LPS treatment than in the control and co-treated samples. This indicates that INSL5 did downregulate *Cd80* in the co-treated samples. However, this effect seems to be either far weaker or absent in the pre-treated samples. Jiménez-Uribe et al. (2019) reported a significant positive correlation between *Cd80* and *Il-6* transcript abundance in macrophages co-stimulated with LPS and the human dialyzable leucocyte extract, Transferon®. While it is possible that *Il-6* upregulates *Cd80* or vice-versa, no causal link has been found. While *Il-6* is a complicated cytokine with pro or anti-inflammatory functions, *Cd80* is more straightforwardly an M1 associated protein. However, it is important to note that M1 and M2 are blurred categories with much overlap. The high transcript abundance of *Cd80* in pre-treated cells compared to co-treated and especially control cells indicates that pre-treated cells were polarized towards the M1 phenotype, therefore INSL5 had little to no anti-inflammatory effect on pre-treated cells. However, given the low *Cd80* transcript abundance found in co-treated cells, the immunological effects of INSL5 appear to be contemporaneous with inflammation, but not preventative. That being said, I still hold that a significant portion of *Il-6* transcript abundance is anti-inflammatory, as if it was all or mostly pro-inflammatory, *Il-10* transcript abundance should be far lower in the pre-treatment samples than it is.

4.2.1 Remaining qPCR Data

INSL5 had no effect on *Tnf-α* transcript abundance as it was significantly highly expressed in the co-treated samples compared to the control samples, and the LPS and pre-treated samples had a similar transcript abundance level compared to the co-treated samples. In fact, average *Tnf-α* transcript abundance was slightly higher in the co-treated samples than in the LPS or pre-treated samples. It therefore seems likely that INSL5 had no effect on the transcript abundance of *Tnf-α*, whether in terms of combating or preventing inflammation.

As we expected INSL5 to have anti-inflammatory properties via binding to RXFP4, we anticipated that *Rxfp4* would serve as an anti-inflammatory marker. Therefore we tested *Rxfp4* to determine whether or not INSL5 would impact the transcript abundance of its cognate receptor. The transcript abundance of *Rxfp4* was significantly reduced in the LPS treatment samples, while average transcript abundance in the co-treated and pre-treated samples was only slightly higher. This indicates that INSL5 had little to no effect on the transcript abundance of its cognate receptor.

Until now, the downstream effects of RXFP4 on SOCS3 had not been studied. There were no significant transcript abundance differences in *Socs3* across various treatments, however average mRNA levels were lower in the control samples than in other treatments, indicating that INSL5 had no effect on the regulation of *Socs3* transcript abundance. *Socs3* is upregulated by M1 macrophages and considered a reliable marker in diagnosing both acute and chronic inflammation, which, along with the *Cd80* results, further indicate that the pre-treated cells were polarized to the M1 phenotype (Chávez-Galán et al., 2015). However, *Socs3* transcript abundance is increased upon stimulation by both pro and anti-inflammatory cytokines including *Il-6, Il-10, Il-12, Tnf-α* and *Ifn-γ*, and by LPS (Miyanaka et al., 2007, Li et al., 2012). SOCS3 restricts the expression of IL-6 but not IL-10, further demonstrating its anti-inflammatory properties (Yoshimura et al., 2012). Yoshimura et al. (2012) reported SOCS3 expression increased in a DSS-treated mouse model, in which it was found to reduce inflammation, there it stands to reason that LPS may induce the same response from SOCS3. SOCS3 negatively regulates the signalling of IFN-γ, which is important in polarizing macrophages to the M1 phenotype, indicating that while SOCS3 is an M1 marker, it is expressed during periods of inflammation as a homeostatic protein (Yoshimura et al., 2012). The *Tnf- α* and *Socs3* results together suggest that the co-treated cells were in a state of inflammation, despite the reduction of M1 markers *Il-6* and *Cd80.*

None of the treatments across the DSS-treated cohort resulted in significantly different gene transcript abundance, and our RNA-seq data suggests that this was because the spleen was preoccupied with maintaining filtering function rather than immune function. Overall, the genetic evidence that INSL5 has an immunological effect in the spleen is sparse, but not non-existent. As discussed previously, INSL5 exerts homeostatic effects on *Cd80* and *Il-6* when co-treated with LPS, however when pre-treated, transcript abundance of *Cd80* and *Il-6* are upregulated. It is likely that INSL5 pre-treatment does not prime naïve splenic macrophages efficiently enough to polarize to an M2 phenotype, and that LPS is able to polarize several macrophages to an M1 phenotype even after 12 hours of INSL5 exposure. The fact that INSL5 had an effect on the transcript abundance of *Il-6, Cd80,* and possibly *Il-10,* but no (or extremely minor) effect on the transcript abundance of *Tnf-α, Rxfp4,* and *Socs3* indicates that INSL5 works via specific pathways. Therefore, it cannot be concluded that INSL5 polarizes macrophages to an M2 phenotype in the murine spleen, as it would have a more ubiquitous effect on the cells, and instead is only a small player in splenic homeostasis. Further research is required to determine the downstream pathways activated by INSL5 to determine which specific downstream pathways of *Rxfp4* it activates in splenic macrophages.

4.3 RNA-SEQ Data

Two of the genes upregulated in control mice were *Fgf21* and *Foxa3,* both of which have been shown to be important for spleen function (Liu et al., 2022, Yu et al., 2023). Additionally, *Fgf21* has been shown to reduce spleen weight and has been reported to function in maintaining a healthy weight (Liu et al., 2022).

Amongst the immune-associated genes was *Socs3,* which was significantly upregulated in the DSS-treated mice, further cementing its role as a pro-inflammatory marker. Additionally, *Cd177* was significantly upregulated in the DSS-treated mice, which indicates that DSS increases neutrophil activity in the spleen, as Cd177 is found exclusively on neutrophils (Demaret et al., 2016). Demaret et al. (2016) reported that out of 364 upregulated and 328 downregulated genes differentially expressed as a result of septic shock, *Cd177* was the most dysregulated (increased significance) out of all of them. *Cd177* plays a role in both the maturation of neutrophils as well as chemotaxis (Demaret et al., 2016), indicating that a major mechanism of DSS-induced inflammation is via boosting both of these functions.

Thompson et al. (2010) reported evidence that claudin family gene claudin 13 (*Cldn13*) has a role in stress-induced erythropoiesis. The erythropoietic genes *Tal1, Trim10, E2f2, Rhd, Gypa,* and *Tmcc2* all cluster with *Cldn13* on microarrays examining erythrocyte development (Thompson et al., 2010). *Tal1, Trim10,* and *E2f2* are important regulators of erythropoiesis, *Rhd* and *Gypa* are erythropoietic membrane proteins, and *Tmcc2* is strongly associated with erythrocyte volume (Thompson et al., 2010). Additionally, *Cldn13* clusters with *Cdca8, Cdkn2d,* and *Cenpk,* all of which are indirectly associated with erythropoiesis (Thompson et al., 2010). The RNA sequencing data revealed that *Cldn13, Trim10, Rhd,* and *Gypa* are all significantly upregulated in the DSS-treated spleen samples compared to the control spleens. Only *E2f2* and *Cdkn2d* showed no difference. This indicates that DSS substantially contributes to the stress-induced erythropoietic pathway, as the spleen becomes a major erythropoietic organ in response to stress (Chen et al., 2021).

4.4 Protein Evidence for INSL5 as an Immunological Hormone in the Spleen

There were several complications that arose when collecting protein data, as discussed below in Section 4.5. As a result, the ELISA data should be viewed with skepticism, as it is skewed by human and technical errors. Therefore, I have overwhelmingly based my analysis of the effect of INSL5 in the spleen on the qPCR and RNA-seq data, while treating the ELISA data as secondary.

We collected cell culture samples from the control, LPS, and pre-treated samples in both cohorts, but not co-treated samples for the ELISA assay. As a result, there was very little effect of INSL5 found in either cohort. In the control cohort, IL-13 was significantly highly expressed in the LPS-treated samples compared to the control samples, while it was variably expressed in the pre-treatment samples, suggesting that perhaps some macrophage cultures were more responsive to INSL5 treatment than others. Average levels of IL-4, IL-6, and IL-12p70 were somewhat higher in both LPS and pre-treated samples than in the control samples, indicating that LPS increased expression of these proteins while INSL5 pre-treatment had no effect. TNF-α was noticeably more highly expressed in the LPS-treated samples than in the control samples, while the average protein level in the pre-treatment sample was somewhere in the middle, indicating that INSL5 had an anti-inflammatory effect. These results are not statistically significant, however.

The DSS-treated samples interestingly showed more variation of protein levels across treatments than the control cohort did. Statistically different levels of LIX, Il-1α, and TNF-α were detected across treatments. LIX was significantly less expressed in the LPS-treated samples than in the control samples, with the pre-treatment samples having a similar albeit more varied level of LIX protein, despite LIX being an LPS-induced protein. LIX is also a homeostatic protein, which may be the reason why it is downregulated in cells exposed to both DSS and LPS. However, in the control cohort, LIX was also expressed less in the LPS-treated samples on average, albeit to a far lower degree, while the average expression in the pre-treated samples was even lower. Perhaps INSL5 downregulates the expression of LIX in situations of moderate inflammation, but not extreme inflammation.

Il-1α was significantly more highly expressed in the pre-treated samples compared to the control samples, with the LPS-treated samples landing in the middle. This suggests that INSL5 may have pro-inflammatory properties in some contexts. TNF-α was significantly highly expressed in the pre-treatment samples compared to the control samples, with the LPS-treated samples also having notably higher protein levels compared to the control samples. In fact, the average level of TNF-α was notably higher in the LPS-treated samples than in the pre-treated samples, however due to the much greater level of variance within the LPS-treated samples, no significance was observed. This suggests that INSL5 may have some role in regulating the expression of TNF-α.

Confusing matters is the fact that, while INSL5 had a far more noticeable effect on the control mouse macrophages according to the qPCR results, the ELISA results suggest that INSL5 had a greater impact on the DSS-treated mouse macrophages. Not every mRNA strand transcribed is translated into a protein, therefore these results are not inherently contradictory. The ELISA results may also be skewed as a result of human and technical error.

As the RNA-Seq data revealed that splenic erythropoietic function was more highly affected than immune function, these results are not unexpected. The spleen functions in both erythrocyte development in addition to it's immune properties, and it seems as though the spleen allocates energy to working towards erythropoietic homeostasis. The erythropoietic effects of colitis on the spleen is a topic that has not previously been explored. This research may generate health sciences funding to further explore the effects of GI disorders on splenic erythrocyte function.

4.5 Limitations

The nature of splenic macrophages provided a severe limitation to the cell culture experiment. As mDCs and macrophages arise from precursor cells in the bone marrow, they do not replicate (Lewis et al., 2011). Murine sDCs die rapidly *in vitro,* with only 30% viability after 24 hours (Chen et al., 2007). Ten million cells were plated per well and left to adhere for sixteen hours before being treated. INSL5 was added to the pre-treated samples for twelve hours, and then the samples were treated and left to incubate for twenty four hours. By the time RNA and cell culture medium was harvested, 52 hours had passed, and the vast majority of macrophages had died. As a result, very little usable RNA was collected, and the cell culture medium needed to be concentrated prior to analysis.

Additionally, there were complications with the culture media used for ELISA, and as such, it is to be viewed as a secondary pool of data to be viewed with extreme skepticism. Due to the low concentration of protein in the cell culture media, it needed to be concentrated via filtration. Unfortunately some of the filters broke during centrifugation resulting in some samples not being filtered properly. As a result, samples were sent with unequal concentrations. This more than likely contributed to the highly variable and confusing ELISA data. Finally, despite our efforts to concentrate the samples, EVE Technologies reported very little expression for most markers.

4.6 Future Directions

Very little research has been conducted which investigates the immunological function of INSL5 and RXFP4. The immunological effects of INSL5 on splenic macrophages appear to be minimal. Vahkal et al. (2021) reported that RXFP4 is expressed on sDCs which monitor the intestinal immune system, and therefore sDCs may be more promising to study the immunological effects of INSL5 in the gut in the context of UC. They showed that INSL5 was significantly upregulated in the murine colon and rectum in UC, while RXFP4 was shown to be downregulated in the murine colon and rectum in UC (Vahkal et al., 2021). Consistent with the results of this thesis, they also found RXFP4 was downregulated in the splenic macrophages of mice suffering from colitis (Vahkal et al., 2021). Additionally, the function of RXFP4 on splenic macrophages and DCs may be to effect homeostatic properties in the gut.

According to the database gutcellatlas.org, RXFP4 is expressed in at least six gut cell types, including IgA plasma cells, ECs, microfold (M)-cells, colonocytes, Paneth cells, and goblet cells, and it may exert other immunomodulatory effects through these cell types. Large quantities of IgA are secreted at the surface of the mucosa by IgA^+ plasma cells to prevent the invasion of pathogens and restricting the entry of commensal microbes to the sub-epithelium (Isho et al., 2021). Around 95% of the body's serotonin is secreted by ECs, which are involved in colonic propulsion (Diwakarla et al., 2017). M-cells are a type of IEC located in peyer's patches, which function to monitor and transport antigens and microbes to the lumen of the sub-epithelium, allowing immune responses to be initiated (Xiang et al., 2024). Colonocytes effect the flora of the gut, shifting between homeostasis and dysbiosis and strengthening the intestinal barrier via modulation of mucosal bacteria (Ge et al., 2022). Paneth cells are similar to neutrophils, in that they release antimicrobial peptides in the form of granules into the crypt of the lumen to regulate the composition of the intestinal microbiota (van Es and Clevers, 2014). Goblet cells are responsible for secreting mucus which forms the protective layer in the gut, which is involved in immunoregulation, selectively trapping harmful microbes and enabling immune responses (Johansson and Hansson, 2022). The fact that all of these common intestinal cell types are involved in the immune system in some form suggests that RXFP4 signalling may play a role in immunological homeostasis on these cells. This hypothesis is strengthened by the high expression of INSL5 in the distal colon and rectum (Grosse et al., 2014). Perhaps INSL5 has little effect on the macrophages of the spleen, however its effect on the various cell types of the gut has yet to be explored, and warrants further investigation.

Conclusion

Since 1999 when Conklin et al. discovered INSL5, it has been hypothesized to be involved with the immune system. Since then, only our lab has investigated this proposition, and recently we have found evidence suggesting that INSL5 has a homeostatic effect in the gut (Vahkal et al., 2021). In this thesis, I investigated the effects of DSS-induced colitis on the spleen and the potential homeostatic effects of INSL5 on splenic macrophages. My results are consistent with the literature regarding the spleen-gut axis and the link between hyposplenism and GI disorders. The spleen and gut are intimately linked primarily via the vagus nerve, and there is a correlation between splenic dysfunction and chronic gut inflammation. Our results also suggest that DSS-induced colitis results in splenic dysfunction via the spleen-gut axis.

The results obtained in this thesis demonstrated an anti-inflammatory effect of INSL5 in the spleen. Our results indicate that *Insl5* works towards an anti-inflammatory state by impacting the transcript abundance of certain pro and anti-inflammatory markers, while having no effect on others. It was shown to prevent inflammation with even less efficiency than it combats inflammation, and in some cases, even upregulates pro-inflammatory marker *Il-6.* This increased transcript abundance of *Il-6* in the pre-treated samples is likely the reason why INSL5 pre-treatment was ineffective in shifting cytokine transcript abundance to favour anti-inflammatory cytokines, however, the reason why *Il-6* was upregulated is unclear. The reduced transcript abundance of *Rxfp4* in all samples treated with LPS implies that RXFP4 has anti-inflammatory properties in the spleen, and therefore so does INSL5. Finally, the RNA-Seq data suggested that DSS has a greater effect on the erythropoietic function of the spleen rather than its immune function. Taken together, it is likely that INSL5 has a minimal role in the immunological properties of the spleen and a greater role in other areas of splenic function. These are not altogether unexpected results, as Vahkal et al. (2021) similarly found that INSL5 downregulated some pro-inflammatory cytokines and chemokines while upregulating others. Vahkal et al. (2021) also reported more significant effects of INSL5 in the gut, however. While INSL5 proved inefficient at alleviating hyposplenism, INSL5 agonists such as INSL5-A13 are shaping up to be a promising treatment for gut disorders. More research into the potential functions of INSL5 is required. If future studies confirm a homeostatic immunological role for INSL5, then it may generate health sciences funding, as well as the engineering of RXFP4 agonists to treat IBD and other forms of chronic inflammation.

References

Albertsen, L., Østergaard, S., Paulsson, J.F., Norrild, J.C. and Strømgaard, K. 2013, "A parallel semisynthetic approach for structure-activity relationship studies of peptide YY", *ChemMedChem,* vol. 8, pp. 1505-1513.

Almeida-Pinto, N., Dschietzig, T.B., Brás-Silva, C. and Adão, R. 2023, "Cardiovascular effects of relaxin-2: therapeutic potential and future perspectives", *Clinical Research in Cardiology*. doi.org/10.1007/s00392-023-02305-1

Andres-Hernando, A., Okamura, K., Bhargava, R., Kiekhaefer, C.M., Soranno, D., Kirkbride-Romeo, L.A., Gil, H.W., Altmann, C. and Faubel, S. 2017, "Circulating IL-6 upregulates IL-10 production in splenic $CD4^+$ T cells and limits acute kidney injury–induced lung inflammation", *Kidney International,* vol. 91, pp. 1057-1069.

Andryukhova, E.S., Tashireva, L.A., Vtorushin, S.V., Zavyalova, M.V. and Perelmuter, V.M. 2022, "Spleen macrophages: Population composition and functions", *Cell and Tissue Biology*, vol. 16, no. 4, pp. 291-301.

Ang, S.Y., Hutchinson, D.S., Patil, N., Evans, B.A., Bathgate, R.A.D., Halls, M.L., Hossain, M.A., Summers, R.J. and Kocan, M. 2017a, "Signal transduction pathways activated by insulin-like peptide 5 at the relaxin family peptide RXFP4 receptor", *British Journal of Pharmacology,* vol. 174, pp. 1077-1089.

Ang, S.Y., Hutchinson, D.S., Evans, B.A., Hossain, M.A., Patil, N., Bathgate, A.D., Kocan, M. and Summers, R.J. 2017b, "The actions of relaxin family peptides on signal transduction pathways activated by the relaxin family peptide receptor RXFP4", *Naunyn-Schmiedeberg's Arch Pharmacol,* vol. 390, pp. 105-111.

Ang, S.Y., Evans, B.A., Poole, D.P., Bron, R., DiCello, J.J., Bathgate, R.A.D., Kocan, M., Hutchinson, D.S. and Summers, R.J. 2018, "INSL5 activates multiple signalling pathways and regulates GLP-1 secretion in NCI-H716 cells", *Journal of Molecular Endocrinology,* vol. 60, no. 3, pp. 213-224.

Arnoldini, M., Cremer, J. and Hwa, T. 2018, "Bacterial growth, flow, and mixing shape human gut microbiota density and composition", *Gut Microbes,* vol. 9, no. 6, pp. 559-566.

Arroyo, J.I., Hoffmann, F.G., Good, S. and Opazo, J.C. 2012, "INSL4 pseudogenes help define the relaxin family peptide repertoire in the common ancestor of placental mammals", *J Mol Evol,* vol. 75, pp. 73-78.

Atri, C., Guerfali, F.Z. and Laouini, D. 2018. "Role of human macrophage polarization in inflammation during infectious diseases", *Int J Mol Sci,* vol. 19.

Avellaneda, N., Coy, C.S.R., Fillmann, H.S., Saad-Hossne, R., Muñoz, J.P., García-Duperly, R., Bellolio, F., Rotholtz, N., Rossi, G., Marquez V, J.R., Cillo, M., Lacerda-Filho, A.,

Carrie, A., Maruyama, B.Y., Fillmann, L.S., Craveiro, M.M.S., Ferro, E., Londoño-Schimmer, E., Iglesias, A., Harriott, C.B., Campana, J.P., Estrada, D.L., Balachandran, R. and Kotze, P.G. 2023, "Risk factors for major complications after surgical treatment of primary ileocecal Crohn's disease. A multicentric Latin American experience", *Cirugía Española (English Edition).*

Awasthi, N., Liongue, C. and Ward, A.C. 2021, "STAT proteins: a kaleidoscope of canonical and non-canonical functions in immunity and cancer", *Journal of Hematology and Oncology,* vol. 14, no. 198.

Bathgate, R.A.D., Halls, M.L., van der Westhuizen, E.T., Callander, G.E., Kocan, M. and Summers, R.J. 2013, "Relaxin family peptides and their receptors", *Physiol Rev,* vol. 93, pp. 405-480.

Bathgate, R.A.D., Samuel, C.S., Burazin, T.C.D., Layfield, S., Claasz, A.A., Reytomas, I.G.T., Dawson, N.F., Zhao, C., Bond, C., Summers, R.J., Parry, L.J., Wade, J.D. and Tregear, G.W. 2002, "Human Relaxin gene 3 (*H3*) and the equivalent mouse Relaxin (*M3*) gene", *The Journal for Biological Chemistry,* vol. 277, no. 2, pp. 1148-1157.

Belgi, A., Bathgate, R.A.D., Tregear, G.W., Wade, J.D. and Hossain, M.A. 2013, "Preliminary structure-function relationship studies on insulin-like peptide 5 (INSL5)", *Int J Pept Res Ther,* vol. 19, pp. 71-79.

Belgi, A., Hossain, M.A., Shabanpoor, F., Chan, L., Zhang, S., Bathgate, R.A.D., Tregear, G.W. and Wade, J.D. 2011, "Structure and function relationship of murine insulin-like peptide 5 (INSL5): free C-terminus is essential for RXFP4 receptor binding and activation", *Biochemistry,* vol. 50, pp. 8352-8361.

Bertani, B. and Ruiz, N. 2018, "Function and biogenesis of lipopolysaccharides", *EcoSal Plus,* vol. 8, no. 1, pp 1-33.

Berthoud, H.R. and Powley, T.L. 1993, "Characterization of vagal innervation to the rat celiac, suprarenal and mesenteric ganglia", *Journal of the Autonomic Nervous System,* vol. 42, no. 2, pp. 153-169.

Bhattacharya, S. and Aggarwal, A. 2019, "M2 macrophages and their role in rheumatic diseases", *Rheumatology International,* vol. 39, pp. 769-780.

Blyth, A.J., Kirk, N.S. and Forbes, B.E. 2020, "Understanding IGF-II action through insights into receptor binding and activation", *Cells,* vol. 9, no. 2276.

Bohlson, S.S., O'Conner, S.D., Hulsebus, H.J., Ho, M.M. and Fraser, D.A. 2014, "Complement, C1q, and C1q-related molecules regulate macrophage polarization", *Frontiers in Immunology,* vol. 5, pp. 1-7.

Bohórquez, D.V., Chandra, R., Samsa, L.A., Rigna, S.R. and Liddle, R.A. 2011, "Characterization of basal-pseudopod-like processes in ileal and colonic PYY cells", *J Mol Hist,* vol. 42, pp. 3-13.

Borovikoka, L.V., Ivanova, S., Zhang, M., Yang, H., Botchkina, G.I., Watkins, L.R., Wang, H., Abumrad, N., Eaton, J.W. and Tracey, K.J. 2000, "Vagus nerve stimulation attenuates the systemic inflammatory response to endotoxin", *Nature,* vol. 405, pp. 458-462.

Brisson, B.K. and Barton, E.R. 2013, "New modulators for IGF-I activity within IGF-I processing products", *Frontiers in Endocrinology,* vol. 4, no. 42.

Browning, K.N., Verheijden, S. and Boeckxstaens, G.E. 2017, "The vagus nerve in appetite regulation, mood, and intestinal inflammation", *Gastroenterology,* vol. 152, pp. 730-744.

Burnicka-Turek, O., Shirneshan, K., Paprotta, I., Grzmil, P., Meinhardt, A., Engel, W. and Adham, I.M. 2009, "Inactivation of insulin-like factor 6 disrupts the progression of spermatogenesis at late meiotic prophase", *Endocrinology*, vol. 150, no. 9, pp. 4348-4357.

Burnicka-Turek, O., Mohamed, B.A., Shirneshan, K., Thanasupawat, T., Hombach-Klonisch, S., Klonisch, T. and Adham, I.M. 2012, "INSL5-deficient mice display an alteration in glucose homeostasis and an impaired fertility", *Endocrinology,* vol. 153, no. 10, pp. 4655-4665.

Chassaing, B., Aitken, J.D.,, Malleshappa, M. and Vijay-Kumar, M. 2015, "Dextran sulfate sodium (DSS)-induced colitis in mice", *Curr Protoc Immunol,* vol. 104.

Chávez-Galán, L., Olleros, M.L., Vesin, D. and Garcia, I. 2015, "Much more than M1 and M2 macrophages, there are also $CD169^+$ and TCR^+ macrophages", *Frontiers in Immunology,* vol. 6, pp. 1-15.

Chen, L., Wang, J., Liu, J., Wang, H., Hillyer, C.D., Blanc, L., An, X. and Mohandas, N. 2021, "Dynamic changes in murine erythropoiesis from birth to adulthood: implications for the study of murine models of anemia", *Blood Advances,* vol. 5, no. 1, pp. 16-25.

Chen, M., Huang, L., Shabier, Z. and Wang, J. 2007, "Regulation of the lifespan in dendritic cell subsets", *Mol Immunol,* vol. 44, no. 10, pp. 2558-2565.

Chen, Y., Deng, M., Chen, Z., Han, S., Chen, J., Zhang, H., Wang, Q., Jin, X., Liu, W. and Zhang, Z. 2022, "Insulin-like peptide 5 (INSL5) positively correlates with anti-Müllerian hormone (AMH) in women with polycystic ovary syndrome in a case-control study", *Journal of Ovarian Research,* vol. 15, no. 118.

Conklin, D., Lofton-Day, C.E., Haldeman, B.A., Ching, A., Whitmore, T.E., Lok, S. and Jaspers, S. 1999, "Identification of INSL5, a new member of the insulin superfamily", *Genomics,* vol. 60, pp. 50-56.

Demaret, J., Venet, F., Plassais, J., Cazalis, M.A., Vallin, H., Friggeri, A., Lepape, A., Rimmelé, T., Textoris, J. and Monneret, G. 2016, "Identification of CD177 as the most dysregulated parameter in a microarray study of purified neutrophils from septic shock patients", *Immunology Letters,* vol. 178, pp. 122-130.

Derewenda, U., Derewenda, Z., Dodson, G.G., Hubbard, R.E. and Korber, F. 1989, "Molecular structure of insulin: the insulin monomer and its assembly", *Br Med Bull,* vol. 45, no. 1, pp. 4-18.

Diwakarla, S., Bathgate, R.A.D., Zhang, X., Hossain, M.A. and Furness, J.B. 2020, "Colokinetic effect of an insulin-like peptide 5-related agonist of the RXFP4 receptor", *Neurogastroenterology & Motility,* vol. 32.

Diwakarla, S., Fothergill, L.J., Fakhry, J., Callaghan, B. and Furness, J.B. 2017, "Heterogeneity of enterochromaffin cells within the gastrointestinal tract", *Neurogastroenterol Motil,* vol. 29, e13101.

Egwuagu, C.E., Yu, C.R., Zhang, M., Mahdi, R.M., Kim, S.J. and Gery, I. 2002, "Suppressors of cytokine signaling proteins are differentially expressed in Th1 and Th2 cells: Implications for Th cell lineage commitment and maintenance", *The Journal of Immunology,* vol. 168, no. 7, pp. 3181-3187.

Eichele, D.D. and Kharbanda, K.K. 2017, "Dextran sodium sulfate colitis murine model: an indispensable tool for advancing our understanding of inflammatory bowel diseases pathogenesis", *World J Gastroenterol,* vol. 23, no. 33, pp. 6016-6029.

Eislmayr, K., Bestehorn, A., Morelli, L., Borroni, M., Walle, L.V., Lamkanfi, M. and Kovarik, P. 2022, "Nonredundancy of IL-1α and IL-1β is defined by distinct regulation of tissues orchestrating resistance versus tolerance to infection", *Sci Adv,* vol. 8, no. 9, eabj7293.

Epelman, S., Lavine, K.J. and Randolph, G.J. 2014, "Origin and functions of tissue macrophages", *Immunity,* vol. 41, no. 1, pp. 21-35.

Esteban-Lopez, M. and Agoulnik, A.I. 2020, "Diverse functions of insulin-like 3 peptide", *J Endocrinol,* vol. 247, no. 1.

Fernando, S.J.A., Wang, Q., Hay, D.L., Bathgate, R.A.D., Shepherd, P.R. and Lee, K.L. 2023, "Evidence that RXFP4 is located in enterochromaffin cells and can regulate production and release of serotonin", *Bioscience Reports,* vol. 43.

Foster, P.N. and Losowsky, M.S. 1987, "Hyposplenism–a review", *Journal of the Royal College of Physicians of London,* vol. 21, no. 3, pp. 188-191.

Ge, L., Qi, J., Shao, B., Ruan, Z., Ren, Y., Sui, S., Wu, X., Sun, X., Liu, S., Li, S., Xu, C. and Song, W. 2022, "Microbial hydrogen economy alleviates colitis by reprogramming

colonocyte metabolism and reinforcing intestinal barrier", *Gut Microbes,* vol. 14, no. 1, e2013764.

Geissmann, F., Manz, M.G., Jung, S., Sieweke, M.H., Merad, M. and Ley, K. 2010, "Development of monocytes, macrophages and dendritic cells", *Science,* vol. 327, no. 5966, pp. 656-661

Ghio, A.J. and Roggli, V.L. 2021, "Perls' Prussian blue stains of lung tissue, bronchoalveolar lavage, and sputum", *J Environ Pathol Toxicol Oncol,* vol. 40, no. 1, pp. 1-15.

Gill, S.R., Pop, M., DeBoy, R.T., Eckburg, P.B., Turnbaugh, P.J., Samuel, B.S., Gordon, J.I., Relman, D.A., Fraser-Liggett, C.M. and Nelson, K.E. 2006, "Metagenomic analysis of the human distal gut microbiome", *Science,* vol. 312, pp. 1355-1359.

Good, S., Yegorov, S., Martijn, J., Franck, J. and Bogerd, J. 2012, "New insights into ligand-receptor pairing and coevolution of relaxin family peptides and their receptors in teleosts", *International Journal of Evolutionary Biology,* vol. 2012.

Gribble, F.M. and Reimann, F. 2016, "Enteroendocrine cells: Chemosensors in the intestinal epithelium", *Annu Rev Physiol,* vol. 78, pp. 277-299.

Gribble, F.M. and Reimann, F. 2019, "Function and mechanisms of enteroendocrine cells and gut hormones in metabolism", *Nature Reviews,* vol. 15, pp. 226-237.

Grosse, J., Heffron, H., Burling, K., Hossain, M.A., Habib, A.M., Rogers, G.J., Richards, P., Larder, R., Rimmington, D., Adriaenssens, A.A., Parton, L., Powell, J., Binda, M., Colledge, W.H., Doran, J., Toyoda, Y., Wade, J.D., Aparicio, S., Carlton, M.B.L., Coll, A.P., Reimann, F., O'Rahilly, S. and Gribble, F.M. 2014, "Insulin-like peptide 5 is an orexigenic gastrointestinal hormone", *PNAS,* vol. 111, no. 30, pp. 11133-11138.

Gualdrón-Lopez, M., Díaz-Varela, M., Toda, H., Aparici-Herraiz, I., Pedró-Cos, L., Lauzurica, R., Lacerda, M.V.G., Femández-Sanmartín, M.A., Fernandez-Becerra, C. and del Portillo, H.A. 2021, "Multiparameter flow cytometry analysis of the human spleen applied to studies of plasma-derived EVs from *Plasmodium vivax* patients", *Frontiers in Cellular and Infection Microbiology,* vol. 11, 596104.

Gupta, V. 2013, "Glucagon-like peptide-1 analogues: An overview", *Indian Journal of Endocrinology and Metabolism,* vol. 17, no. 3, pp. 413-421.

Haugaard-Jōnsson, L.M., Hossain, M.A., Daly, N.L., Craik, D.J., Wade, J.D. and Rosengren, K.J. 2009, "Structure of human insulin-like peptide 5 and characterization of conserved hydrogen bonds and electrostatic interactions within the relaxin framework", *Biochem J,* vol. 419, pp. 619-627.

Hechter, D., Vahkal, B., Tiede, T. and Good, S.V. 2022, "Reviewing the physiological roles of the novel hormone-receptor pair INSL5-RXFP4: a protective energy sensor?", *Journal of Molecular Endocrinology,* vol. 69, no. 1, pp. 45-62.

Hecquet, C., Lefevre, G., Valtink, M., Engelmann, K. and Mascarelli, F. 2002, "Activation and role of MAP kinase-dependent pathways in retinal pigment epithelial cells: ERK and RPE cell proliferation", *Ophthalmology & Visual Science,* vol. 43, no. 9, pp. 3091-3098.

Hoehn, K.B., Pybus, O.G., Kleinstein, S.H. 2022, "Phylogenetic analysis of migration, differentiation, and class switching in B cells", *PLOS Computational Biology,* vol. 18, no. 4, e1009885.

Hu, M.J., Shao, X.X., Wang, J.H., Wei, D., Guo, Y.Q., Liu, Y.L., Xu, Z.G. and Guo, Z.Y. 2016, "Mechanism for insulin-like peptide 5 distinguishing the homologous relaxin family peptide receptor 3 and 4", *Scientific Reports,* vol. 6, 29648.

Hu, X., Li, J., Fu, M., Zhao, X. and Wang, W. 2021, "The JAK/STAT signaling pathway: from bench to clinic", *Signal Transduction and Targeted Therapy,* vol. 6, no. 402.

Isho, B., Florescu, A., Wang, A.A. and Gommerman, J.L. 2021, "Fantastic IgA plasma cells and where to find them", *Immunological Reviews,* vol. 303, pp. 119-137.

Iwasaki, A. and Medzhitov, R. 2015, "Control of adaptive immunity by the innate immune system", *Nature immunology,* vol. 16, no. 4, pp. 343-353.

Jewell, D.P. 2007, "Crohn's disease", *Medicine,* vol. 35, no. 5, pp. 283-289.

Jiménez-Uribe, A., Valencia-Martínes, H., Carballo-Uicab, G., Vallejo-Castillo, L., Medina-Rivero, E., Chacón-Salinas, R., Pavón, L., Velasco-Velázquez, A., Mellado-Sánchez, G., Estrada-Parra, S. and Pérez-Tapia, S.M. 2019, "CD80 expression correlates with IL-6 production in THP-1-like macrophages costimulated with LPS and dialyzable leukocyte extract (Transferon®)", *Journal of Immunology Research,* vol. 2019, Article ID 2198508.

Johansson, M.E.V. and Hansson, G.C. 2022, "Goblet cells need some stress", *J Clin Invest,* vol, 132, no.17, e162030.

Kerkhofs, C., Stevens, S.J.C., Faust, S.N., Rae, W., Williams, A.P., Wurm, P., Østern, R., Fockens, P., Würfel, C., Laass, M., Kokke, F., Stegmann, A.P.A. and Brunner, H.G. 2019, "Mutations in *RPSA* and *NKX2-3* link development of the spleen and intestinal vasculature', *Human Mutation,* vol. 41, pp. 196-202.

Kohli, S., Shahzad, K., Jouppila, A., Holthöfer, H., Isermann, B. and Lassila, R. 2022, "Thrombosis and inflammation – a dynamic interplay and the role of glycosaminoglycans and activated protein C", *Frontiers in Cardiovascular Medicine,* vol. 9, article 866751.

Kirkineska, L., Perifanis, V. and Vasiliadis, T. 2014, “Functional hyposplenism”, *Hippokratia,* vol. 18, no. 1, pp. 7-11.

Kuchipudi, S.V., Tellabati, M., Nelli, R.K., White, G.A., Perez, B.B., Sebastian, S., Slomka, M.J., Brookes, S.M., Brown, I.H., Dunham, S.P. and Chang, K.C. 2012, “18s rRNAi is a reliable normalisation gene for real time PCR based on influenza virus infected cells”, *Virology Journal,* vol. 9, no. 230.

Lafferty, R.A., Flatt, P.R. and Irwin, N. 2018, “Emerging therapeutic potential for peptide YY for obesity-diabetes”, *Peptides,* vol. 100, pp. 269-274.

Laron, Z. 2001, “Insulin-like growth factor 1 (IGF-1): a growth hormone”, *J Clin Pathol: Mol Pathol,* vol. 54, pp. 311-316.

Lee, Y.S., Vadder, F.D., Tremaroli, V., Wichmann, A., Mithieux, G. and Bäckhed, F. 2016, “Insulin-like peptide 5 is a microbially regulated peptide that promotes hepatic glucose production”, *Molecular Metabolism,* vol. 5, pp. 263-270.

Lenti, M.V., Aronico, N., Pellegrino, I., Boveri, E., Giuffrida, P., de Andreis, F.B., Morbini, P., Vanelli, L., Pasini, A., Ubezio, C., Melazzini, F., Rascaroli, A., Antoci, V., Merli, S., Di Terlizzi, F., Sabatini, U., Cambiè, G., Tenore, A., Picone, C., Vanoli, A., Arcaini, L., Baldanti, F., Paulli, M., Corazza, G.R. and Di Sabatino, A. 2020, “Depletion of circulating IgM memory B cells predicts unfavourable outcome in COVID-19”, *Scientific Reports,* vol. 10, 20836.

Lenti, M.V., Luu, S., Carsetti, R., Osier, F., Ogwang, R., Nnodu, O.E., Wiedermann, U., Spencer, J., Locatelli, F., Corazza, G.R. and Di Sabatino, A. 2022, “Asplenia and spleen hypofunction”, *Nature Reviews Disease Primers,* vol. 8, no. 71.

Lewis, J.E., Woodward, O.R.M., Nuzzaci, D., Smith, C.A., Adriaenssens, A.E., Billing, L., Brighton, C., Phillips, B.U., Tadross, J.A., Kinston, S.J., Clabatti, E., Göttgens, B., Tripodi, M., Hornigold, D., Baker, D., Gribble, F.M. and Reimann, F. 2022, “Relaxin/insulin-like family peptide receptor 4 (*Rxfp4*) expressing hypothalamic neurons modulate food intake and preference in mice”, *Molecular Metabolism,* vol. 66, 101604.

Lewis, K.L., Caton, M.L., Bogunovic, M., Greter, M., Grajkowska, L.T., Ng, D., Klinakis, A., Charo, I.F., Jung, S., Gommerman, J.L., Ivanov, I.I., Liu, K., Merad, M. and Reizis, B. 2011, “Notch2 receptor signaling controls functional differentiation of dendritic cells in the spleen and intestine”, *Immunity,* vol. 35, pp. 780-791.

Li, M., van Esch, B.C.A.M., Wagenaar, G.T.M., Garssen, J., Folkerts, G., Henricks, P.A.J. 2018, “Pro- and anti-inflammatory effects of short chain fatty acids on immune and endothelial cells”, *European Journal of Pharmacology,* vol. 831, no. 52-59.

Li, S.B., Liu, Y.Y., Yuan, L., Ji, M.F., Zhang, A., Li, H.Y., Tang, L.Q., Fang, S.G., Zhang, H., Xing, S., Li, M.Z., Zhong, Q., Lin, S.J., Liu, W.L., Huang, P., Zeng, Y.X., Zheng, Y.M.,

Ling, Z.Q., Sui, J.H. and Zeng, M.S. 2020, "Autocrine INSL5 promotes tumor progression and glycolysis via activation of STAT5 signaling", *EMBO Molecular Medicine,* vol. 12, e12050.

Li, Y., de Harr, C., Pebbelenbosch, M.P. and van der Woude, C.J. 2012, "SOCS3 in immune regulation of inflammatory bowel idease and inflammatory bowel disease-related cancer", *Cytokine & Growth Factor Reviews,* vol. 23, pp. 127-138.

Lillie, R.D. and Greer, J.C. 1965, "On the relation of enterosiderosis pigments of man and guinea pig. Melanosis and pseudomelanosis of colon and villi and the intestinal iron uptake and storage mechanism", *The American Journal of Pathology,* vol. 47, no. 6, pp. 965-1009.

Livak, K. and Schmittgen, T.D. 2001, "Analysis of relative gene expression data using real time quantitative PCR and the $2^{-\Delta\Delta Ct}$ method", *Methods,* vol. 25, pp. 402-408.

Liu, C., Schönke, M., Zhou, E., Li, Z., Kooijman, S., Boon, M.R., Larsson, M., Wallenius, K., Dekker, N., Barlind, L., Peng, X.R., Wang, Y. and Rensen, P.C.N. 2022, "Pharmacological treatmen with FGF21 strongly improves plasma cholesterol metabolism to reduce atherosclerosis", *Cardiovascular Research,* vol. 118, pp. 489-502.

Liu, M., Weiss, M.A., Arunagiri, A., Yong, J., Rege, N., Sun, J., Haataja, L., Kaufman, R.J. and Arvan, P. 2018, "Biosynthesis, structure, and folding of the insulin precursor protein", *Diabetes Obes Metab,* vol. 20, no. 2, pp. 28-50.

Loftus, E.V. 2004, "Clinical epidemiology of inflammatory bowel disease incidence, prevalence, and environmental influences", *Gastroenterology,* vol. 126, no. 6, pp. 1504-1517.

Ma, S., Smith, C.M., Blasiak, A. and Gundlach, A.L. 2017, "Distribution, physiology and pharmacology of relaxin-3/RXFP3 systems in brain", *British Journal of Pharmacology,* vol. 174, pp. 1034-1048.

Mashima, H., Ohno, H., Yamada, Y., Sakai, T. and Ohnishi, H. 2013, "INSL5 may be a unique marker of colorectal endocrine cells and neuroendocrine tumors", *Biochemical and Biophysical Research Communications,* vol. 432, pp. 586-592.

McDaniel, D.K., Eden, K., Ringel, V.M. and Allen, I.C. 2016, "Emerging roles for noncanonical NF-kB signaling in the Modulation of Inflammatory Bowel Disease Pathobiology", *Basic Inflamm Bowel Dis,* vol. 22, no. 9, pp. 2265-2279.

McDermott, J.R., Leslie, F.C., D'Amato, M., Thompson, D.G., Grencis, R.K. and McLaughlin, J.T. 2006, "Immune control of food intake: enteroendocrine cells are regulated by $CD4^+$ T lymphocytes during small intestinal inflammation", *Gut,* vol. 55, pp. 492-497.

Meers, G.K., Bohnenberger, H., Reichardt, H.M., Lühder, F. and Reichardt, S.D. 2018, "Impaired resolution of DSS-induced colitis in mice lacking the glucocorticoid receptor in myeloid cells", *PLoS ONE,* vol. 13, no. 1.

Miyanaka, Y., Ueno, Y., Tanaka, S., Yoshioka, K., Hatakeyama, T., Shimamoto, M., Sumii, M. and Chayama, K. 2007, "Clinical significance of mucosal suppressors of cytokine signaling 3 expression in ulcerative colitis", *World J Gastroenterol,* vol. 13, no. 21, pp. 2939-2944.

Mohamed, M.E., Gamal, R.M., El-Mokhtar, M.A., Hassan, A.T., Abozaid, H.S.M., Ghandour, A.M., Ismail, S.A.A., Yousef, H.A., El-Hakeim, E.H., Makarem, Y.S. and Awad, A.A. 2021, "Peripheral cells from patients with systemic sclerosis disease co-expressing M1 and M2 monocyte/macrophage surface markers: Relation to the degree of skin involvement", *Human Immunology,* vol. 82, pp. 634-639.

Muller and Toghill. 1995, "Hyposplenism in gastrointestinal disease", *Gut,* vol. 36, pp. 165-167.

Murotomi, K., Arai, S., Uchida, S., Endo, S., Mitsuzumi, H., Tabei, Y., Yoshida, Y. and Nakajima, Y. 2016, "Involvement of splenic iron accumulation in the development of non-alcoholic steatohepatitis in Tsumura Suzuki Obese Diabetes mice", *Scientific Reports,* vol. 6, 22476.

Oldak, B., Cruz-Rivera, Flisser, A. and Mendlovic, F. 2018, "RNA purity, real-time PCR sensitivity, and colon segment influence mRNA relative expression in murine dextran sodium sulfate experimental colitis", *Journal of Biomolecular Techniques,* vol. 29, pp. 61-70.

Peyrin-Biroulet, L., Panés, J., Sandborn, W.J., Vermeire, S., Danese, S., Feagan, B.G., Colombel, J.F., Hanauer, S.B. and Rycroft, B. 2016, "Defining disease severity in inflammatory bowel diseases: Current and future directions", *Clinical Gastroenterology and Hepatology,* vol. 14, no. 3., pp. 348-354.

Pfeffer, L.A., Brisson, B.K., Lei, H. and Barton, E.R. 2009, "The insulin-like growth factor (IGF)-I E-peptides modulate cell entry of the mature IGF-I protein", *Molecular Biology of the Cell,* vol. 20, pp. 3810-3817.

Phillips, I., Eykyn, S., King, B.A., Jenkins, C., Warren, C.A. and Shannon, K.P. 1977, "The *in vitro* antibacterial activity of nine aminoglycosides and spectinomycin on clinical isolates of common Gram-negative bacteria", *Journal of Antimicrobial Chemotherapy,* vol. 3, pp. 403-410.

Praveen, P., Bathgate, R.A.D., Hossain, M.A. 2019, "Engineering of chimeric peptides as antagonists for the G protein coupled receptor, RXFP4", *Scientific Reports,* vol. 9.

Psichas, A., Reimann, F. and Gribble, F.M. 2015, "Gut chemosensing mechanisms", *The Journal of Clinical Investigation,* vol. 125, no. 3, pp. 908-917.

Rosado, M.M., Aranburu, A., Scarsella, M., Cascioli, S., Giorda, E., Chierico, F.D., Mortera, S.L., Mortari, E.P., Petrini, S., Putignani, L. and Carsetti, R. 2018, "Spleen development is modulated by neonatal gut microbiota", *Immunology letters,* vol. 199, pp. 1-15.

Rotwein, P. and Baral, K. 2019, "The *insulin-like growth factor 2* gene in mammals: Organizational complexity within a conserved locus", *PLoS ONE,* vol. 14, no. 6.

Sands, B.E., Sandborn, W.J., Feagan, B., Löfberg, F., Hibi, T., Wang, T., Gustofson, L.M., Wong, C.J., Vandervoort, M.K., Hanauer, S. and the Adacolumn Study Group. 2008, "A randomized, double-blind, sham-controlled study of granulocyte/monocyte apheresis for active ulcerative colitis", *Gastroenterology,* vol. 135, no. 2, pp. 400-409.

Sann, H., von Erichsen, J., Hessman, M., Pahl, A. and Hoffmeyer, A. 2013, "Efficacy of drugs used in the treatment of IBD and combinations thereof in acute DSS-induced colitis in mice", *Life Sciences,* vol. 92, pp. 708-718.

Sawyer, R.T., Strausbauch, P.H. and Volkman, A. 1982, "Resident macrophage proliferation in mice depleted of blood monocytes by strontium-89", *Lab Invest,* vol. 46, no. 2, pp. 165-170.

Seong-Min, L., Hae-Bin, P. and Jun-O, Jin. 2021, "Polysaccharide from *Astragalus membranaceus*promotes the activation of human peripheral blood and mouse spleen dendritic cells". *Chinese Journal of Natural Medicines,* vol. 19, no. 1, pp. 56-62.

Sherwood, O.D. 2004, "Relaxin's physiological roles and other diverse actions", *Endocrine Reviews,* vol. 25, no. 2, pp. 205-234.

Silva, P.Y., Bernardi, A. and Frozza, L. 2020, "The role of short-chain fatty acids from gut microbiota in gut-brain communication", *Frontiers in Endocrinology,* vol. 11.

Skok, D.J., Hauptman, N., Jerala, M. and Zidar, N. 2021, "Expression of cytokine-coding genes BMP8B, LEFTY1 and INSL5 could distinguish between Ulcerative colitis and Crohn's disease", *Genes,* vol. 12.

Steinman, R.M. and Cohn, Z.A. 1973, "Identification of a novel cell type in peripheral lymphoid organs in mice. I. Morphology, quantification, tissue distribution", *J Exp Med,* vol. 137, no. 5, pp. 1142-1162.

Suzuki, A., Hanada, T., Mitsuyama, K., Yoshida, T., Kamizono, S., Hoshino, T., Kubo, M., Yamashita, A., Okabe, M., Takeda, K., Akira, S., Matsumoto, S., Toyonaga, A., Sata, M. and Yoshimura, A. 2001, "CIS3/SOCS3/SSI3 plays a negative regulatory role in STAT3 activation and intestinal inflammation", *J Exp Med,* vol. 193, no. 4, pp. 471-481.

Tesmer, L.A., Lundy, S.K., Sarkar, S. and Fox, D.A. 2008, "Th17 cells in human disease", *Immunol Rev,* vol. 223, pp. 87-113.

Thanasupawat, T., Hammje, K., Adham, I., Ghia, J.E., Del Bigio, M.R., Krcek, J., Hoang-Vu, C., Klonisch, T. and Hombach-Klonisch, S. 2013, "INSL5 is a novel marker for human enteroendocrine cells of the large intestine and neuroendocrine tumours", *Oncology Reports,* vol. 29, pp. 149-154.

Thompson, P.D., Tipney, H., Brass, A., Noyes, H., Kemp, S., Naessens, J. and Tassabehji, M. 2010, "Claudin 13, a member of the claudin family regulated in mouse stress induced erythropoiesis", *PLoS One,* vol. 5, no. 9, e12667.

Thomsen, R.W., Schoonen, W.M., Farkas, D.K., Riis, A., Fryzek, J.P. and Sørensen, H.T. 2010, "Risk of venous thromboembolism in splenectomised patients compared with the general population and appendectomized patients: a 10-year nationwide cohort study", *J Thromb Haemost,* vol. 8, pp. 1413-1444.

Vahkal, B., Yegerov, S., Onyilagha, C., Donner, J., Reddick, D., Shrivastav, A., Uzonna, J. and Good, S.V. 2021, "Immune system effects of insulin-like peptide 5 in a mouse model", *Frontiers in Endocrinology,* vol. 11.

Van Es, J.H. and Clevers, H. 2014, "Paneth cells", *Current Biology,* vol. 24, no. 12, pp. 547-548.

Van Furth, R. and Cohn, Z.A. 1968, "The origin and kinetics of mononuclear phagocytes", *J Exp Med,* vol. 128, no. 3, pp. 415-435.

Villumsen, M., Schelde, A.B., Jimenez-Solem, E., Jess, T. and Allin, K.H. 2021, "GLP-1 based therapies and disease course of inflammatory bowel disease", *EClinicalMedicine,* vol. 37.

Walker, J.A. and McKenzie, A.N.J. 2018, "T_H2 cell development and function", *Nature Reviews Immunology,* vol. 18, pp.121-133.

Wang, Y., Tu, S., Huang, Y., Qin, K. and Chen, Z. 2022, "MicroRNA-181a regulates Treg functions via TGF- β1/Smad axis in the spleen of mice with acute gouty arthritis induced by MSU crystals", *Braz J Med Res,* vol. 55, e12002.

Wichmann, A., Allahyar, A., Greiner, T.U., Plovier, H., Lundén, G.Ö., Larsson, T., Drucker, D.J., Delzenne, N.M., Cani, P.D. and Bäckhed, F. 2013, "Microbial modulation of energy availability in the colon regulates intestinal transit", *Cell Host & Microbe,* vol. 14, pp. 582-590.

Wei, G., Jie, Y., Chaoneng, W., Dong, H., Jianbing, Z., Junjie, G., Leilei, M., Hongtao, S., Yunzeng, Z. and Junbo, G. 2017, "Dendritic cells derived exosomes migration to spleen and induction of inflammation are regulated by CCR7", *Scientific Reports,* vol. 7.

Weisheit, C.K., Engel, D.R. and Kurts, C. 2015, "Dendritic cells and macrophages: Sentinels in the kidney", *Clin J Am Soc Nephrol,* vol. 10, pp. 1841-1851.

Wortzel, I. and Seger, R. 2011, “The ERK cascade: Distinct functions within various subcellular organelles”, *Genes & Cancer,* vol. 2, no. 3, pp. 195-209.

Xiang, L., Pan, W., Chen, H., Du, W., Xie, S., Liang, X., Yang, F., Niu, R., Huang, C., Luo, M., Xu, Y., Geng, L., Gong, S., Xu, W. and Zhao, J. 2024, “Sorbitol destroyed intestinal microfold cells (M cells) development through inhibition of PDE4-mediated RANKL expression”, *Mediators of Inflammation,* vol. 2024, Article ID 7524314.

Xing, Z., Gauldie, J., Cox, G., Baumann, H., Jordana, M., Lei, X.F. and Achong, M.K. 1998, “IL-6 is an antiinflammatory cytokine required for controlling local or systemic acute inflammatory responses”, *J Clin Invest,* vol. 101, no. 2, pp. 311-320.

Xu, T., Sun, D., Chen, Y. and Ouyang, L. 2020, “Targeting mTOR for fighting diseases: A revisited review of mTOR inhibitors”, *European Journal of Medicinal Chemistry,* vol. 199, 112391.

Yang, R., Li, S.W., Chen, Z., Zhou, X., Ni, Wei., Fu, D.A., Lu, J., Kaye, F.J. and Wu, L. 2019, “Role of INSL4 signaling in sustaining the growth and viability of LKB1-inactivated lung cancer”, *JNCI J Natl Cancer Inst,* vol. 111, no. 7, pp. 664-674.

Yang, Y., Shu, H., Hu, J., Li, L., Wang, J., Chen, T., Zhen, J., Sun, J., Feng, W., Xiong, X., Huang, Y., Li, X., Zhang, K., Fan, Z., Guo, H. and Liu, M. 2022, “A novel nonsense *INS* mutation causes inefficient preproinsulin translocation into the endoplasmic reticulum”, *Frontiers in Endocrinology,* vol. 12, article 774634.

Ye, Y., Gaugler, B., Mohty, M. and Malard, F. 2020, “Plasmacytoid dendritic cell biology and its role in immune-mediated diseases”, *Clinical & Translational Immunology,* vol. 9, e1139.

Yeganeh, I.S., Taromchi, A.H., Fathabadi, F.F., Nejatbakhsh, R., Novin, M.G. and Shokri, S. 2017, “Expression and localization of relaxin family peptide receptor 4 in human spermatozoa and impact of insulin-like peptide 5 on sperm functions”, *Reproductive Biology,* vol. 17, pp. 327-332.

Yoshimura, A., Suzuki, M., Sakaguchi, R., Hanada, T. and Yasukawa, H. 2012, “SOCS, inflammation, and autoimmunity”, *Frontiers in Immunology,* vol. 3, no. 20.

Yu, C., Li, X., Zhao, Y. and Hu, Y. 2023, “The role of FOXA family transcription factors in glucolipid metabolism and NAFLD”, *Frontiers in Endocrinology,* vol. 14, 1081500.

Zhang, W. and Liu, H.T. 2002, “MAPK signal pathways in the regulation of cell proliferation in mammalian cells”, *Cell Research,* vol. 12, no. 1, pp. 9-18.

Zhang, X., Bathgate, R.A.D. and Hossain, M.A. 2020, “Human insulin-like peptide 5 (INSL5). Identification of a simplified version of two-chain analog A13”, *ACS Med Chem Lett,* vol. 11, pp. 2455-2460.

Zhang, Y., Xie, B., Chen, X., Zhang, J. and Yuan, S. 2021, “A key role of gut microbiota-vagus nerve/spleen axis in sleep deprivation-mediated aggravation of systemic inflammation after LPS administration”, *Life Sciences,* vol. 265, 118736.

Zhu, J., Kuei, C., Sutton, S., Kamme, F., Yu, J., Bonaventure, P., Atack, J., Lovenberg, T.W. and Liu, C. 2008, “Identification of the domains in RXFP4 (GPCR142) responsible for the high binding and agonistic activity of INSL5 at RXFP4 compared to RXFP3 (GPCR135)”, *European Journal of Pharmacology,* vol. 590, pp. 43-52.

Appendices

Appendix A: Recipes for solutions used in Prussian blue experiment.

Solution	Reagent	Amount
Potassium Ferrocyanide Solution	Potassium Ferrocyanide 6M HCl Distilled water	300 mg 0.8 mL 29.3 mL
Eosin Y Stock Solution	Eosin Y 70% Ethanol Glacial acetic acid	1 gm 1 L 5 mL
Eosin Y Working Solution	Eosin Y stock 70% Ethanol Glacial acetic acid	15 mL 15 mL 2 drops

Appendix B: List of dissected mice with total weight from November–December 2022 dissections.

Individual	**Cohort**	**Spleen Weight (g)**
C2M	CTL	0.081
C2U	CTL	0.089
D2M	CTL	0.084
D2U	CTL	0.08
E2M	CTL	0.101
E2U	CTL	0.086
F2M	CTL	0.067
F2U	CTL	0.088
C3M	DSS	0.082
C3U	DSS	0.126
D3U	DSS	0.086
D3M	DSS	0.09
E3M	DSS	0.115
E3U	DSS	0.088
F3M	DSS	0.112
F3U	DSS	0.115

Appendix C: Howell-Jolly and Hypochromic Erythrocyte Counts

Control Mice

Mouse ID	Total Cells	Howell-Jollies	Hypochromic Erythrocytes
C1.1_1W2	1000	32	0
C1.1_2W2		19	6
C1.1_3W2		23	11
C2.3_1W2		64	19
C2.3_2W2		52	7
C2.3_3W2		38	15
C1.2_1W3		22	13
C1.2_2W3		12	11
C1.2_3W3		26	0
C2.2_1W3		27	3
C2.2_2W3		31	9
C2.2_3W3		33	1
C1.2_1W4		5	8
C1.2_2W4		2	10
C1.2_3W4		7	14
C2.1_1W4		4	29
C2.1_2W4		6	34
C2.1_3W4		11	48

DSS Mice

Mouse ID	Total Cells	Howell-Jollies	Hypochromic Erythrocytes
Co1.2_1W2	1000	26	254
Co1.2_2W2		91	439
Co1.2_3W2		36	379
Co1.5_1W2		34	165
Co1.5_2W2		48	82
Co1.5_3W2		69	477
Co1.6_1W3		39	280
Co1.6_2W3		51	173
Co1.6_3W3		51	93
Co2.3_1W3		105	585
Co2.3_2W3		20	392
Co2.3_3W3		25	476
Co1.1_1W4		136	599
Co1.1_2W4		77	661
Co1.1_3W4		93	786
Co2.3_1W4		50	690
Co2.3_2W4		41	509
Co2.3_3W4		35	572

Appendix D: K-Means Cluster Enrichment Data

	Group	FDR	nGenes	Pathway size	Fold enriched	Pathway
1	1	5.02E-05	6	124	24.85192308	Digestion
2	1	5.02E-05	6	99	25.50592105	Zymogen activation
3	1	9.57E-04	16	1863	3.473924731	Proteolysis
4	1	1.27E-02	6	276	8.501973684	Protein processing
5	1	2.15E-02	2	6	107.6916667	Cell wall disruption in another organism
6	1	3.16E-02	6	343	6.684310345	Protein maturation
7	1	4.58E-02	2	11	64.615	Regulation of nitric oxide mediated signal transduction
8	1	4.62E-02	5	230	7.583920188	Endothelial cell migration
9	1	4.73E-02	2	15	53.84583333	Intestinal cholesterol absorption
10	1	4.73E-02	3	119	17.94861111	Antimicrobial humoral immune response mediated by antimicrobial peptide
11	2	1.38E-14	69	983	3.195964932	Organic acid metabolic process
12	2	1.27E-13	66	958	3.12810319	Oxoacid metabolic process
13	2	1.64E-13	65	940	3.123435949	Carboxylic acid metabolic process
14	2	3.18E-10	90	1817	2.189712173	Small molecule metabolic process
15	2	2.19E-08	73	1436	2.252151576	Lipid metabolic process
16	2	2.47E-08	24	195	5.19691689	Alpha-amino acid metabolic process
17	2	2.58E-08	17	99	7.749788345	Zymogen activation
18	2	4.69E-08	23	197	5.174419414	Cellular modified amino acid metabolic process
19	2	4.69E-08	43	651	3.02187189	Monocarboxylic acid metabolic process
20	2	1.41E-07	26	267	4.330764075	Cellular amino acid metabolic process
21	3	6.07E-10	15	133	13.62802306	Erythrocyte differentiation
22	3	9.40E-10	15	144	12.63327685	Erythrocyte homeostasis
23	3	9.40E-10	10	43	28.84598214	Erythrocyte development
24	3	1.69E-08	15	186	9.89005102	Myeloid cell homeostasis
25	3	9.30E-08	11	91	14.75840947	Myeloid cell development
26	3	2.51E-07	46	2595	2.479056849	Immune system process

27	3	2.82E-07	19	430	5.6795198	Myeloid cell differentiation
28	3	4.35E-06	16	340	5.823794502	Homeostasis of number of cells
29	3	2.14E-05	6	41	26.62706044	Peptide cross-linking
30	3	2.46E-05	6	83	25.64087302	Antibacterial humoral response
31	4	5.21E-05	28	774	3.289191892	Response to bacterium
32	4	5.21E-05	42	1489	2.436966263	Response to external biotic stimulus
33	4	5.21E-05	42	1485	2.43907985	Response to other organism
34	4	9.07E-05	42	1528	2.365230502	Response to biotic stimulus
35	4	1.46E-04	62	2831	1.884443964	Response to external stimulus
36	4	4.52E-04	42	1643	2.197077396	Biological process involved in interspecies interaction between organisms
37	4	1.85E-03	40	1642	2.120619136	Defense response
38	4	1.97E-03	30	1083	2.458698258	Defense response to other organism
39	4	3.54E-03	11	269	5.186929869	Humoral immune response
40	4	3.54E-03	8	83	7.652405625	Chemokine-mediated signaling pathway
41	5	1.15E-28	113	879	3.390808147	Mitotic cell cycle
42	5	1.15E-28	103	733	3.661752488	Mitotic cell cycle process
43	5	1.45E-28	77	464	4.786987059	Nuclear division
44	5	2.23E-28	70	367	5.238285503	Chromosome segregation
45	5	1.04E-26	79	515	4.363135559	Organelle fission
46	5	1.90E-26	155	1784	2.517143794	Cell cycle
47	5	3.49E-26	125	1187	2.905774043	Cell cycle process
48	5	4.24E-26	61	307	5.539297735	Nuclear chromosome segregation
49	5	4.55E-24	112	1026	2.980820203	Chromosome organization
50	5	4.89E-22	81	615	3.616773605	Cell division

	Genes
1	ENSMUSG00000024225, ENSMUSG00000026818, ENSMUSG00000031957, ENSMUSG00000057163, ENSMUSG00000046008, ENSMUSG00000029193
2	ENSMUSG00000063903, ENSMUSG00000036938, ENSMUSG00000054106, ENSMUSG00000057163, ENSMUSG00000071519, ENSMUSG00000071521
3	ENSMUSG00000011463, ENSMUSG00000023031, ENSMUSG00000023433, ENSMUSG00000031896, ENSMUSG00000031957, ENSMUSG00000034139, ENSMUSG00000036938, ENSMUSG00000054106, ENSMUSG00000054446, ENSMUSG00000057163, ENSMUSG00000058579, ENSMUSG00000063903, ENSMUSG00000071519, ENSMUSG00000071521, ENSMUSG00000071553, ENSMUSG00000024503
4	ENSMUSG00000063903, ENSMUSG00000036938, ENSMUSG00000054106, ENSMUSG00000057163, ENSMUSG00000071519, ENSMUSG00000071521
5	ENSMUSG00000059654, ENSMUSG00000068341
6	ENSMUSG00000063903, ENSMUSG00000036938, ENSMUSG00000054106, ENSMUSG00000057163, ENSMUSG00000071519, ENSMUSG00000071521
7	ENSMUSG00000024503, ENSMUSG00000024039
8	ENSMUSG00000036938, ENSMUSG00000054106, ENSMUSG00000057163, ENSMUSG00000071519, ENSMUSG00000071521
9	ENSMUSG00000026818, ENSMUSG00000046008
10	ENSMUSG00000059654, ENSMUSG00000068341, ENSMUSG00000029522
11	ENSMUSG00000002769, ENSMUSG00000003053, ENSMUSG00000009614, ENSMUSG00000010651, ENSMUSG00000019762, ENSMUSG00000019987, ENSMUSG00000020017, ENSMUSG00000020150, ENSMUSG00000021416, ENSMUSG00000021953, ENSMUSG00000023070, ENSMUSG00000023963, ENSMUSG00000025140, ENSMUSG00000025991, ENSMUSG00000026621, ENSMUSG00000027199, ENSMUSG00000028011, ENSMUSG00000028179, ENSMUSG00000028186, ENSMUSG00000028307, ENSMUSG00000028601, ENSMUSG00000029445, ENSMUSG00000029695, ENSMUSG00000030382, ENSMUSG00000032079, ENSMUSG00000032083, ENSMUSG00000034456, ENSMUSG00000038754, ENSMUSG00000041798, ENSMUSG00000042251, ENSMUSG00000044005, ENSMUSG00000052520, ENSMUSG00000052974, ENSMUSG00000054827, ENSMUSG00000060613, ENSMUSG00000062480, ENSMUSG00000068086, ENSMUSG00000070985, ENSMUSG00000090145, ENSMUSG00000094806, ENSMUSG00000000567, ENSMUSG00000001670, ENSMUSG00000019278, ENSMUSG00000025481, ENSMUSG00000056973, ENSMUSG00000074768, ENSMUSG00000005373, ENSMUSG00000006378, ENSMUSG00000017950, ENSMUSG00000020098, ENSMUSG00000020256, ENSMUSG00000022546, ENSMUSG00000027048, ENSMUSG00000028518, ENSMUSG00000030088, ENSMUSG00000030717, ENSMUSG00000034785, ENSMUSG00000035735, ENSMUSG00000037798, ENSMUSG00000054422, ENSMUSG00000006345, ENSMUSG00000026398, ENSMUSG00000029304, ENSMUSG00000029556, ENSMUSG00000004035, ENSMUSG00000030659, ENSMUSG00000057400, ENSMUSG00000061959, ENSMUSG00000040562

12	ENSMUSG00000002769, ENSMUSG00000003053, ENSMUSG00000009614, ENSMUSG00000010651, ENSMUSG00000019762, ENSMUSG00000019987, ENSMUSG00000020017, ENSMUSG00000020150, ENSMUSG00000021416, ENSMUSG00000021953, ENSMUSG00000023070, ENSMUSG00000023963, ENSMUSG00000025140, ENSMUSG00000025991, ENSMUSG00000026621, ENSMUSG00000027199, ENSMUSG00000028011, ENSMUSG00000028179, ENSMUSG00000028307, ENSMUSG00000028601, ENSMUSG00000029445, ENSMUSG00000029695, ENSMUSG00000030382, ENSMUSG00000032079, ENSMUSG00000032083, ENSMUSG00000034456, ENSMUSG00000038754, ENSMUSG00000041798, ENSMUSG00000042251, ENSMUSG00000044005, ENSMUSG00000052974, ENSMUSG00000054827, ENSMUSG00000060613, ENSMUSG00000062480, ENSMUSG00000068086, ENSMUSG00000070985, ENSMUSG00000090145, ENSMUSG00000094806, ENSMUSG00000000567, ENSMUSG00000001670, ENSMUSG00000019278, ENSMUSG00000056973, ENSMUSG00000074768, ENSMUSG00000005373, ENSMUSG00000006378, ENSMUSG00000017950, ENSMUSG00000020098, ENSMUSG00000020256, ENSMUSG00000022546, ENSMUSG00000027048, ENSMUSG00000028518, ENSMUSG00000030088, ENSMUSG00000030717, ENSMUSG00000034785, ENSMUSG00000035735, ENSMUSG00000037798, ENSMUSG00000054422, ENSMUSG00000006345, ENSMUSG00000026398, ENSMUSG00000029556, ENSMUSG00000004035, ENSMUSG00000030659, ENSMUSG00000052520, ENSMUSG00000057400, ENSMUSG00000061959, ENSMUSG00000040562
13	ENSMUSG00000002769, ENSMUSG00000003053, ENSMUSG00000009614, ENSMUSG00000010651, ENSMUSG00000019762, ENSMUSG00000019987, ENSMUSG00000020017, ENSMUSG00000020150, ENSMUSG00000021416, ENSMUSG00000021953, ENSMUSG00000023070, ENSMUSG00000023963, ENSMUSG00000025140, ENSMUSG00000025991, ENSMUSG00000027199, ENSMUSG00000028011, ENSMUSG00000028179, ENSMUSG00000028307, ENSMUSG00000028601, ENSMUSG00000029445, ENSMUSG00000029695, ENSMUSG00000030382, ENSMUSG00000032079, ENSMUSG00000032083, ENSMUSG00000034456, ENSMUSG00000038754, ENSMUSG00000041798, ENSMUSG00000042251, ENSMUSG00000044005, ENSMUSG00000052974, ENSMUSG00000054827, ENSMUSG00000060613, ENSMUSG00000062480, ENSMUSG00000068086, ENSMUSG00000070985, ENSMUSG00000090145, ENSMUSG00000094806, ENSMUSG00000000567, ENSMUSG00000001670, ENSMUSG00000019278, ENSMUSG00000056973, ENSMUSG00000074768, ENSMUSG00000005373, ENSMUSG00000006378, ENSMUSG00000017950, ENSMUSG00000020098, ENSMUSG00000020256, ENSMUSG00000022546, ENSMUSG00000027048, ENSMUSG00000028518, ENSMUSG00000030088, ENSMUSG00000030717, ENSMUSG00000034785, ENSMUSG00000035735, ENSMUSG00000037798, ENSMUSG00000054422, ENSMUSG00000006345, ENSMUSG00000026398, ENSMUSG00000029556, ENSMUSG00000004035, ENSMUSG00000030659, ENSMUSG00000052520, ENSMUSG00000057400, ENSMUSG00000061959, ENSMUSG00000040562
14	ENSMUSG00000002769, ENSMUSG00000003053, ENSMUSG00000005681, ENSMUSG00000009614, ENSMUSG00000010651, ENSMUSG00000019762,

	ENSMUSG00000019987, ENSMUSG00000020017, ENSMUSG00000020150, ENSMUSG00000021416, ENSMUSG00000021953, ENSMUSG00000023070, ENSMUSG00000023963, ENSMUSG00000025140, ENSMUSG00000025481, ENSMUSG00000025991, ENSMUSG00000026621, ENSMUSG00000027199, ENSMUSG00000028011, ENSMUSG00000028179, ENSMUSG00000028186, ENSMUSG00000028307, ENSMUSG00000028601, ENSMUSG00000029445, ENSMUSG00000029695, ENSMUSG00000030382, ENSMUSG00000032079, ENSMUSG00000032083, ENSMUSG00000034456, ENSMUSG00000034570, ENSMUSG00000038754, ENSMUSG00000041261, ENSMUSG00000041798, ENSMUSG00000042251, ENSMUSG00000044005, ENSMUSG00000052520, ENSMUSG00000052974, ENSMUSG00000054827, ENSMUSG00000060613, ENSMUSG00000061808, ENSMUSG00000062480, ENSMUSG00000068086, ENSMUSG00000070985, ENSMUSG00000073988, ENSMUSG00000090145, ENSMUSG00000094806, ENSMUSG00000000567, ENSMUSG00000001670, ENSMUSG00000019278, ENSMUSG00000024747, ENSMUSG00000029644, ENSMUSG00000035540, ENSMUSG00000037025, ENSMUSG00000056973, ENSMUSG00000074768, ENSMUSG00000000215, ENSMUSG00000005373, ENSMUSG00000006378, ENSMUSG00000017950, ENSMUSG00000020098, ENSMUSG00000020256, ENSMUSG00000020609, ENSMUSG00000022546, ENSMUSG00000024924, ENSMUSG00000024990, ENSMUSG00000027048, ENSMUSG00000028518, ENSMUSG00000029556, ENSMUSG00000029630, ENSMUSG00000029727, ENSMUSG00000030088, ENSMUSG00000030717, ENSMUSG00000034785, ENSMUSG00000035735, ENSMUSG00000037798, ENSMUSG00000040134, ENSMUSG00000053647, ENSMUSG00000054422, ENSMUSG00000056035, ENSMUSG00000061959, ENSMUSG00000006345, ENSMUSG00000009545, ENSMUSG00000026398, ENSMUSG00000028150, ENSMUSG00000029304, ENSMUSG00000004035, ENSMUSG00000030659, ENSMUSG00000057400, ENSMUSG00000040562, ENSMUSG00000073834
15	ENSMUSG00000003053, ENSMUSG00000005681, ENSMUSG00000010651, ENSMUSG00000020609, ENSMUSG00000021416, ENSMUSG00000023963, ENSMUSG00000027761, ENSMUSG00000028601, ENSMUSG00000030382, ENSMUSG00000032079, ENSMUSG00000032083, ENSMUSG00000034570, ENSMUSG00000038754, ENSMUSG00000042251, ENSMUSG00000047822, ENSMUSG00000052974, ENSMUSG00000054827, ENSMUSG00000056973, ENSMUSG00000057400, ENSMUSG00000060613, ENSMUSG00000061959, ENSMUSG00000062480, ENSMUSG00000068086, ENSMUSG00000070985, ENSMUSG00000079434, ENSMUSG00000094806, ENSMUSG00000000215, ENSMUSG00000000567, ENSMUSG00000028518, ENSMUSG00000035540, ENSMUSG00000037025, ENSMUSG00000053647, ENSMUSG00000066513, ENSMUSG00000000049, ENSMUSG00000005373, ENSMUSG00000008461, ENSMUSG00000017950, ENSMUSG00000019278, ENSMUSG00000023070, ENSMUSG00000023232, ENSMUSG00000024924, ENSMUSG00000024972, ENSMUSG00000024990, ENSMUSG00000025991, ENSMUSG00000027048, ENSMUSG00000027249, ENSMUSG00000028179, ENSMUSG00000029304, ENSMUSG00000029630, ENSMUSG00000029727, ENSMUSG00000031286, ENSMUSG00000034528, ENSMUSG00000035735, ENSMUSG00000040134,

	ENSMUSG00000040562, ENSMUSG00000042429, ENSMUSG00000054422, ENSMUSG00000056035, ENSMUSG00000056553, ENSMUSG00000061808, ENSMUSG00000020256, ENSMUSG00000020964, ENSMUSG00000026398, ENSMUSG00000028150, ENSMUSG00000029556, ENSMUSG00000004035, ENSMUSG00000024907, ENSMUSG00000030659, ENSMUSG00000030827, ENSMUSG00000052520, ENSMUSG00000072115, ENSMUSG00000073834, ENSMUSG00000052430
16	ENSMUSG00000002769, ENSMUSG00000009614, ENSMUSG00000019762, ENSMUSG00000019987, ENSMUSG00000021953, ENSMUSG00000025140, ENSMUSG00000025991, ENSMUSG00000028011, ENSMUSG00000028179, ENSMUSG00000029445, ENSMUSG00000029695, ENSMUSG00000044005, ENSMUSG00000001670, ENSMUSG00000074768, ENSMUSG00000006378, ENSMUSG00000017950, ENSMUSG00000020017, ENSMUSG00000020098, ENSMUSG00000022546, ENSMUSG00000034456, ENSMUSG00000037798, ENSMUSG00000006345, ENSMUSG00000019278, ENSMUSG00000020150
17	ENSMUSG00000029102, ENSMUSG00000044485, ENSMUSG00000063089, ENSMUSG00000063713, ENSMUSG00000066512, ENSMUSG00000066513, ENSMUSG00000066515, ENSMUSG00000000049, ENSMUSG00000001249, ENSMUSG00000019851, ENSMUSG00000033831, ENSMUSG00000033860, ENSMUSG00000038224, ENSMUSG00000027249, ENSMUSG00000028001, ENSMUSG00000062751, ENSMUSG00000006345
18	ENSMUSG00000000308, ENSMUSG00000002769, ENSMUSG00000004035, ENSMUSG00000006345, ENSMUSG00000009614, ENSMUSG00000019762, ENSMUSG00000020150, ENSMUSG00000027199, ENSMUSG00000027313, ENSMUSG00000040562, ENSMUSG00000073987, ENSMUSG00000020256, ENSMUSG00000022949, ENSMUSG00000023232, ENSMUSG00000030004, ENSMUSG00000030088, ENSMUSG00000053644, ENSMUSG00000074768, ENSMUSG00000001249, ENSMUSG00000019278, ENSMUSG00000028179, ENSMUSG00000033634, ENSMUSG00000057103
19	ENSMUSG00000003053, ENSMUSG00000010651, ENSMUSG00000020150, ENSMUSG00000021416, ENSMUSG00000023963, ENSMUSG00000027199, ENSMUSG00000028307, ENSMUSG00000028601, ENSMUSG00000030382, ENSMUSG00000032079, ENSMUSG00000032083, ENSMUSG00000038754, ENSMUSG00000041798, ENSMUSG00000052974, ENSMUSG00000054827, ENSMUSG00000060613, ENSMUSG00000062480, ENSMUSG00000068086, ENSMUSG00000070985, ENSMUSG00000090145, ENSMUSG00000094806, ENSMUSG00000000567, ENSMUSG00000056973, ENSMUSG00000005373, ENSMUSG00000020017, ENSMUSG00000023070, ENSMUSG00000027048, ENSMUSG00000028518, ENSMUSG00000030717, ENSMUSG00000034456, ENSMUSG00000035735, ENSMUSG00000042251, ENSMUSG00000054422, ENSMUSG00000020256, ENSMUSG00000026398, ENSMUSG00000029556, ENSMUSG00000004035, ENSMUSG00000017950, ENSMUSG00000030659, ENSMUSG00000052520, ENSMUSG00000057400, ENSMUSG00000061959, ENSMUSG00000040562
20	ENSMUSG00000002769, ENSMUSG00000009614, ENSMUSG00000019762, ENSMUSG00000019987, ENSMUSG00000020017, ENSMUSG00000021953,

	ENSMUSG00000025140, ENSMUSG00000025991, ENSMUSG00000028011, ENSMUSG00000028179, ENSMUSG00000029445, ENSMUSG00000029695, ENSMUSG00000034456, ENSMUSG00000042251, ENSMUSG00000044005, ENSMUSG00000001670, ENSMUSG00000074768, ENSMUSG00000006378, ENSMUSG00000017950, ENSMUSG00000020098, ENSMUSG00000022546, ENSMUSG00000034785, ENSMUSG00000037798, ENSMUSG00000006345, ENSMUSG00000019278, ENSMUSG00000020150
21	ENSMUSG00000025270, ENSMUSG00000016526, ENSMUSG00000028717, ENSMUSG00000031162, ENSMUSG00000073400, ENSMUSG00000023216, ENSMUSG00000054191, ENSMUSG00000006574, ENSMUSG00000022099, ENSMUSG00000023926, ENSMUSG00000023995, ENSMUSG00000026815, ENSMUSG00000031543, ENSMUSG00000037124, ENSMUSG00000051910
22	ENSMUSG00000025270, ENSMUSG00000016526, ENSMUSG00000028717, ENSMUSG00000031162, ENSMUSG00000073400, ENSMUSG00000023216, ENSMUSG00000054191, ENSMUSG00000006574, ENSMUSG00000022099, ENSMUSG00000023926, ENSMUSG00000023995, ENSMUSG00000026815, ENSMUSG00000031543, ENSMUSG00000037124, ENSMUSG00000051910
23	ENSMUSG00000025270, ENSMUSG00000023216, ENSMUSG00000031162, ENSMUSG00000006574, ENSMUSG00000022099, ENSMUSG00000023926, ENSMUSG00000028717, ENSMUSG00000031543, ENSMUSG00000037124, ENSMUSG00000051910
24	ENSMUSG00000025270, ENSMUSG00000016526, ENSMUSG00000028717, ENSMUSG00000031162, ENSMUSG00000073400, ENSMUSG00000023216, ENSMUSG00000054191, ENSMUSG00000006574, ENSMUSG00000022099, ENSMUSG00000023926, ENSMUSG00000023995, ENSMUSG00000026815, ENSMUSG00000031543, ENSMUSG00000037124, ENSMUSG00000051910
25	ENSMUSG00000025270, ENSMUSG00000023216, ENSMUSG00000031162, ENSMUSG00000006574, ENSMUSG00000022099, ENSMUSG00000023926, ENSMUSG00000028717, ENSMUSG00000031543, ENSMUSG00000037124, ENSMUSG00000051910, ENSMUSG00000032496
26	ENSMUSG00000006235, ENSMUSG00000020125, ENSMUSG00000020490, ENSMUSG00000020641, ENSMUSG00000025270, ENSMUSG00000026815, ENSMUSG00000028644, ENSMUSG00000032496, ENSMUSG00000033688, ENSMUSG00000037124, ENSMUSG00000051748, ENSMUSG00000052212, ENSMUSG00000052270, ENSMUSG00000056054, ENSMUSG00000056071, ENSMUSG00000069792, ENSMUSG00000073400, ENSMUSG00000004552, ENSMUSG00000016526, ENSMUSG00000022797, ENSMUSG00000028717, ENSMUSG00000031162, ENSMUSG00000053338, ENSMUSG00000022126, ENSMUSG00000023216, ENSMUSG00000025889, ENSMUSG00000026822, ENSMUSG00000030000, ENSMUSG00000040314, ENSMUSG00000054191, ENSMUSG00000057729, ENSMUSG00000005800, ENSMUSG00000006574, ENSMUSG00000009350, ENSMUSG00000022026, ENSMUSG00000022099, ENSMUSG00000023926, ENSMUSG00000023995, ENSMUSG00000026532, ENSMUSG00000031543, ENSMUSG00000051910, ENSMUSG00000022651, ENSMUSG00000000157, ENSMUSG00000027562, ENSMUSG00000068417, ENSMUSG00000093973

27	ENSMUSG00000025270, ENSMUSG00000016526, ENSMUSG00000026815, ENSMUSG00000028717, ENSMUSG00000031162, ENSMUSG00000073400, ENSMUSG00000023216, ENSMUSG00000054191, ENSMUSG00000057729, ENSMUSG00000006574, ENSMUSG00000022099, ENSMUSG00000022797, ENSMUSG00000023926, ENSMUSG00000023995, ENSMUSG00000031543, ENSMUSG00000037124, ENSMUSG00000051910, ENSMUSG00000027562, ENSMUSG00000032496
28	ENSMUSG00000025270, ENSMUSG00000016526, ENSMUSG00000028717, ENSMUSG00000031162, ENSMUSG00000073400, ENSMUSG00000023216, ENSMUSG00000054191, ENSMUSG00000006574, ENSMUSG00000022099, ENSMUSG00000023926, ENSMUSG00000023995, ENSMUSG00000026532, ENSMUSG00000026815, ENSMUSG00000031543, ENSMUSG00000037124, ENSMUSG00000051910
29	ENSMUSG00000023216, ENSMUSG00000022902, ENSMUSG00000059657, ENSMUSG00000071561, ENSMUSG00000071562, ENSMUSG00000079597
30	ENSMUSG00000032496, ENSMUSG00000033688, ENSMUSG00000051748, ENSMUSG00000069792, ENSMUSG00000020125, ENSMUSG00000040314
31	ENSMUSG00000029371, ENSMUSG00000029380, ENSMUSG00000105096, ENSMUSG00000023992, ENSMUSG00000030017, ENSMUSG00000054072, ENSMUSG00000020889, ENSMUSG00000027513, ENSMUSG00000031778, ENSMUSG00000040264, ENSMUSG00000044701, ENSMUSG00000061356, ENSMUSG00000022878, ENSMUSG00000025479, ENSMUSG00000027559, ENSMUSG00000031517, ENSMUSG00000049436, ENSMUSG00000061780, ENSMUSG00000062515, ENSMUSG00000066363, ENSMUSG00000078921, ENSMUSG00000078922, ENSMUSG00000102758, ENSMUSG00000040627, ENSMUSG00000031551, ENSMUSG00000034730, ENSMUSG00000026405, ENSMUSG00000035352
32	ENSMUSG00000009185, ENSMUSG00000020676, ENSMUSG00000022887, ENSMUSG00000027718, ENSMUSG00000029371, ENSMUSG00000029380, ENSMUSG00000029915, ENSMUSG00000030017, ENSMUSG00000031778, ENSMUSG00000035352, ENSMUSG00000040627, ENSMUSG00000067297, ENSMUSG00000079516, ENSMUSG00000105096, ENSMUSG00000023992, ENSMUSG00000037440, ENSMUSG00000044701, ENSMUSG00000054072, ENSMUSG00000078921, ENSMUSG00000078922, ENSMUSG00000020889, ENSMUSG00000026405, ENSMUSG00000026874, ENSMUSG00000027513, ENSMUSG00000028885, ENSMUSG00000034730, ENSMUSG00000038037, ENSMUSG00000040264, ENSMUSG00000059201, ENSMUSG00000061356, ENSMUSG00000061780, ENSMUSG00000022878, ENSMUSG00000025479, ENSMUSG00000027559, ENSMUSG00000031517, ENSMUSG00000049436, ENSMUSG00000062515, ENSMUSG00000066363, ENSMUSG00000102758, ENSMUSG00000031551, ENSMUSG00000039699, ENSMUSG00000022865
33	ENSMUSG00000009185, ENSMUSG00000020676, ENSMUSG00000022887, ENSMUSG00000027718, ENSMUSG00000029371, ENSMUSG00000029380, ENSMUSG00000029915, ENSMUSG00000030017, ENSMUSG00000031778, ENSMUSG00000035352, ENSMUSG00000040627, ENSMUSG00000067297, ENSMUSG00000079516, ENSMUSG00000105096, ENSMUSG00000023992,

	ENSMUSG00000037440, ENSMUSG00000044701, ENSMUSG00000054072, ENSMUSG00000078921, ENSMUSG00000078922, ENSMUSG00000020889, ENSMUSG00000026405, ENSMUSG00000026874, ENSMUSG00000027513, ENSMUSG00000028885, ENSMUSG00000034730, ENSMUSG00000038037, ENSMUSG00000040264, ENSMUSG00000059201, ENSMUSG00000061356, ENSMUSG00000061780, ENSMUSG00000022878, ENSMUSG00000025479, ENSMUSG00000027559, ENSMUSG00000031517, ENSMUSG00000049436, ENSMUSG00000062515, ENSMUSG00000066363, ENSMUSG00000102758, ENSMUSG00000031551, ENSMUSG00000039699, ENSMUSG00000022865
34	ENSMUSG00000009185, ENSMUSG00000020676, ENSMUSG00000022887, ENSMUSG00000027718, ENSMUSG00000029371, ENSMUSG00000029380, ENSMUSG00000029915, ENSMUSG00000030017, ENSMUSG00000031778, ENSMUSG00000035352, ENSMUSG00000040627, ENSMUSG00000067297, ENSMUSG00000079516, ENSMUSG00000105096, ENSMUSG00000023992, ENSMUSG00000037440, ENSMUSG00000044701, ENSMUSG00000054072, ENSMUSG00000078921, ENSMUSG00000078922, ENSMUSG00000020889, ENSMUSG00000026405, ENSMUSG00000026874, ENSMUSG00000027513, ENSMUSG00000028885, ENSMUSG00000034730, ENSMUSG00000038037, ENSMUSG00000040264, ENSMUSG00000059201, ENSMUSG00000061356, ENSMUSG00000061780, ENSMUSG00000022878, ENSMUSG00000025479, ENSMUSG00000027559, ENSMUSG00000031517, ENSMUSG00000049436, ENSMUSG00000062515, ENSMUSG00000066363, ENSMUSG00000102758, ENSMUSG00000031551, ENSMUSG00000039699, ENSMUSG00000022865
35	ENSMUSG00000009185, ENSMUSG00000020676, ENSMUSG00000021804, ENSMUSG00000022887, ENSMUSG00000023992, ENSMUSG00000027513, ENSMUSG00000027718, ENSMUSG00000029371, ENSMUSG00000029380, ENSMUSG00000029915, ENSMUSG00000030017, ENSMUSG00000031778, ENSMUSG00000035352, ENSMUSG00000040627, ENSMUSG00000048480, ENSMUSG00000048915, ENSMUSG00000059201, ENSMUSG00000067297, ENSMUSG00000079516, ENSMUSG00000105096, ENSMUSG00000022878, ENSMUSG00000037440, ENSMUSG00000044701, ENSMUSG00000054072, ENSMUSG00000078921, ENSMUSG00000078922, ENSMUSG00000013584, ENSMUSG00000020889, ENSMUSG00000022865, ENSMUSG00000026405, ENSMUSG00000026874, ENSMUSG00000028885, ENSMUSG00000031980, ENSMUSG00000032725, ENSMUSG00000034730, ENSMUSG00000037541, ENSMUSG00000038037, ENSMUSG00000039323, ENSMUSG00000040264, ENSMUSG00000046186, ENSMUSG00000061356, ENSMUSG00000061780, ENSMUSG00000062515, ENSMUSG00000063415, ENSMUSG00000025479, ENSMUSG00000027559, ENSMUSG00000027840, ENSMUSG00000031517, ENSMUSG00000049436, ENSMUSG00000066363, ENSMUSG00000102758, ENSMUSG00000002771, ENSMUSG00000014704, ENSMUSG00000027071, ENSMUSG00000031551, ENSMUSG00000033498, ENSMUSG00000039699, ENSMUSG00000063063, ENSMUSG00000109564, ENSMUSG00000000301, ENSMUSG00000027070, ENSMUSG00000038155
36	ENSMUSG00000009185, ENSMUSG00000020676, ENSMUSG00000022887, ENSMUSG00000027718, ENSMUSG00000029371, ENSMUSG00000029380,

	ENSMUSG00000029915, ENSMUSG00000030017, ENSMUSG00000031778, ENSMUSG00000035352, ENSMUSG00000040627, ENSMUSG00000067297, ENSMUSG00000079516, ENSMUSG00000105096, ENSMUSG00000023992, ENSMUSG00000037440, ENSMUSG00000044701, ENSMUSG00000054072, ENSMUSG00000078921, ENSMUSG00000078922, ENSMUSG00000020889, ENSMUSG00000026405, ENSMUSG00000026874, ENSMUSG00000027513, ENSMUSG00000028885, ENSMUSG00000034730, ENSMUSG00000038037, ENSMUSG00000040264, ENSMUSG00000059201, ENSMUSG00000061356, ENSMUSG00000061780, ENSMUSG00000022878, ENSMUSG00000025479, ENSMUSG00000027559, ENSMUSG00000031517, ENSMUSG00000049436, ENSMUSG00000062515, ENSMUSG00000066363, ENSMUSG00000102758, ENSMUSG00000031551, ENSMUSG00000039699, ENSMUSG00000022865
37	ENSMUSG00000009185, ENSMUSG00000020676, ENSMUSG00000022887, ENSMUSG00000023992, ENSMUSG00000027718, ENSMUSG00000029371, ENSMUSG00000029380, ENSMUSG00000029915, ENSMUSG00000031778, ENSMUSG00000035148, ENSMUSG00000035352, ENSMUSG00000040627, ENSMUSG00000054072, ENSMUSG00000067297, ENSMUSG00000068606, ENSMUSG00000078921, ENSMUSG00000078922, ENSMUSG00000105096, ENSMUSG00000022878, ENSMUSG00000030017, ENSMUSG00000037440, ENSMUSG00000044701, ENSMUSG00000022548, ENSMUSG00000026405, ENSMUSG00000026874, ENSMUSG00000028885, ENSMUSG00000034730, ENSMUSG00000038037, ENSMUSG00000039196, ENSMUSG00000040264, ENSMUSG00000059201, ENSMUSG00000061780, ENSMUSG00000062515, ENSMUSG00000079516, ENSMUSG00000020889, ENSMUSG00000029026, ENSMUSG00000031551, ENSMUSG00000039699, ENSMUSG00000063415, ENSMUSG00000022865
38	ENSMUSG00000009185, ENSMUSG00000020676, ENSMUSG00000022887, ENSMUSG00000027718, ENSMUSG00000029915, ENSMUSG00000031778, ENSMUSG00000035352, ENSMUSG00000040627, ENSMUSG00000067297, ENSMUSG00000105096, ENSMUSG00000023992, ENSMUSG00000029380, ENSMUSG00000030017, ENSMUSG00000037440, ENSMUSG00000044701, ENSMUSG00000054072, ENSMUSG00000078921, ENSMUSG00000078922, ENSMUSG00000026405, ENSMUSG00000026874, ENSMUSG00000028885, ENSMUSG00000034730, ENSMUSG00000038037, ENSMUSG00000040264, ENSMUSG00000059201, ENSMUSG00000061780, ENSMUSG00000029371, ENSMUSG00000039699, ENSMUSG00000022865, ENSMUSG00000079516
39	ENSMUSG00000022887, ENSMUSG00000026405, ENSMUSG00000029371, ENSMUSG00000029380, ENSMUSG00000030017, ENSMUSG00000079516, ENSMUSG00000026874, ENSMUSG00000061780, ENSMUSG00000023992, ENSMUSG00000009185, ENSMUSG00000035352
40	ENSMUSG00000009185, ENSMUSG00000020676, ENSMUSG00000029371, ENSMUSG00000029380, ENSMUSG00000031778, ENSMUSG00000035352, ENSMUSG00000023992, ENSMUSG00000048480
41	ENSMUSG00000000028, ENSMUSG00000002068, ENSMUSG00000004031, ENSMUSG00000012443, ENSMUSG00000015880, ENSMUSG00000017499, ENSMUSG00000017861, ENSMUSG00000019773, ENSMUSG00000019942,

	ENSMUSG00000020897, ENSMUSG00000021714, ENSMUSG00000021965, ENSMUSG00000022422, ENSMUSG00000023940, ENSMUSG00000024301, ENSMUSG00000024660, ENSMUSG00000024791, ENSMUSG00000026039, ENSMUSG00000026202, ENSMUSG00000026605, ENSMUSG00000026683, ENSMUSG00000027115, ENSMUSG00000027306, ENSMUSG00000027330, ENSMUSG00000027454, ENSMUSG00000027469, ENSMUSG00000027490, ENSMUSG00000027496, ENSMUSG00000027699, ENSMUSG00000027715, ENSMUSG00000028212, ENSMUSG00000028312, ENSMUSG00000028587, ENSMUSG00000028873, ENSMUSG00000029414, ENSMUSG00000030867, ENSMUSG00000031004, ENSMUSG00000032218, ENSMUSG00000032254, ENSMUSG00000034023, ENSMUSG00000034311, ENSMUSG00000034906, ENSMUSG00000036752, ENSMUSG00000036777, ENSMUSG00000037474, ENSMUSG00000038379, ENSMUSG00000038943, ENSMUSG00000040084, ENSMUSG00000041431, ENSMUSG00000042029, ENSMUSG00000042417, ENSMUSG00000042489, ENSMUSG00000043091, ENSMUSG00000044201, ENSMUSG00000045273, ENSMUSG00000046591, ENSMUSG00000048922, ENSMUSG00000051378, ENSMUSG00000062248, ENSMUSG00000068744, ENSMUSG00000069910, ENSMUSG00000072082, ENSMUSG00000079553, ENSMUSG00000005233, ENSMUSG00000006398, ENSMUSG00000017146, ENSMUSG00000017716, ENSMUSG00000018983, ENSMUSG00000021221, ENSMUSG00000074476, ENSMUSG00000020020, ENSMUSG00000020185, ENSMUSG00000001517, ENSMUSG00000002055, ENSMUSG00000003779, ENSMUSG00000006715, ENSMUSG00000020235, ENSMUSG00000020541, ENSMUSG00000020649, ENSMUSG00000020900, ENSMUSG00000022018, ENSMUSG00000026622, ENSMUSG00000026779, ENSMUSG00000027323, ENSMUSG00000027379, ENSMUSG00000027883, ENSMUSG00000028551, ENSMUSG00000028678, ENSMUSG00000028718, ENSMUSG00000029177, ENSMUSG00000029516, ENSMUSG00000029752, ENSMUSG00000030528, ENSMUSG00000030677, ENSMUSG00000030978, ENSMUSG00000036223, ENSMUSG00000036768, ENSMUSG00000037313, ENSMUSG00000037725, ENSMUSG00000038252, ENSMUSG00000041147, ENSMUSG00000041498, ENSMUSG00000045328, ENSMUSG00000050107, ENSMUSG00000058290, ENSMUSG00000061878, ENSMUSG00000096472, ENSMUSG00000026955, ENSMUSG00000028068, ENSMUSG00000046179, ENSMUSG00000047844, ENSMUSG00000027510, ENSMUSG00000060860
42	ENSMUSG00000000028, ENSMUSG00000002068, ENSMUSG00000012443, ENSMUSG00000015880, ENSMUSG00000017499, ENSMUSG00000019773, ENSMUSG00000019942, ENSMUSG00000020897, ENSMUSG00000021714, ENSMUSG00000022422, ENSMUSG00000023940, ENSMUSG00000024301, ENSMUSG00000024660, ENSMUSG00000024791, ENSMUSG00000026039, ENSMUSG00000026605, ENSMUSG00000026683, ENSMUSG00000027115, ENSMUSG00000027306, ENSMUSG00000027330, ENSMUSG00000027454, ENSMUSG00000027469, ENSMUSG00000027490, ENSMUSG00000027496, ENSMUSG00000027699, ENSMUSG00000027715, ENSMUSG00000028212, ENSMUSG00000028312, ENSMUSG00000028587, ENSMUSG00000028873, ENSMUSG00000029414, ENSMUSG00000031004, ENSMUSG00000032218,

	ENSMUSG00000032254, ENSMUSG00000034023, ENSMUSG00000034311, ENSMUSG00000034906, ENSMUSG00000036777, ENSMUSG00000037474, ENSMUSG00000038379, ENSMUSG00000038943, ENSMUSG00000040084, ENSMUSG00000041431, ENSMUSG00000042029, ENSMUSG00000042417, ENSMUSG00000042489, ENSMUSG00000044201, ENSMUSG00000045273, ENSMUSG00000046591, ENSMUSG00000048922, ENSMUSG00000051378, ENSMUSG00000068744, ENSMUSG00000069910, ENSMUSG00000072082, ENSMUSG00000079553, ENSMUSG00000005233, ENSMUSG00000006398, ENSMUSG00000017146, ENSMUSG00000017716, ENSMUSG00000018983, ENSMUSG00000021221, ENSMUSG00000074476, ENSMUSG00000017861, ENSMUSG00000020020, ENSMUSG00000020185, ENSMUSG00000001517, ENSMUSG00000002055, ENSMUSG00000003779, ENSMUSG00000020235, ENSMUSG00000020541, ENSMUSG00000020649, ENSMUSG00000020900, ENSMUSG00000022018, ENSMUSG00000026622, ENSMUSG00000026779, ENSMUSG00000027323, ENSMUSG00000027379, ENSMUSG00000027883, ENSMUSG00000028551, ENSMUSG00000028678, ENSMUSG00000028718, ENSMUSG00000029177, ENSMUSG00000029516, ENSMUSG00000030528, ENSMUSG00000030677, ENSMUSG00000030867, ENSMUSG00000030978, ENSMUSG00000036768, ENSMUSG00000037313, ENSMUSG00000037725, ENSMUSG00000038252, ENSMUSG00000041147, ENSMUSG00000041498, ENSMUSG00000045328, ENSMUSG00000050107, ENSMUSG00000058290, ENSMUSG00000096472, ENSMUSG00000061878, ENSMUSG00000062248, ENSMUSG00000026955, ENSMUSG00000028068, ENSMUSG00000027510, ENSMUSG00000060860
43	ENSMUSG00000012443, ENSMUSG00000015880, ENSMUSG00000019773, ENSMUSG00000020914, ENSMUSG00000021714, ENSMUSG00000022422, ENSMUSG00000023940, ENSMUSG00000024301, ENSMUSG00000024533, ENSMUSG00000024660, ENSMUSG00000024791, ENSMUSG00000026039, ENSMUSG00000026683, ENSMUSG00000027115, ENSMUSG00000027306, ENSMUSG00000027323, ENSMUSG00000027469, ENSMUSG00000028312, ENSMUSG00000028873, ENSMUSG00000029414, ENSMUSG00000031004, ENSMUSG00000032254, ENSMUSG00000034023, ENSMUSG00000034906, ENSMUSG00000038379, ENSMUSG00000038943, ENSMUSG00000040084, ENSMUSG00000041431, ENSMUSG00000042029, ENSMUSG00000048922, ENSMUSG00000051378, ENSMUSG00000055385, ENSMUSG00000058290, ENSMUSG00000068744, ENSMUSG00000069910, ENSMUSG00000078773, ENSMUSG00000079553, ENSMUSG00000003824, ENSMUSG00000005233, ENSMUSG00000006398, ENSMUSG00000017716, ENSMUSG00000020897, ENSMUSG00000021221, ENSMUSG00000074476, ENSMUSG00000017861, ENSMUSG00000020020, ENSMUSG00000020235, ENSMUSG00000032218, ENSMUSG00000041147, ENSMUSG00000002055, ENSMUSG00000017499, ENSMUSG00000020541, ENSMUSG00000022018, ENSMUSG00000026622, ENSMUSG00000027379, ENSMUSG00000027496, ENSMUSG00000028678, ENSMUSG00000030346, ENSMUSG00000030677, ENSMUSG00000030867, ENSMUSG00000034311, ENSMUSG00000036768, ENSMUSG00000038252, ENSMUSG00000041498, ENSMUSG00000045328, ENSMUSG00000050107,

	ENSMUSG00000002068, ENSMUSG00000028212, ENSMUSG00000046101, ENSMUSG00000061878, ENSMUSG00000026779, ENSMUSG00000027330, ENSMUSG00000033952, ENSMUSG00000035455, ENSMUSG00000062248, ENSMUSG00000082079, ENSMUSG00000060860
44	ENSMUSG00000005233, ENSMUSG00000015880, ENSMUSG00000020914, ENSMUSG00000021714, ENSMUSG00000021965, ENSMUSG00000022034, ENSMUSG00000022422, ENSMUSG00000023940, ENSMUSG00000024660, ENSMUSG00000024791, ENSMUSG00000026039, ENSMUSG00000026605, ENSMUSG00000026622, ENSMUSG00000026683, ENSMUSG00000027115, ENSMUSG00000027306, ENSMUSG00000027326, ENSMUSG00000028312, ENSMUSG00000028873, ENSMUSG00000029414, ENSMUSG00000031004, ENSMUSG00000032254, ENSMUSG00000034023, ENSMUSG00000034906, ENSMUSG00000038379, ENSMUSG00000038943, ENSMUSG00000040084, ENSMUSG00000041431, ENSMUSG00000042029, ENSMUSG00000045273, ENSMUSG00000048922, ENSMUSG00000051378, ENSMUSG00000055385, ENSMUSG00000058290, ENSMUSG00000068744, ENSMUSG00000069910, ENSMUSG00000072980, ENSMUSG00000074476, ENSMUSG00000003824, ENSMUSG00000006398, ENSMUSG00000017716, ENSMUSG00000020897, ENSMUSG00000021221, ENSMUSG00000020020, ENSMUSG00000002055, ENSMUSG00000017146, ENSMUSG00000017499, ENSMUSG00000019773, ENSMUSG00000024742, ENSMUSG00000027379, ENSMUSG00000027654, ENSMUSG00000027699, ENSMUSG00000028678, ENSMUSG00000030677, ENSMUSG00000030867, ENSMUSG00000031756, ENSMUSG00000034311, ENSMUSG00000036223, ENSMUSG00000038252, ENSMUSG00000041498, ENSMUSG00000045328, ENSMUSG00000050107, ENSMUSG00000002068, ENSMUSG00000028212, ENSMUSG00000046101, ENSMUSG00000082079, ENSMUSG00000024301, ENSMUSG00000041147, ENSMUSG00000047844, ENSMUSG00000079553
45	ENSMUSG00000012443, ENSMUSG00000015880, ENSMUSG00000019773, ENSMUSG00000019992, ENSMUSG00000020914, ENSMUSG00000021714, ENSMUSG00000022422, ENSMUSG00000023940, ENSMUSG00000024301, ENSMUSG00000024533, ENSMUSG00000024660, ENSMUSG00000024791, ENSMUSG00000026039, ENSMUSG00000026683, ENSMUSG00000027115, ENSMUSG00000027306, ENSMUSG00000027323, ENSMUSG00000027469, ENSMUSG00000027601, ENSMUSG00000028312, ENSMUSG00000028873, ENSMUSG00000029414, ENSMUSG00000031004, ENSMUSG00000032254, ENSMUSG00000034023, ENSMUSG00000034906, ENSMUSG00000038379, ENSMUSG00000038943, ENSMUSG00000040084, ENSMUSG00000041431, ENSMUSG00000042029, ENSMUSG00000048922, ENSMUSG00000051378, ENSMUSG00000055385, ENSMUSG00000058290, ENSMUSG00000068744, ENSMUSG00000069910, ENSMUSG00000078773, ENSMUSG00000079553, ENSMUSG00000003824, ENSMUSG00000005233, ENSMUSG00000006398, ENSMUSG00000017716, ENSMUSG00000020897, ENSMUSG00000021221, ENSMUSG00000074476, ENSMUSG00000017861, ENSMUSG00000020020, ENSMUSG00000020235, ENSMUSG00000032218, ENSMUSG00000041147, ENSMUSG00000002055, ENSMUSG00000017499, ENSMUSG00000020541,

	ENSMUSG00000022018, ENSMUSG00000026622, ENSMUSG00000027379, ENSMUSG00000027496, ENSMUSG00000028678, ENSMUSG00000030346, ENSMUSG00000030677, ENSMUSG00000030867, ENSMUSG00000034311, ENSMUSG00000036768, ENSMUSG00000038252, ENSMUSG00000041498, ENSMUSG00000045328, ENSMUSG00000050107, ENSMUSG00000002068, ENSMUSG00000028212, ENSMUSG00000046101, ENSMUSG00000061878, ENSMUSG00000026779, ENSMUSG00000027330, ENSMUSG00000033952, ENSMUSG00000035455, ENSMUSG00000062248, ENSMUSG00000082079, ENSMUSG00000060860
46	ENSMUSG00000000028, ENSMUSG00000002068, ENSMUSG00000004031, ENSMUSG00000006715, ENSMUSG00000012443, ENSMUSG00000015880, ENSMUSG00000017499, ENSMUSG00000017716, ENSMUSG00000017861, ENSMUSG00000019773, ENSMUSG00000019942, ENSMUSG00000020897, ENSMUSG00000020914, ENSMUSG00000021714, ENSMUSG00000021965, ENSMUSG00000022034, ENSMUSG00000022422, ENSMUSG00000023940, ENSMUSG00000024301, ENSMUSG00000024533, ENSMUSG00000024660, ENSMUSG00000024791, ENSMUSG00000026039, ENSMUSG00000026202, ENSMUSG00000026605, ENSMUSG00000026683, ENSMUSG00000027115, ENSMUSG00000027306, ENSMUSG00000027323, ENSMUSG00000027326, ENSMUSG00000027330, ENSMUSG00000027454, ENSMUSG00000027469, ENSMUSG00000027490, ENSMUSG00000027496, ENSMUSG00000027654, ENSMUSG00000027699, ENSMUSG00000027715, ENSMUSG00000028212, ENSMUSG00000028312, ENSMUSG00000028587, ENSMUSG00000028873, ENSMUSG00000029414, ENSMUSG00000030867, ENSMUSG00000031004, ENSMUSG00000032218, ENSMUSG00000032254, ENSMUSG00000034023, ENSMUSG00000034311, ENSMUSG00000034906, ENSMUSG00000036752, ENSMUSG00000036777, ENSMUSG00000037474, ENSMUSG00000038379, ENSMUSG00000038943, ENSMUSG00000040084, ENSMUSG00000041431, ENSMUSG00000042029, ENSMUSG00000042417, ENSMUSG00000042489, ENSMUSG00000043091, ENSMUSG00000044201, ENSMUSG00000045273, ENSMUSG00000046591, ENSMUSG00000048922, ENSMUSG00000051378, ENSMUSG00000055385, ENSMUSG00000058290, ENSMUSG00000062248, ENSMUSG00000068744, ENSMUSG00000069910, ENSMUSG00000072082, ENSMUSG00000078521, ENSMUSG00000078773, ENSMUSG00000079553, ENSMUSG00000003824, ENSMUSG00000005233, ENSMUSG00000006398, ENSMUSG00000017146, ENSMUSG00000018983, ENSMUSG00000021221, ENSMUSG00000041147, ENSMUSG00000074476, ENSMUSG00000020020, ENSMUSG00000020185, ENSMUSG00000020235, ENSMUSG00000028551, ENSMUSG00000030978, ENSMUSG00000096472, ENSMUSG00000001228, ENSMUSG00000001517, ENSMUSG00000002055, ENSMUSG00000002190, ENSMUSG00000002835, ENSMUSG00000003779, ENSMUSG00000003813, ENSMUSG00000004864, ENSMUSG00000007659, ENSMUSG00000020493, ENSMUSG00000020541, ENSMUSG00000020649, ENSMUSG00000020900, ENSMUSG00000020990, ENSMUSG00000022018, ENSMUSG00000022945, ENSMUSG00000023505, ENSMUSG00000024742, ENSMUSG00000025408, ENSMUSG00000026027, ENSMUSG00000026463, ENSMUSG00000026622,

	ENSMUSG00000026646, ENSMUSG00000026779, ENSMUSG00000026955, ENSMUSG00000027379, ENSMUSG00000027510, ENSMUSG00000027883, ENSMUSG00000028063, ENSMUSG00000028678, ENSMUSG00000028718, ENSMUSG00000028906, ENSMUSG00000029177, ENSMUSG00000029516, ENSMUSG00000029752, ENSMUSG00000030346, ENSMUSG00000030528, ENSMUSG00000030677, ENSMUSG00000032221, ENSMUSG00000032411, ENSMUSG00000033952, ENSMUSG00000035683, ENSMUSG00000036223, ENSMUSG00000036768, ENSMUSG00000036825, ENSMUSG00000037313, ENSMUSG00000037725, ENSMUSG00000038252, ENSMUSG00000038822, ENSMUSG00000041498, ENSMUSG00000045328, ENSMUSG00000046101, ENSMUSG00000046179, ENSMUSG00000047534, ENSMUSG00000049551, ENSMUSG00000049932, ENSMUSG00000050107, ENSMUSG00000056596, ENSMUSG00000060860, ENSMUSG00000061878, ENSMUSG00000072980, ENSMUSG00000073542, ENSMUSG00000028068, ENSMUSG00000035455, ENSMUSG00000047844, ENSMUSG00000082079
47	ENSMUSG00000000028, ENSMUSG00000002068, ENSMUSG00000012443, ENSMUSG00000015880, ENSMUSG00000017499, ENSMUSG00000019773, ENSMUSG00000019942, ENSMUSG00000020897, ENSMUSG00000020914, ENSMUSG00000021714, ENSMUSG00000022034, ENSMUSG00000022422, ENSMUSG00000023940, ENSMUSG00000024301, ENSMUSG00000024533, ENSMUSG00000024660, ENSMUSG00000024791, ENSMUSG00000026039, ENSMUSG00000026605, ENSMUSG00000026683, ENSMUSG00000027115, ENSMUSG00000027306, ENSMUSG00000027323, ENSMUSG00000027326, ENSMUSG00000027330, ENSMUSG00000027454, ENSMUSG00000027469, ENSMUSG00000027490, ENSMUSG00000027496, ENSMUSG00000027654, ENSMUSG00000027699, ENSMUSG00000027715, ENSMUSG00000028212, ENSMUSG00000028312, ENSMUSG00000028587, ENSMUSG00000028873, ENSMUSG00000029414, ENSMUSG00000030867, ENSMUSG00000031004, ENSMUSG00000032218, ENSMUSG00000032254, ENSMUSG00000034023, ENSMUSG00000034311, ENSMUSG00000034906, ENSMUSG00000036777, ENSMUSG00000037474, ENSMUSG00000038379, ENSMUSG00000038943, ENSMUSG00000040084, ENSMUSG00000041431, ENSMUSG00000042029, ENSMUSG00000042417, ENSMUSG00000042489, ENSMUSG00000044201, ENSMUSG00000045273, ENSMUSG00000046591, ENSMUSG00000048922, ENSMUSG00000051378, ENSMUSG00000055385, ENSMUSG00000058290, ENSMUSG00000068744, ENSMUSG00000069910, ENSMUSG00000072082, ENSMUSG00000078521, ENSMUSG00000078773, ENSMUSG00000079553, ENSMUSG00000003824, ENSMUSG00000005233, ENSMUSG00000006398, ENSMUSG00000017146, ENSMUSG00000017716, ENSMUSG00000018983, ENSMUSG00000021221, ENSMUSG00000041147, ENSMUSG00000074476, ENSMUSG00000017861, ENSMUSG00000020020, ENSMUSG00000020185, ENSMUSG00000020235, ENSMUSG00000030978, ENSMUSG00000096472, ENSMUSG00000001517, ENSMUSG00000002055, ENSMUSG00000003779, ENSMUSG00000006715, ENSMUSG00000007659, ENSMUSG00000020541, ENSMUSG00000020649, ENSMUSG00000020900, ENSMUSG00000022018, ENSMUSG00000024742, ENSMUSG00000026463, ENSMUSG00000026622,

	ENSMUSG00000026779, ENSMUSG00000027379, ENSMUSG00000027883, ENSMUSG00000028063, ENSMUSG00000028551, ENSMUSG00000028678, ENSMUSG00000028718, ENSMUSG00000029177, ENSMUSG00000029516, ENSMUSG00000030346, ENSMUSG00000030528, ENSMUSG00000030677, ENSMUSG00000033952, ENSMUSG00000036768, ENSMUSG00000036825, ENSMUSG00000037313, ENSMUSG00000037725, ENSMUSG00000038252, ENSMUSG00000041498, ENSMUSG00000045328, ENSMUSG00000050107, ENSMUSG00000073542, ENSMUSG00000046101, ENSMUSG00000061878, ENSMUSG00000062248, ENSMUSG00000026955, ENSMUSG00000028068, ENSMUSG00000035455, ENSMUSG00000046179, ENSMUSG00000082079, ENSMUSG00000027510, ENSMUSG00000060860
48	ENSMUSG00000015880, ENSMUSG00000020914, ENSMUSG00000021714, ENSMUSG00000022034, ENSMUSG00000022422, ENSMUSG00000023940, ENSMUSG00000024660, ENSMUSG00000024791, ENSMUSG00000026039, ENSMUSG00000026605, ENSMUSG00000026683, ENSMUSG00000027115, ENSMUSG00000027306, ENSMUSG00000027326, ENSMUSG00000028312, ENSMUSG00000028873, ENSMUSG00000029414, ENSMUSG00000032254, ENSMUSG00000034023, ENSMUSG00000034906, ENSMUSG00000038379, ENSMUSG00000038943, ENSMUSG00000040084, ENSMUSG00000041431, ENSMUSG00000042029, ENSMUSG00000051378, ENSMUSG00000055385, ENSMUSG00000058290, ENSMUSG00000068744, ENSMUSG00000069910, ENSMUSG00000003824, ENSMUSG00000005233, ENSMUSG00000006398, ENSMUSG00000017716, ENSMUSG00000020897, ENSMUSG00000021221, ENSMUSG00000074476, ENSMUSG00000020020, ENSMUSG00000002055, ENSMUSG00000017499, ENSMUSG00000019773, ENSMUSG00000024742, ENSMUSG00000026622, ENSMUSG00000027379, ENSMUSG00000027654, ENSMUSG00000027699, ENSMUSG00000028678, ENSMUSG00000030677, ENSMUSG00000030867, ENSMUSG00000034311, ENSMUSG00000038252, ENSMUSG00000041498, ENSMUSG00000045328, ENSMUSG00000050107, ENSMUSG00000002068, ENSMUSG00000028212, ENSMUSG00000046101, ENSMUSG00000082079, ENSMUSG00000024301, ENSMUSG00000041147, ENSMUSG00000079553
49	ENSMUSG00000002835, ENSMUSG00000005470, ENSMUSG00000015880, ENSMUSG00000017146, ENSMUSG00000020914, ENSMUSG00000021714, ENSMUSG00000022034, ENSMUSG00000022422, ENSMUSG00000022945, ENSMUSG00000023940, ENSMUSG00000024791, ENSMUSG00000026039, ENSMUSG00000026683, ENSMUSG00000027115, ENSMUSG00000027306, ENSMUSG00000027323, ENSMUSG00000028312, ENSMUSG00000028873, ENSMUSG00000029414, ENSMUSG00000030528, ENSMUSG00000032254, ENSMUSG00000034023, ENSMUSG00000034906, ENSMUSG00000038379, ENSMUSG00000038943, ENSMUSG00000040084, ENSMUSG00000041064, ENSMUSG00000041431, ENSMUSG00000042029, ENSMUSG00000047246, ENSMUSG00000049539, ENSMUSG00000051378, ENSMUSG00000051627, ENSMUSG00000052565, ENSMUSG00000055385, ENSMUSG00000058385, ENSMUSG00000058773, ENSMUSG00000060639, ENSMUSG00000060678, ENSMUSG00000060981, ENSMUSG00000061482, ENSMUSG00000062727,

	ENSMUSG00000064288, ENSMUSG00000068744, ENSMUSG00000069268, ENSMUSG00000069300, ENSMUSG00000069308, ENSMUSG00000069910, ENSMUSG00000072980, ENSMUSG00000075031, ENSMUSG00000095217, ENSMUSG00000105827, ENSMUSG00000114279, ENSMUSG00000003824, ENSMUSG00000005233, ENSMUSG00000006398, ENSMUSG00000017716, ENSMUSG00000020897, ENSMUSG00000021221, ENSMUSG00000024660, ENSMUSG00000027454, ENSMUSG00000074476, ENSMUSG00000020020, ENSMUSG00000054582, ENSMUSG00000000028, ENSMUSG00000001228, ENSMUSG00000002055, ENSMUSG00000017499, ENSMUSG00000019214, ENSMUSG00000019773, ENSMUSG00000019942, ENSMUSG00000021391, ENSMUSG00000024742, ENSMUSG00000025330, ENSMUSG00000026622, ENSMUSG00000026646, ENSMUSG00000027379, ENSMUSG00000028678, ENSMUSG00000029177, ENSMUSG00000030677, ENSMUSG00000030867, ENSMUSG00000031262, ENSMUSG00000031756, ENSMUSG00000034206, ENSMUSG00000034311, ENSMUSG00000038252, ENSMUSG00000041498, ENSMUSG00000045273, ENSMUSG00000045328, ENSMUSG00000046101, ENSMUSG00000050107, ENSMUSG00000058290, ENSMUSG00000063856, ENSMUSG00000063952, ENSMUSG00000078773, ENSMUSG00000082079, ENSMUSG00000002068, ENSMUSG00000028212, ENSMUSG00000041147, ENSMUSG00000031004, ENSMUSG00000024301, ENSMUSG00000028063, ENSMUSG00000069265, ENSMUSG00000099517, ENSMUSG00000101972, ENSMUSG00000015217, ENSMUSG00000054717, ENSMUSG00000069310, ENSMUSG00000074403, ENSMUSG00000079553, ENSMUSG00000099583, ENSMUSG00000064220
50	ENSMUSG00000020897, ENSMUSG00000022129, ENSMUSG00000024533, ENSMUSG00000024660, ENSMUSG00000027306, ENSMUSG00000027496, ENSMUSG00000027699, ENSMUSG00000030867, ENSMUSG00000036777, ENSMUSG00000017716, ENSMUSG00000028873, ENSMUSG00000002055, ENSMUSG00000002068, ENSMUSG00000003779, ENSMUSG00000003824, ENSMUSG00000005233, ENSMUSG00000006398, ENSMUSG00000007659, ENSMUSG00000012443, ENSMUSG00000015880, ENSMUSG00000017499, ENSMUSG00000019773, ENSMUSG00000019942, ENSMUSG00000020020, ENSMUSG00000020235, ENSMUSG00000020900, ENSMUSG00000021965, ENSMUSG00000023505, ENSMUSG00000023940, ENSMUSG00000024791, ENSMUSG00000026039, ENSMUSG00000026622, ENSMUSG00000026683, ENSMUSG00000026779, ENSMUSG00000026955, ENSMUSG00000027326, ENSMUSG00000027330, ENSMUSG00000027469, ENSMUSG00000027654, ENSMUSG00000027715, ENSMUSG00000027883, ENSMUSG00000028212, ENSMUSG00000028312, ENSMUSG00000028678, ENSMUSG00000028906, ENSMUSG00000029177, ENSMUSG00000029414, ENSMUSG00000029516, ENSMUSG00000030528, ENSMUSG00000032218, ENSMUSG00000032254, ENSMUSG00000033952, ENSMUSG00000034311, ENSMUSG00000034906, ENSMUSG00000036223, ENSMUSG00000037725, ENSMUSG00000038252, ENSMUSG00000038943, ENSMUSG00000040084, ENSMUSG00000041431, ENSMUSG00000041498, ENSMUSG00000042029, ENSMUSG00000042417, ENSMUSG00000042680, ENSMUSG00000044201, ENSMUSG00000047534,

	ENSMUSG00000048922, ENSMUSG00000051378, ENSMUSG00000060860, ENSMUSG00000062248, ENSMUSG00000068744, ENSMUSG00000069910, ENSMUSG00000072082, ENSMUSG00000072980, ENSMUSG00000074476, ENSMUSG00000079553, ENSMUSG00000018486, ENSMUSG00000020185, ENSMUSG00000020914, ENSMUSG00000041147, ENSMUSG00000046179

Appendix E: RNA Sequencing Significant Values (Control vs DSS)
Blue: immune-associated genes
Red: Erythrocyte associated genes

Symbol	Ensembl_ID	User_ID	log2FC	Adjusted P-Value
CHI3L1	CHI3L1	CHI3L1	-3.502238326	4.55E-11
Lrg1	ENSMUSG00000037095	LRG1	-2.28650956	2.32E-08
Mmp9	ENSMUSG00000017737	MMP9	-2.080043943	2.32E-08
Hdc	ENSMUSG00000027360	HDC	-2.789656059	2.94E-07
Wfdc17	ENSMUSG00000069792	WFDC17	-2.911309798	3.47E-07
Hp	ENSMUSG00000031722	HP	-2.445868203	4.38E-07
Ly6g	ENSMUSG00000022582	LY6G	-6.214014941	4.38E-07
Cstdc4	ENSMUSG00000079597	CSTDC4	-4.438884333	6.96E-07
S100a9	ENSMUSG00000056071	S100A9	-3.709382736	9.93E-07
Il36g	ENSMUSG00000044103	IL36G	-2.404618713	9.93E-07
Lcn2	ENSMUSG00000026822	LCN2	-4.595406604	1.09E-06
Stfa2l1	ENSMUSG00000059657	STFA2L1	-3.629699907	1.46E-06
S100a8	ENSMUSG00000056054	S100A8	-3.834910306	1.73E-06
Mrgpra2b	ENSMUSG00000096719	MRGPRA2B	-3.993748142	2.24E-06
C5ar1	ENSMUSG00000049130	C5AR1	-1.967259593	9.99E-06
Retnlg	ENSMUSG00000022651	RETNLG	-3.674875292	1.17E-05
Slc25a21	ENSMUSG00000035472	SLC25A21	-4.183155158	2.04E-05
Car1	ENSMUSG00000027556	CAR1	-2.304506808	2.28E-05
Wfdc21	ENSMUSG00000051748	WFDC21	-3.344594085	2.52E-05
Capn11	ENSMUSG00000058626	CAPN11	-7.890694568	2.52E-05
Saa3	ENSMUSG00000040026	SAA3	-4.982909018	4.21E-05
Slfn4	ENSMUSG00000000204	SLFN4	-3.274574457	7.18E-05
Mmp8	ENSMUSG00000005800	MMP8	-4.489072403	0.000122014
Fpr2	ENSMUSG00000052270	FPR2	-2.727415118	0.000126048
Ifitm1	ENSMUSG00000025491	IFITM1	-1.528914907	0.000972137
Prtn3	ENSMUSG00000057729	PRTN3	-3.300615797	0.000972137
Clec4e	ENSMUSG00000030142	CLEC4E	-2.526941183	0.001613932
Acod1	ENSMUSG00000022126	ACOD1	-3.584665131	0.001613932
Mgam	ENSMUSG00000068587	MGAM	-3.418965309	0.001613932
Trem3	ENSMUSG00000041754	TREM3	-2.415837501	0.001999854
Gm867	ENSMUSG00000050157	GM867	-6.676717123	0.002225466
Mrgpra2a	ENSMUSG00000093973	MRGPRA2A	-6.79884356	0.002225466
Klf1	ENSMUSG00000054191	KLF1	-4.876526172	0.002527662
Redrum	ENSMUSG00000096982	REDRUM	-4.546975139	0.002684858
Ypel4	ENSMUSG00000034059	YPEL4	-6.057383979	0.00278366
Lipg	ENSMUSG00000053846	LIPG	-4.47260012	0.003254283
Stfa2	ENSMUSG00000022902	STFA2	-6.925216073	0.003332788
Phospho1	ENSMUSG00000050860	PHOSPHO1	-2.237493762	0.003963559

Btnl10	ENSMUSG00000020490	BTNL10	-5.855335792	0.004139503
Elane	ENSMUSG00000020125	ELANE	-2.957167126	0.004139503
Epb42	ENSMUSG00000023216	EPB42	-5.352958815	0.004269439
Ctsg	ENSMUSG00000040314	CTSG	-3.233144409	0.004699764
Emilin2	ENSMUSG00000024053	EMILIN2	-1.992142471	0.005971496
Rhd	ENSMUSG00000028825	RHD	-5.370983911	0.006189535
Fcgr4	ENSMUSG00000059089	FCGR4	-2.050240633	0.006189535
Tspan8	ENSMUSG00000034127	TSPAN8	-4.756157802	0.006189535
Slc4a1	ENSMUSG00000006574	SLC4A1	-5.334941787	0.006636322
AHSP	AHSP	AHSP	-5.337010884	0.006636322
Steap4	ENSMUSG00000012428	STEAP4	-1.54303349	0.007691583
Fgf21	ENSMUSG00000030827	FGF21	6.146197809	0.007691583
Gm20161	ENSMUSG00000117534	GM20161	-5.66948558	0.008361506
Apol8	ENSMUSG00000056656	APOL8	-5.923364694	0.00939958
Gypa	ENSMUSG00000051839	GYPA	-4.889813148	0.009772425
Dsp	ENSMUSG00000054889	DSP	4.545628572	0.009772425
Slc16a3	ENSMUSG00000025161	SLC16A3	-1.330506644	0.009940253
Cldn13	ENSMUSG00000008843	CLDN13	-4.771040843	0.010026092
Pklr	ENSMUSG00000041237	PKLR	-2.141099007	0.010026092
GM32208	GM32208	GM32208	-5.985660084	0.010026092
Arg2	ENSMUSG00000021125	ARG2	-2.24879593	0.010026092
GM41235	GM41235	GM41235	-3.376409896	0.010026092
Cstdc5	ENSMUSG00000071561	CSTDC5	-6.549493324	0.010026092
Trem1	ENSMUSG00000042265	TREM1	-1.818449975	0.010259347
Gfap	ENSMUSG00000020932	GFAP	-5.576473904	0.010564508
Ltb4r1	ENSMUSG00000046908	LTB4R1	-1.887623188	0.010564508
Apol10a	ENSMUSG00000050982	APOL10A	-5.549356871	0.010573736
Kel	ENSMUSG00000029866	KEL	-5.028953987	0.010795753
Foxa3	ENSMUSG00000040891	FOXA3	7.275093318	0.011039245
Slfn14	ENSMUSG00000082101	SLFN14	-5.345017664	0.011970977
Chil3	ENSMUSG00000040809	CHIL3	-3.275797927	0.012466518
Add2	ENSMUSG00000030000	ADD2	-4.584751375	0.013074295
Phyhip	ENSMUSG00000003469	PHYHIP	-4.853836099	0.013380216
Ms4a6d	ENSMUSG00000024679	MS4A6D	-2.14450178	0.014289929
Dmtn	ENSMUSG00000022099	DMTN	-4.906079596	0.016680161
Itgb2l	ENSMUSG00000000157	ITGB2L	-3.462661525	0.016787365
Hapln4	ENSMUSG00000007594	HAPLN4	6.81278951	0.016787365
Ermap	ENSMUSG00000028644	ERMAP	-4.098207707	0.016859528
Itih2	ENSMUSG00000037254	ITIH2	5.552697893	0.016859528
Rhag	ENSMUSG00000023926	RHAG	-4.914335486	0.017609182
Asprv1	ENSMUSG00000033508	ASPRV1	-1.526707766	0.018968962
Gm38825	ENSMUSG00000107799	GM38825	-4.752438057	0.018968962
Abcg4	ENSMUSG00000032131	ABCG4	-4.323087189	0.019218682

Sphk1	ENSMUSG00000061878	SPHK1	-2.044407051	0.021076813
Prok2	ENSMUSG00000030069	PROK2	-7.652108586	0.021432578
Padi4	ENSMUSG00000025330	PADI4	-1.935621257	0.022782286
Tarm1	ENSMUSG00000053338	TARM1	-2.940358864	0.022789269
Apol11b	ENSMUSG00000091694	APOL11B	-4.938372967	0.023707012
Lin28a	ENSMUSG00000050966	LIN28A	-4.802948828	0.023707012
Hemgn	ENSMUSG00000028332	HEMGN	-4.882044463	0.024037867
Sowaha	ENSMUSG00000044352	SOWAHA	-5.139778572	0.025320294
GM40180	GM40180	GM40180	-4.861990158	0.026236922
Il1r2	ENSMUSG00000026073	IL1R2	-2.595719549	0.027439035
Ank1	ENSMUSG00000031543	ANK1	-4.521696022	0.028332127
Plk1	ENSMUSG00000030867	PLK1	-1.879473523	0.028443519
Cdkn3	ENSMUSG00000037628	CDKN3	-2.98169632	0.028443519
Tfr2	ENSMUSG00000029716	TFR2	-2.101571548	0.028443519
GM41604	GM41604	GM41604	-6.239234872	0.028443519
Cd177	ENSMUSG00000052212	CD177	-3.36980746	0.029199092
Tmod1	ENSMUSG00000028328	TMOD1	-4.55269738	0.031000732
Cdc20	ENSMUSG00000006398	CDC20	-1.751436451	0.032224851
Ccdc92b	ENSMUSG00000069814	CCDC92B	-4.946375661	0.032224851
Olfm4	ENSMUSG00000022026	OLFM4	-2.985309688	0.032277293
Tmem125	ENSMUSG00000050854	TMEM125	7.355935411	0.03232171
Samd11	ENSMUSG00000096351	SAMD11	-5.014089828	0.032509638
Fpr1	ENSMUSG00000045551	FPR1	-1.462218832	0.032509638
Ifitm6	ENSMUSG00000059108	IFITM6	-2.055412546	0.034110377
Apol11a	ENSMUSG00000091650	APOL11A	-4.610796122	0.03469283
Lilrb4b	ENSMUSG00000112023	LILRB4B	-1.871246345	0.036314545
Cd5l	ENSMUSG00000015854	CD5L	-1.308723654	0.037200939
Sema3g	ENSMUSG00000021904	SEMA3G	-1.094431557	0.037200939
Parpbp	ENSMUSG00000035365	PARPBP	-2.061697303	0.037747795
Trim10	ENSMUSG00000073400	TRIM10	-4.242687019	0.037977743
Slc38a3	ENSMUSG00000010064	SLC38A3	6.945191164	0.03808367
Atp7b	ENSMUSG00000006567	ATP7B	-2.063000564	0.038104991
9830107B12Rik	ENSMUSG00000073386	9830107B12RIK	-2.327747792	0.038896007
Tspo2	ENSMUSG00000023995	TSPO2	-4.164490379	0.041360508
Siglece	ENSMUSG00000030474	SIGLECE	-1.255580934	0.043073876
5430401H09Rik	ENSMUSG00000112071	5430401H09RIK	-4.8177798	0.043073876
Hbq1b	ENSMUSG00000073063	HBQ1B	-4.222051757	0.043073876
Pnp2	ENSMUSG00000068417	PNP2	-4.359116375	0.04328404
Gm47252	ENSMUSG00000111895	GM47252	-6.699027206	0.04328404
Socs3	ENSMUSG00000053113	SOCS3	-1.466857772	0.049756628

Appendix F: Enrichment Pathways associated with the 158 differentially expressed genes identified using DESEQ2

Database	Name	P-value	Adjusted p-value	Odds Ratio	Combined score
GTEx Aging Signatures 2021	GTEx Spleen 20-29 vs 30-39 Up	1.71E-20	4.30E-18	16.27	740.29
	GTEx Blood 20-29 vs 40-49 Down	1.09E-14	1.37E-12	12.27	394.44
	GTEx Liver 20-29 vs 60-69 Down	1.64E-10	1.37E-08	9.38	211.24
	GTEx Lung 20-29 vs 40-49 Down	1.53E-09	9.61E-08	8.69	176.39
	GTEx Pituitary 20-29 vs 70-79 Up	1.33E-08	6.67E-07	8.02	145.47
	GTEx Blood 20-29 vs 30-39 Up	7.86E-07	0.00002817	6.72	94.51
	GTEx Breast 20-29 vs 70-79 Up	7.86E-07	0.00002817	6.72	94.51
	GTEx Liver 20-29 vs 70-79 Down	5.302E-06	0.0001479	6.1	74.05
	GTEx Blood 20-29 vs 50-59 Down	5.302E-06	0.0001479	6.1	74.05
	GTEx Muscle 20-29 vs 30-39 Down	0.00003254	0.0005833	5.48	56.64
Clinvar 2019	hereditary spherocytosis	2.98E-11	2.98E-10	99205	2404351.39

HDSigDB Mouse 2021	Genes Up-Regulated During Hematopoietic Differentiation PMID19128795	5.31E-20	8.78E-17	6.99	310.4
GWAS Catalog 2023	Mean Sphered Cell Volume	1.54E-08	0.00001058	48.59	874.02
	Mean Corpuscular Hemoglobin Concentration	0.00000382	0.00131	5.72	71.4
	Reticulocyte Count	6.735E-06	0.00154	4.63	55.18
	Immature Fraction Of Reticulocytes	0.00001593	0.002467	5.39	59.52
	Reticulocyte Fraction Of Red Cells	0.00001798	0.002467	4.51	49.3
	Mean Spheric Corpuscular Volume	0.00003091	0.003534	3.8	39.4
GO Biological Process 2023	Erythrocyte Differentiation (GO:0030218)	2.421E-06	0.002177	18.06	233.48
	Cellular Component Disassembly (GO:0022411)	0.00003141	0.009425	15.68	162.57

	Neutrophil Migration (GO:1990266)	0.00003418	0.009425	10.92	112.3
GO cellular compartment	Specific Granule (GO:0042581)	5.47E-09	3.38E-07	10.94	208.07
	Tertiary Granule (GO:0070820)	6.76E-09	3.38E-07	10.72	201.6
MGI mammalian Phenotype	increased erythrocyte osmotic fragility MP:0031085	1.63E-13	1.44E-10	131.34	3867.55
	spherocytosis MP:0002812	2.90E-12	1.28E-09	152.24	4044.71
	reticulocytosis MP:0002640	1.72E-10	4.12E-08	22.5	505.89
	microcytosis MP:0002813	1.86E-10	4.12E-08	65.22	1461.25
	abnormal erythrocyte morphology MP:0002447	6.00E-10	1.06E-07	19.52	414.39
	decreased hematocrit MP:0000208	1.21E-09	1.79E-07	11.02	226.31
	poikilocytosis MP:0002643	1.81E-09	2.29E-07	43.46	874.98
	anemia MP:0001577	2.91E-09	3.21E-07	9.11	179.14

	increased kidney iron level MP:0010375	2.26E-08	0.00000222	91.99	1619.7
	increased nucleated erythrocyte cell number MP:0009395	3.75E-08	0.000003322	26.06	445.58
Reactome 2022	Neutrophil Degranulation R-HSA-6798695	1.54E-10	4.11E-08	6.6	149.17
	Innate Immune System R-HSA-168249	0.00000767	0.0008623	3.15	37.06
Encode Histone Modification	H3K4me1 bone marrow macrophage mm9	7.72E-07	0.0003128	2.76	38.87